Prediction of bubbles in presence of α-stable aggregates moving averages

Gilles de Truchis[1], Sébastien Fries[2], Arthur Thomas[3]

PRELIMINARY DRAFT - PLEASE DO NOT CIRCULATE

Abstract

Financial markets frequently exhibit boom-and-bust cycles that are incompatible with standard linear time series models. While anticipative heavy-tailed linear processes offer a promising alternative for modeling such phenomena, they impose uniform bubble patterns across different episodes, contradicting empirical evidence. This paper introduces a new model based on α-stable moving average aggregates that accommodates heterogeneous bubble dynamics. We establish the theoretical properties of this model, demonstrating that it admits a semi-norm representation on a unit cylinder, thereby enabling the prediction of extreme trajectories with varying growth dynamics. We develop a minimum distance estimation procedure based on the joint characteristic function and establish its asymptotic properties. Monte Carlo simulations confirm the estimator's good finite-sample performance across various specifications. Our empirical application to the CBOE Crude Oil ETF Volatility Index successfully decomposes observed volatility dynamics into distinct components with different persistence properties, revealing that what appears as a single bubble episode actually consists of multiple superimposed processes with heterogeneous growth rates and crash probabilities.

Keywords: Aggregated processes, Stable random vectors, Spectral representation, Anticipative processes, Financial bubbles

[1]Université d'Orléans, Laboratoire d'Economie d'Orléans (LEO), 45000 PARIS, FRANCE, gilles.detruchis@univ-orleans.fr.
[2]Department of Econometrics and Data Science, Vrije Universiteit Amsterdam, Amsterdam, Netherlands
[3]Corresponding author: Université Paris Dauphine, Université PSL, LEDA, CNRS, IRD, 75016 PARIS, FRANCE, arthur.thomas@dauphine.psl.eu.

1. Introduction

Speculative assets on financial markets often exhibit periods of rapid price increases followed by sudden crashes. These fluctuations, known as rational asset pricing bubbles when driven by deviations from the fundamental value (as outlined by Blanchard and Watson , 1982; Tirole , 1985), have become increasingly evident in global financial markets, alongside the well-established characteristics of heavy-tailed distributions and clustered volatility. To explain how bubbles originate in markets, researchers have generally relied on standard martingale theory (see e.g. Biagini et al. , 2014; Jarrow et al. , 2010; Protter , 2012), or added further assumptions such as portfolio constraints or defaultable claims (see e.g. Biagini and Nedelcu , 2015; Hugonnier, 2012; Jarrow et al. , 2012). More recent work has examined the role of zombie credits (Acharya et al. , 2024), liquidity constraints (Acharya and Rajan , 2024), and risk premia (Allen et al. , 2023) in bubble formation. A substantial literature documents the impact of bubbles on economic growth (Martin and Ventura , 2012; Carvalho et al. , 2012) or on unemployment (Hashimoto and Im , 2016, 2019; Miao , 2014; Miao et al. , 2016).

A growing body of economic literature emphasizes the significance of bubble phenomena beyond finance, extending to macroeconomic modeling (Gouriéroux et al. , 2020; Hirano and Toda , 2024; Hirano et al. , 2025).[4] From a theoretical perspective, Hirano and Toda (2024) develop a comprehensive framework for bubble economics, establishing conditions under which rational bubbles can emerge and persist even with infinitely-lived representative agents deriving utility from wealth holdings. Lux and Sornette (2002) demonstrates how agent interactions can create bubble formation, with bubbles growing in seemingly rational ways driven by investor expectations. Their model effectively captures sudden dramatic crashes and replicates the "fat tails" observed in empirical financial market data, suggesting that traditional representative rational agent models inadequately explain these phenomena. Agliari et al. (2018) develop a stock market participation model with heterogeneous traders that produces boom-bust dynamics through the interplay of different trading strategies, further highlighting how agent heterogeneity contributes to the emergence of bubbles. Gouriéroux et al. (2020) show that linear rational expectation models admit multiple stationary dynamic equilibria due to nonlinear stationary solutions, which can exhibit speculative bubbles and volatility-induced mean reversion while remaining consistent with transversality conditions in intertemporal optimization models.

From an empirical perspective, the so-called mixed-causal (or anticipative) models appears as good candidates (see e.g. Cavaliere et al. , 2020; Cubadda et al. , 2017; Fries and Zakoian , 2019; Gouriéroux et al. , 2020; Gouriéroux and Zakoian , 2017; Hecq et al. , 2016, 2017a; Hencic and Gouriéroux, 2015) to account the non-linear dynamics of the bubble and the non-Gaussian environment characterized by Lux and Sornette (2002) and Gouriéroux et al. (2020). Indeed, future-oriented models may generate intermittent

[4] While our paper's empirical focus remains on finance, we reserve potential macroeconomic applications for future research.

periods of explosive growth and relative stability in a stationarity linear framework while also admitting a regular time representation involving non-linear dynamics or non-i.i.d. innovations. Among others we can mention Andrews et al. (2009); Behme (2011); Behme et al. (2011); Chen et al. (2017); Gouriéroux and Jasiak (2016, 2017); Lanne and Saikkonen (2011, 2013); Saikkonen and Sandberg (2016). Most importantly, this framework exhibits intriguing properties, such as a predictive distribution with lighter tails than the marginal distribution. This enables more accurate predictions of higher-order moments (see e.g. Fries, 2022) and forecasts based on pattern recognition (see Dumitrescu and Thomas , 2024; de Truchis et al. , 2025a) which are critical for informed investment decisions (see de Truchis et al. , 2024). As emphasized by Gouriéroux et al. (2020) this framework offers a robust approach to modeling bubble dynamics as it relaxes the finite variance constraint while maintaining stationarity.

However, anticipative models impose a similar increase rate for all bubbles, fully determined by the non-causal autoregressive coefficients Gouriéroux and Zakoian (2017). This lack of flexibility might conflicts with empirical evidence on financial markets where the surge of explosive episodes can exhibit very different pattern. Moreover, Gouriéroux et al. (2021) recall that aggregation implies various sources of noise and is hence very different from mixed-causal AR processes and more generally, different from any two-sided moving average. As it incorporates independent unobservable stochastic factors aggregation it is more suitable for financial applications. For instance, if one want to build derivatives to hedge portfolios against the uncertainty associated with the anticipative components and the risk of sudden bubble crashes, the two factor of risk should be priced and accounted for in the derivatives.

In this paper, we make two contributions to the literature on econometric modeling of financial bubbles. First, we introduce a novel flexible framework built on α-stable moving average aggregates that overcomes a key limitation of existing anticipative heavy-tailed models, which impose uniform growth patterns across different bubble episodes. Our approach allows for diverse bubble dynamics by aggregating multiple latent components, each with distinct stochastic properties. We derive the theoretical tail properties of this model and demonstrate that, similar to non-aggregated processes, it admits a semi-norm representation on a unit cylinder, expect if one of the underling component is purely non-anticipative, thereby enabling the prediction of extreme trajectories with heterogeneous growth patterns.

Second, we develop an inference procedure for anticipative stable aggregates, departing from Gouriéroux and Zakoian (2017) and building upon Knight and Yu (2002). While Gouriéroux and Zakoian (2017) focus on continuous support distributions for the aggregation weights in the specific case of anticipative Cauchy AR(1) processes, our approach extends to the general α-stable case with discrete support, a framework more suitable for empirical applications. We propose a deconvolution minimum distance estimator based on the joint characteristic function that effectively identifies the model parameters. Our methodology draws from Knight and Yu (2002), who established asymptotic theory for minimum distance estimation using the empirical characteristic function in stationary time series, but we extend their approach to handle the

heavy-tailed stable distributions. We also incorporate elements from Xu and Knight (2010), who explored empirical characteristic function estimation of mixtures of normal parameters, adapting their insights to our non-Gaussian, dependent context. The resulting procedure transforms the intractable likelihood into a computationally feasible estimation method that simultaneously handles all parameters of interest, including both the AR coefficients and the distribution parameters of the innovations. We establish the asymptotic properties of our estimator under suitable regularity conditions, proving consistency and asymptotic normality with an explicit characterization of the asymptotic variance-covariance matrix. In contrast to existing methods, our procedure estimates all model parameters simultaneously while maintaining computational tractability, addressing a gap in the literature on stable ARMA modeling.

The Section 2 introduces the stable aggregates model and suggests a new minimum distance estimator base on the characteristic functions of the unobserved latent components. Section 3 extends the representation theorem of de Truchis et al. (2025a) to stable aggregates and theoretically derive the conditions under which the forecast of a stable aggregate is possible. The finite sample performance of the minimum estimator are documented in Section 4 and an application to the CBOE Crude Oil ETF Volatility Index is proposed in Section 5. Section 6 concludes and all proofs are postponed in the Appendix 7.

2. Estimating stable-aggregate of moving average

Consider X_t an α-stable moving average defined by

$$X_t = \sum_{k\in\mathbb{Z}} d_k \varepsilon_{t+k}, \qquad \varepsilon_t \overset{i.i.d.}{\sim} \mathcal{S}(\alpha,\beta,\sigma,0) \tag{2.1}$$

with (d_k) a real deterministic sequence such that if $\alpha \neq 1$ or $(\alpha,\beta) = (1,0)$,

$$0 < \sum_{k\in\mathbb{Z}} |d_k|^s < +\infty, \qquad \text{for some} \quad s \in (0,\alpha)\cap[0,1], \tag{2.2}$$

and if $\alpha = 1$ and $\beta \neq 0$,

$$0 < \sum_{k\in\mathbb{Z}} |d_k| \Big| \ln |d_k| \Big| < +\infty. \tag{2.3}$$

For $d_k = \rho^k$, X_t is a simple strictly stationary anticipative AR(1). Adding the $(\alpha,\beta) = (1,0)$ restrictions (let say $\mathcal{S}1\mathcal{S}$), X_t actually comes down to the so-called anticipative Cauchy AR(1) studied, e.g., in Gouriéroux and Jasiak (2018). As emphasized in the introduction, stable moving averages of the form (2.1) generate trajectories bound to feature the same pattern $t \mapsto cd_{\tau-t}$ (up to a scaling c and a time shift τ) recurrently through time. This can be seen as a strong limitation when it comes to time series modelling as argued by Gouriéroux and Zakoian (2017) in the context of explosive bubbles. They suggest to alleviate this restriction by considering processes resulting from the linear combination of different models.

Definition 2.1. *Let $(X_{1,t}), \dots, (X_{J,t})$ be $J \geq 1$ stable moving averages, each satisfying (2.1)-(2.3), for some coefficients sequences $(d_{j,k})_k$ and mutually independent error sequences $\varepsilon_{j,t} \overset{i.i.d.}{\sim} \mathcal{S}(\alpha, \beta_j, 1, 0)$, $j = 1, \dots, J$. Let also $(\pi_j)_{j=1,\dots,J}$ be positive numbers summing to 1, $\sigma > 0$ be a scale parameter and define*

$$\mathcal{X}_t = \sigma \sum_{j=1}^{J} \pi_j X_{j,t}, \qquad \text{for} \quad t \in \mathbb{Z}.$$

We will call such process $\mathcal{X}_t$ a stable aggregate, and call $X_{j,t}$, $j = 1, \dots, J$ the latent components of $\mathcal{X}_t$.

The estimator we propose is valid for any strictly stationary stable aggregate, but in practice, it requires to formally derive the characteristic function of the latent components which can be tedious. In the rest of this section, we hence restrict our attention to $d_{j,k} = \rho_j^k$ and $\beta_j = \beta$. We relax this hypothesis in Section 3 as linear combinations of stable moving averages fit naturally into the framework of de Truchis et al. (2025a) that deals with the general α-stable moving average in (2.1). Notice that even in this specific AR(1) framework, these aggregations feature much richer dynamics than single-component stable anticipative processes. In particular, they are able to mimic most of financial assets dynamics, as illustrated in Figure 1.

The occurrence of each component is governed by the weights π_j, also crucially involved in the strict stationarity condition of $\mathcal{X}_t$

$$\sum_{j=0}^{J} \frac{\pi_j^s}{(1 - |\rho_j|^s)} < \infty$$

for $s \in (0, \alpha) \cap [0, 1]$. Considering a continuum of values of parameter ρ in the aggregation,

$$\mathcal{X}_t = \int_{(-1,1)} X_{\rho,t} d\pi(\rho),$$

Gouriéroux and Zakoian (2017) also provide identification and estimation conditions by deriving the joint characteristic function of $(\mathcal{X}_t, \mathcal{X}_{t-1})$ for the anticipative Cauchy AR(1). Under Cauchy assumption they derive a non-parametric estimator of the probability measure π. Unfortunately, their results no longer old when we relax the restriction $\alpha = 1$. We hence restrict our attention on a discrete support for π while extending their approach to the (general) α-Stable family, hereafter referred as $\mathcal{G}\alpha\mathcal{S}$. To disentangle the elements of $\mathcal{X}_t$ we rely on the independence of the AR(1) components, the joint characteristic function

$$\varphi_{\mathcal{X}}(u, v) = \mathbb{E}\Big(\exp\{i(u\mathcal{X}_t + v\mathcal{X}_{t+1})\} \Big) = \exp\left(\sum_{j \in \mathbb{N}} \pi_j (\varphi_{X_j}(u, v) \right) \tag{2.4}$$

and the joint characteristic function of each latent component

$$\varphi_{X_j}(u, v) = \mathbb{E}\Big(\exp i(uX_{j,t} + vX_{j,t+1}) \Big) = \mathbb{E}\Big(\exp i(\rho_j u + v) X_{j,t+1} \Big) \mathbb{E}\Big(\exp iu\sigma\varepsilon_{j,t} \Big) \tag{2.5}$$

for $(u, v) \in \mathbb{R}^2$. It follows that we have

$$\log \mathbb{E}\Big(\exp i(\rho_j u + v) X_{j,t+1} \Big) = -\sigma^\alpha \frac{|\rho_j u + v|^\alpha}{1 - |\rho_j|^\alpha} \left(1 - \beta i \operatorname{sign}(\rho_j u + v) \tan\left(\frac{\pi\alpha}{2} \right) \right)$$

$$\log \mathbb{E}\Big(\exp iu\sigma\varepsilon_{j,t} \Big) = -\sigma^\alpha \left(1 - \beta i \operatorname{sign}(u) \tan\left(\frac{\pi\alpha}{2} \right) \right) |u|$$

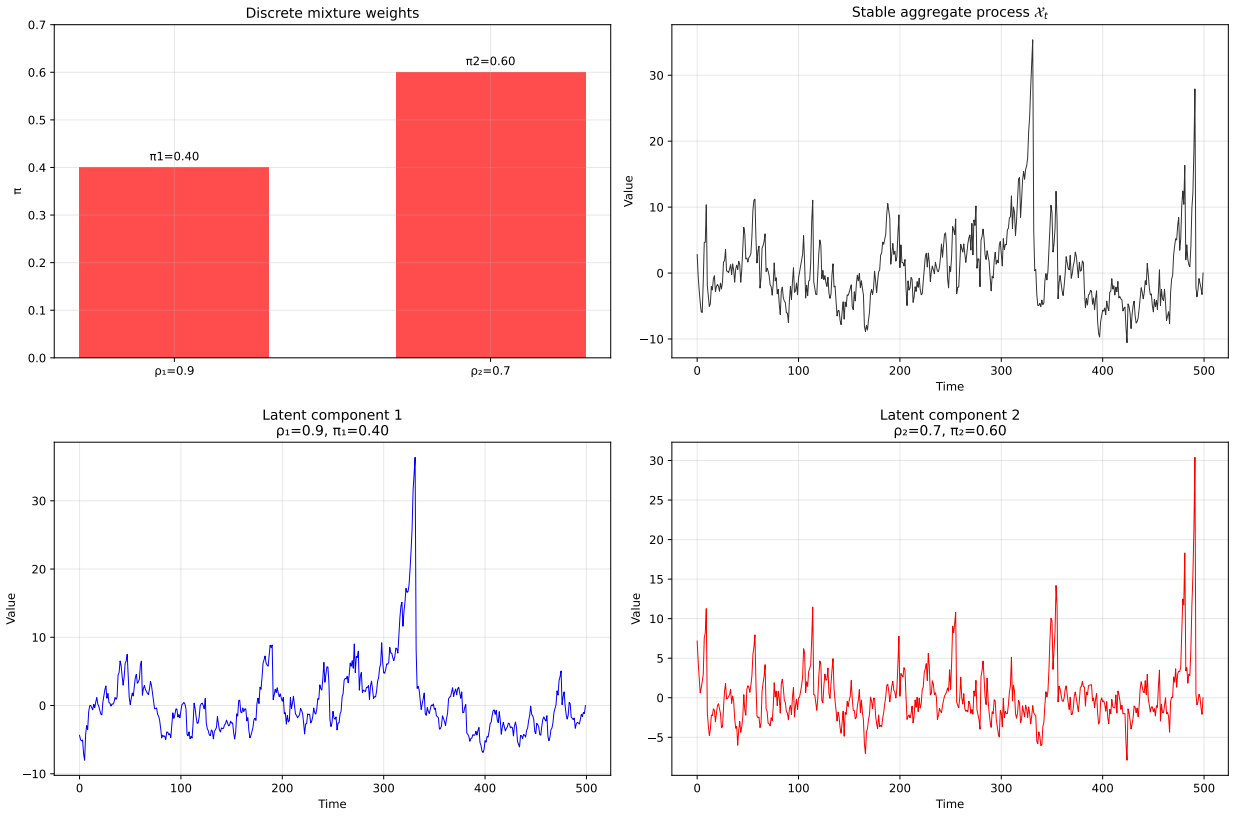

Figure 1: Simulated stable aggregate dynamics with two components. Top left: Distribution of weights for the two components with $\rho_1 = 0.90$, $\pi_1 = 0.40$ for the first component and $\rho_2 = 0.70$, $\pi_2 = 0.60$ for the second component. Top right: The resulting trajectory of the aggregated process $\mathcal{X}_t$. Middle and bottom panels: The individual latent component processes with different persistence parameters.

and the Cauchy case is recovered for $\alpha = 1$, $\beta = 0$:

$$\log \mathbb{E}\Big(\exp i(\rho_j u + v) X_{j,t} \Big) = -\sigma \frac{|\rho_j u + v|}{1 - |\rho_j|}$$
$$\log \mathbb{E}\Big(\exp iu\sigma\varepsilon_{j,t} \Big) = -\sigma|u|$$

As suggested by Knight and Yu (2002) and Gouriéroux and Zakoian (2017), one can rely on the empirical counterpart of the joint characteristic function (ECF) to build a minimum distance estimator (MDE). The ECF is simply defined as

$$\varphi_n(u, v) = \frac{1}{n-1} \sum_{j=1}^{n-1} \exp(i(u\mathcal{X}_{j+1} + v\mathcal{X}_j)) \tag{2.6}$$

which can be decomposed into real and imaginary parts:

$$\varphi_n(u, v) = \frac{1}{n-1} \sum_{j=1}^{n-1} \cos(u\mathcal{X}_{j+1} + v\mathcal{X}_j) + \frac{1}{n-1} \sum_{j=1}^{n-1} i \sin(u\mathcal{X}_{j+1} + v\mathcal{X}_j) \tag{2.7}$$

By the law of large numbers, $\varphi_n(u, v) \xrightarrow{P} \varphi(u, v; \theta_0)$ as $n \to \infty$, where θ_0 denotes the true parameter values. Then, the identification of the parameters $\theta = (\sigma, \rho_1, \ldots, \rho_J, \pi_1, \ldots, \pi_J, \alpha, \beta)$ relies on distinct asymptotic behaviors of the joint characteristic function for different values of (u, v). For small values of u, the limit behavior of (2.6) is dominated by the α-stable distribution's properties. Specifically, for $u > 0$,

$$\alpha = \lim_{u \to 0} \frac{\log \log |\varphi_n(u, 0)|^{-1}}{\log |u|} \tag{2.8}$$

and

$$\beta = -\lim_{u \to 0} \frac{\mathrm{Im}(\log \varphi_n(u, 0))}{\mathrm{Re}(\log \varphi_n(u, 0))} \cdot \cot \frac{\pi\alpha}{2}. \tag{2.9}$$

For the identification of the remaining parameters, we exploit the behavior of the function

$$g_n(\lambda) = \lim_{u \to 0} \frac{\log |\varphi_n(u, \lambda u)|}{|u|^\alpha} \approx -\sigma^\alpha \sum_{j=1}^{J} \pi_j^\alpha \left[\frac{|1 + \rho_k \lambda|^\alpha}{1 - |\rho_j|^\alpha} + |\lambda|^\alpha \right] \tag{2.10}$$

for $v = \lambda u$ and $\lambda \in \mathbb{R}$. By evaluating $g_n(\lambda)$ for $2J + 1$ different values of λ, we can obtain a system of equations to identify $(\sigma, \rho_1, \ldots, \rho_J, \pi_1, \ldots, \pi_J)$. Now we can define the MDE estimator as the minimizer of the objective distance measure

$$D_{\mathcal{X}}(\theta) = \int_{-\infty}^{+\infty} \int_{-\infty}^{+\infty} |\varphi_n(u, v) - \varphi(u, v; \theta)|^2 w(u, v) du dv \tag{2.11}$$

where $w(u, v)$ is a weighting function ensuring the convergence of the integral. The MDE estimator is then defined as

$$\hat{\theta}_n = \arg\min_{\theta} D_{\mathcal{X}}(\theta). \tag{2.12}$$

Knight and Yu (2002), show that under the following regularity conditions, the MDE estimator has standard limit theory. They suggest that it could accommodate α-stable models. Actually, some of their assumptions, listed hereafter, does not readily extend to the α-stable case. The characteristic functions of α-stable distributions are likely to exhibit singularities in their derivatives when $\alpha \in (0, 2)$, particularly near points where $|\rho_j u+v|^\alpha$ vanishes. Without appropriate regularization through the weight function, these singularities can cause the integrals defining the first and second derivatives of (2.11) to diverge. The following lemma establishes the precise conditions under which Assumption A2 remains valid for α-stable AR(1) aggregates.

Lemma 2.1. *Consider the MDE objective function defined by:*

$$D_{\mathcal{X}}(\theta) = \int_{-\infty}^{+\infty} \int_{-\infty}^{+\infty} |\varphi_n(u, v) - \varphi(u, v; \theta)|^2 w(u, v)\, du\, dv \tag{2.13}$$

where $w(u, v) = \exp(-\kappa(u^2 + v^2))$ *with* $\kappa > 0$ *a positive constant.*

Then,

(ι) For any $\alpha > 0$*, the objective function* $D_{\mathcal{X}}(\theta)$ *belongs to the differentiability class* $C^1(\Theta)$*.*

(ιι) For any $\alpha > 1$*, the objective function* $D_{\mathcal{X}}(\theta)$ *belongs to* $C^2(\Theta)$ *and Assumption 3, 6, 7 and 8 are satisfied.*

Lemma 2.1, shows that we need to reduce the parameter space of α by introducing Assumption 2, in addition to whole set of assumptions of Knight and Yu (2002), to recover their asymptotic theory in presence of α-stable model. It also reveals the critical role of the decaying exponential weights $w(u, v)$.

Assumption 1. $\theta \in \Theta$ *where the parameter space* $\Theta \subset \mathbb{R}^{2J+3}$ *is a compact set with* $\theta_0 \in Int(\Theta)$*.*

Assumption 2. *The tail parameter space is such that* $\alpha \in (1, 2)$ *and* $w(u, v)$ *is an exponential weight function of form* $\exp(-\kappa(u^2 + v^2))$ *with* $\kappa > 0$ *a positive constant.*

Assumption 3. *With probability one,* $D_{\mathcal{X}}(\theta)$ *is twice continuously differentiable under the integral sign with respect to* θ *over* Θ*.*

Assumption 4. *The sequence* $\{\mathcal{X}_t\}$ *is strictly stationary and ergodic.*

Assumption 5. *Let* $D_0(\theta) = \iint |\varphi(u, v; \theta_0) - \varphi(u, v; \theta)|^2 w(u, v) du dv$ *and* $D_0(\theta) = 0$ *only if* $\theta = \theta_0$*.*

Assumption 6. $K(x; \theta)$ *is a measurable function of* x *for all* θ *and bounded, where*

$$\begin{aligned} K(x;\theta) = \iint \Bigg[&(\cos(ux_{j+1} + vx_j) - Re\ \varphi(u, v; \theta)) \frac{\partial Re\ \varphi(u, v; \theta)}{\partial \theta} \\ &+ (\sin(ux_{j+1} + vx_j) - Im\ \varphi(u, v; \theta)) \frac{\partial Im\ \varphi(u, v; \theta)}{\partial \theta} \Bigg] w(u, v) du dv. \end{aligned} \tag{2.14}$$

Assumption 7. *The matrix*

$$\Sigma(\theta_0) = \iint \left(\frac{\partial \varphi(u,v;\theta_0)}{\partial \theta}\right)\left(\frac{\partial \overline{\varphi}(u,v;\theta_0)}{\partial \theta'}\right) w(u,v)dudv$$

is nonsingular and

$$\frac{\partial^2 \varphi(u,v;\theta)}{\partial \theta \partial \theta'}$$

is uniformly bounded by a w-integrable function over Θ.

Assumption 8. *Let $\mathcal{F}_j$ be a σ-algebra such that $\{K_j, \mathcal{F}_j\}$ is an adapted stochastic sequence, where $K_j = K(x_j;\theta)$. We can think of $\mathcal{F}_j$ as being the σ-algebra generated by the entire current and past history of K_j. Let $\nu_j = \mathbb{E}[K_0|K_j, K_{j-1}, \ldots] - \mathbb{E}[K_0|K_{j-1}, K_{j-2}, \ldots]$ for $j \geq 0$. Assume that $\mathbb{E}(K_0|\mathcal{F}_{-m})$ converges in mean square to 0 as $m \to \infty$ and $\sum_{j=0}^{\infty} \mathbb{E}[\nu_j' \nu_j]^{1/2} < \infty$.*

Proposition 2.1. *Under Assumptions 1-8*

$$\sqrt{n}(\hat{\theta}_n - \theta_0) \xrightarrow{d} N(0, \Sigma^{-1}\Omega\Sigma^{-1}) \tag{2.15}$$

where Σ and Ω are $(2J+2) \times (2J+2)$ matrices with the (i,k)-th elements given by:

$$\Sigma_{ik} = \mathbb{E}\left(\frac{\partial^2 D_{\mathcal{X}}(\theta)}{\partial \theta_i \partial \theta_k}\right) \tag{2.16}$$

$$\Omega_{ik} = \mathbb{E}\left(\frac{\partial D_{\mathcal{X}}(\theta)}{\partial \theta_i}\frac{\partial D_{\mathcal{X}}(\theta)}{\partial \theta_k}\right) \tag{2.17}$$

where Ω can also be expressed as:

$$\Omega = var(K(x_1;\theta_0)) + 2\sum_{j=2}^{\infty} cov(K(x_1;\theta_0), K(x_j;\theta_0)) \tag{2.18}$$

The proof of this theorem is omitted as, by Lemma 2.1, it follows from a straightforward extension of Theorem 2.1 of Knight and Yu (2002). Notice that in our α-stable framework, unlike Xu and Knight (2010), Σ and Ω have no closed-form solutions. Moreover, to alleviate the optimization problem from a numerical standpoint, we directly estimate the products $\varsigma = \sigma \times \pi_j$ for $j = 1, \ldots, J$.

3. Forecasting aggregation of moving averages

This section begins by summarizing relevant findings from de Truchis et al. (2025a), DFT henceforth, concerning the description of stable random vectors on the unit cylinder.[5] Let the vector $\boldsymbol{X} = (X_1, \ldots, X_d)$

[5] We exclude the Gaussian case from further discussion as anticipative dynamics are not identifiable when $\alpha = 2$.

be an α-stable random vector, Γ a finite spectral measure on the Euclidean unit sphere S_d and $\boldsymbol{\mu}^0$ a non-random vector in $\mathbb{R}^d$, such that,

$$\mathbb{E}\Big[e^{i\langle \boldsymbol{u},\boldsymbol{X}\rangle}\Big] = \exp\left\{ -\int_{S_d} |\langle \boldsymbol{u},\boldsymbol{s}\rangle|^\alpha \Big(1 - i\,\mathrm{sign}(\langle \boldsymbol{u},\boldsymbol{s}\rangle) w(\alpha,\langle \boldsymbol{u},\boldsymbol{s}\rangle)\Big)\Gamma(d\boldsymbol{s}) + i\,\langle \boldsymbol{u},\boldsymbol{\mu}^0\rangle \right\}, \quad \forall \boldsymbol{u}\in\mathbb{R}^d, \tag{3.1}$$

where $\langle\cdot,\cdot\rangle$ denotes the canonical scalar product, $w(\alpha,s) = \mathrm{tg}\left(\frac{\pi\alpha}{2}\right)$, if $\alpha \neq 1$, and $w(1,s) = -\frac{2}{\pi}\ln|s|$ otherwise, for $s\in\mathbb{R}$. Drawing on DFT, we explore alternative representations of $\boldsymbol{X}$ where the integration is performed over a unit cylinder $C_d^{\|\cdot\|} := \{\boldsymbol{s}\in\mathbb{R}^d : \ \|\boldsymbol{s}\| = 1\}$, defined by a semi-norm $\|\cdot\|$ on $\mathbb{R}^d$, in presence of stable aggregates. The reason why we are interested in alternative representations is that, in the presence of the Euclidean norm, the spectral measure encodes information in all directions of $\mathbb{R}^d$ and does not allow us to predict future elements of the vector $\boldsymbol{X}$ while ensuring that these future elements are not themselves carriers of information for prediction. By contrast, the semi-norm $\|\cdot\|$ is flexible enough to force some directions $\mathbb{R}^d$ to vanish.

We will say that $\boldsymbol{X}$ is representable on $C_d^{\|\cdot\|}$ if $\boldsymbol{X}$ can be written as in (3.1) with $(S_d,\Gamma,\boldsymbol{\mu}^0)$ replaced by $(C_d^{\|\cdot\|},\Gamma^{\|\cdot\|},\boldsymbol{\mu}^0_{\|\cdot\|})$. As demonstrated in DFT for the single-component model, $\boldsymbol{X}$ is representable on $C_d^{\|\cdot\|} \iff \Gamma(K^{\|\cdot\|}) = 0$ when $\alpha\neq 1$ or if $\boldsymbol{X}$ is $\mathcal{S}1\mathcal{S}$. Moreover, $\Gamma^{\|\cdot\|}(d\boldsymbol{s}) = \|\boldsymbol{s}\|_e^{-\alpha}\,\Gamma\circ T^{-1}_{\|\cdot\|}(d\boldsymbol{s})$ with $T_{\|\cdot\|} : S_d\setminus K^{\|\cdot\|} \longrightarrow C_d^{\|\cdot\|}$ defined by $T_{\|\cdot\|}(\boldsymbol{s}) = \boldsymbol{s}/\|\boldsymbol{s}\|$. Importantly, this new representation inherits from the traditional representation the following asymptotic conditional tail property: for any Borel sets $A,B\subset C_d^{\|\cdot\|}$ with $\Gamma^{\|\cdot\|}\Big(\partial(A\cap B)\Big) = \Gamma^{\|\cdot\|}\big(\partial B\big) = 0$, and $\Gamma^{\|\cdot\|}(B) > 0$,

$$\mathbb{P}_x^{\|\cdot\|}(\boldsymbol{X},A|B) \underset{x\to+\infty}{\longrightarrow} \frac{\Gamma^{\|\cdot\|}(A\cap B)}{\Gamma^{\|\cdot\|}(B)}, \tag{3.2}$$

where ∂B (resp. $\partial(A\cap B)$) denotes the boundary of B (resp. $A\cap B$), and

$$\mathbb{P}_x^{\|\cdot\|}(\boldsymbol{X},A|B) := \mathbb{P}\left(\frac{\boldsymbol{X}}{\|\boldsymbol{X}\|}\in A \,\middle|\, \|\boldsymbol{X}\| > x, \frac{\boldsymbol{X}}{\|\boldsymbol{X}\|}\in B\right).$$

To build a forecasting strategy upon these theoretical results, DFT considers vectors of the form $\boldsymbol{X_t} = (X_{t-m},\ldots,X_t,X_{t+1},\ldots,X_{t+h})$, $m\geq 0$, $h\geq 1$, derived from a stable moving average process and choose, without loss of generality, semi-norms satisfying

$$\|(x_{-m},\ldots,x_0,x_1,\ldots,x_h)\| = 0 \iff x_{-m} = \ldots = x_0 = 0, \tag{3.3}$$

for any $(x_{-m},\ldots,x_h)\in\mathbb{R}^{m+h+1}$. They show that for $\alpha\neq 1$ and $(\alpha,\beta) = (1,0)$, the representability of $\boldsymbol{X_t}$ on a semi-norm unit cylinder depends on the number of observation $m+1$ but not on the prediction horizon h. More precisely, they find that sequences of consecutive zero values in must either be of finite length or extend infinitely to the left :

$$\forall k\in\mathbb{Z}, \quad \Big[(d_{k+m},\ldots,d_k) = \mathbf{0} \quad\Longrightarrow\quad \forall \ell\leq k-1, \quad d_\ell = 0\Big]. \tag{3.4}$$

This result surprisingly establishes that the anticipativeness of a stable moving average is a necessary condition (and sufficient for $\alpha \neq 1$ and $(\alpha, \beta) = (1, 0)$) to make use of (3.2) in order to feasibly predict $\boldsymbol{X_t}$. The more non-anticipative a moving average is (i.e., the larger the gaps of zeros in its forward-looking coefficients), the larger m must be to achieve representability of $(X_{t-m}, \ldots, X_t, X_{t+1}, \ldots, X_{t+h})$ on the appropriate unit cylinder.

3.1. Extending the representation to stable aggregates

To extend these results to stable aggregates, we first provide the spectral representation of paths of the aggregated process $\mathcal{X}_t$ on the Euclidean unit sphere.

Lemma 3.1. *Let $\mathcal{X}_t$ be an α-stable aggregate with latent moving averages $(X_{1,t}), \ldots, (X_{J,t})$ as in Definition 2.1, but now allowing $\beta_j \in [-1, 1]$ to vary across components, and $\boldsymbol{X_t} = (\mathcal{X}_{t-m}, \ldots, \mathcal{X}_t, \mathcal{X}_{t+1}, \ldots, \mathcal{X}_{t+h})$ for any $m \geq 0$, $h \geq 1$.*

Then, $\boldsymbol{X}_t$ is α-stable and its spectral representation $(\Gamma, \boldsymbol{\mu}^0)$ on the Euclidean unit sphere S_{m+h+1} writes

$$\Gamma = \sigma^\alpha \sum_{j=1}^{J} \sum_{\vartheta \in S_1} \sum_{k \in \mathbb{Z}} w_{j,\vartheta} \pi_j^\alpha \|\boldsymbol{d}_{j,k}\|_e^\alpha \delta \left\{ \frac{\vartheta \boldsymbol{d}_{j,k}}{\|\boldsymbol{d}_{j,k}\|_e} \right\}, \tag{3.5}$$

$$\boldsymbol{\mu}^0 = \begin{cases} \mathbf{0}, & \text{if } \alpha \neq 1 \\ -\frac{2\sigma}{\pi} \sum_{j=1}^{J} \sum_{k \in \mathbb{Z}} \pi_j \beta_j \boldsymbol{d}_{j,k} \ln \|\sigma \pi_j \boldsymbol{d}_{j,k}\|_e, & \text{if } \alpha = 1 \end{cases}$$

where $\boldsymbol{d}_{j,k} = (d_{j,k+m}, \ldots, d_{j,k}, d_{j,k-1}, \ldots, d_{j,k-h})$, $w_{j,\vartheta} = (1 + \vartheta\beta_j)/2$, for any $k \in \mathbb{Z}$, $j = 1, \ldots, J$, δ is the Dirac mass, $\vartheta \in S_1$ with $S_1 = \{-1, +1\}$, and if $\boldsymbol{d}_{j,k} = \mathbf{0}$, the term vanishes by convention from the sums.

Notice that $\Gamma = \sigma^\alpha \sum_{j=1}^{J} \pi_j^\alpha \Gamma_j$, where Γ_j denotes the spectral measure of the path $\boldsymbol{X}_{j,t}$ from the moving average $(X_{j,t})$, $j = 1, \ldots, J$. If all the $\boldsymbol{X}_{j,t}$'s are symmetric ($\beta_j = 0$ for all j), then $\boldsymbol{X}_t$ and Γ are symmetric as well, but the reciprocal however does not hold true. The measure Γ will be symmetric if and only if $\sigma^\alpha \sum_{j=1}^{J} \pi_j^\alpha \Big(\Gamma_j(A) - \Gamma_j(-A)\Big) = 0$ for any Borel set $A \subset S_{m+h+1}$. The latter condition is necessary and sufficient for $\boldsymbol{X}_t$ to be symmetric in the case where $\alpha \neq 1$, whereas for $\alpha = 1$, it guarantees that $\boldsymbol{X}_t$ will be symmetric up to an additive shifting, as $\boldsymbol{\mu}^0$ may be non-zero. The symmetry of paths intervenes in the representability conditions provided in the following lemma.

Lemma 3.2. *Let $\mathcal{X}_t$ be an α-stable aggregate with latent moving averages $(X_{1,t}), \ldots, (X_{J,t})$ as in Definition 2.1, where each component j has asymmetry parameter $\beta_j \in [-1, 1]$. Let $m \geq 0$, $h \geq 1$ and $\|\cdot\|$ be a semi-norm on $\mathbb{R}^{m+h+1}$ satisfying (3.3). When either $\alpha \neq 1$ or $\boldsymbol{X}_t \sim \mathcal{S}1\mathcal{S}$, the vector $\boldsymbol{X}_t$ is representable on $C_{m+h+1}^{\|\cdot\|}$ if and only if condition (3.4) holds with m for all coefficient sequences $(d_{j,k})_k$, $j = 1, \ldots, J$. For $\alpha = 1$ and $\boldsymbol{X}_t$ asymmetric, the vector $\boldsymbol{X}_t$ is representable on $C_{m+h+1}^{\|\cdot\|}$ if and only if (3.4) holds and*

$$\sum_{k \in \mathbb{Z}} \|\boldsymbol{d}_{j,k}\|_e \left| \ln \Big(\|\boldsymbol{d}_{j,k}\| / \|\boldsymbol{d}_{j,k}\|_e \Big) \right| < +\infty, \quad \forall j \in \{1, \ldots, J\} \tag{3.6}$$

hold with m and h for all sequences $(d_{j,k})_k$, $j = 1, \dots, J$.

The next proposition extends to stable aggregated processes the notion of past-representability introduced in DFT and helps to understand to what extent anticipativeness is crucial in this more general framework.

Proposition 3.1. *Let $\mathcal{X}_t$ be an α-stable aggregate with latent moving averages $(X_{1,t}), \dots, (X_{J,t})$ as in Definition 2.1, where $\mathcal{X}_t = \sigma \sum_{j=1}^{J} \pi_j X_{j,t}$ with scale parameter $\sigma > 0$.*

(ι) Define for $j = 1, \dots, J$ the sets $\mathcal{M}_j = \{m \geq 1 : \ \exists k \in \mathbb{Z}, \ d_{j,k+m} = \dots = d_{j,k+1} = 0, \ d_{j,k} \neq 0\}$, and

$$m_{0,j} = \begin{cases} \sup \mathcal{M}_j, & \text{if} \quad \mathcal{M}_j \neq \emptyset, \\ 0, & \text{if} \quad \mathcal{M}_j = \emptyset. \end{cases} \tag{3.7}$$

(a) For $\alpha \neq 1$, the aggregated process $\mathcal{X}_t$ is past-representable if and only if $(X_{j,t})$ is past-representable for all $j = 1, \dots, J$, i.e.,

$$\sup_{j=1,\dots,J} m_{0,j} < +\infty. \tag{3.8}$$

Moreover, letting $m \geq 0$, $h \geq 1$, $\mathcal{X}_t$ is (m,h)-past-representable if and only if (3.8) holds and $m \geq \max_{j=1,\dots,J} m_{0,j}$.

(b) For $\alpha = 1$, the process $\mathcal{X}_t$ is past-representable if and only if (3.8) holds and there exists a pair (m,h), $m \geq \max_{j=1,\dots,J} m_{0,j}$, $h \geq 1$ such that either

$$\boldsymbol{X}_t \ \text{is} \ \mathcal{S}1\mathcal{S}, \qquad \text{or,} \qquad \boldsymbol{X}_t \ \text{asymmetric and (3.6) holds for all sequences } (d_{j,k})_k.$$

If such a pair exists, then the process $\mathcal{X}_t$ is (m,h)-past-representable.

($\iota\iota$) Let $\|\cdot\|$ be a semi-norm satisfying (3.3) and assume that $\mathcal{X}_t$ is (m,h)-past-representable for some $m \geq 0$, $h \geq 1$. The spectral representation $(\Gamma^{\|\cdot\|}, \boldsymbol{\mu}^{\|\cdot\|})$ of the vector $\boldsymbol{X_t} = (\mathcal{X}_{t-m}, \dots, \mathcal{X}_t, \mathcal{X}_{t+1}, \dots, \mathcal{X}_{t+h})$ on $C_{m+h+1}^{\|\cdot\|}$ is given by:

$$\Gamma^{\|\cdot\|} = \sigma^\alpha \sum_{j=1}^{J} \sum_{\vartheta \in S_1} \sum_{k \in \mathbb{Z}} w_{j,\vartheta} \pi_j^\alpha \|\boldsymbol{d}_{j,k}\|^\alpha \delta_{\left\{ \frac{\vartheta \boldsymbol{d}_{j,k}}{\|\boldsymbol{d}_{j,k}\|} \right\}}, \tag{3.9}$$

$$\boldsymbol{\mu}^{\|\cdot\|} = \begin{cases} \mathbf{0}, & \text{if } \alpha \neq 1 \\ -\frac{2\sigma}{\pi} \sum_{j=1}^{J} \sum_{k \in \mathbb{Z}} \pi_j \beta_j \boldsymbol{d}_{j,k} \ln \|\sigma \pi_j \boldsymbol{d}_{j,k}\|, & \text{if } \alpha = 1 \end{cases} \tag{3.10}$$

where $\boldsymbol{d}_{j,k} = (d_{j,k+m}, \dots, d_{j,k}, d_{j,k-1}, \dots, d_{j,k-h})$, $w_{j,\vartheta} = (1 + \vartheta \beta_j)/2$, for any $k \in \mathbb{Z}$, $j = 1, \dots, J$, δ is the Dirac mass, $\vartheta \in S_1$ with $S_1 = \{-1, +1\}$, and if $\boldsymbol{d}_{j,k} = \mathbf{0}$, the term vanishes by convention from the sums.

The necessary condition (3.8) extends what was noticed in the Proposition 3 of de de Truchis et al. (2025a), namely, that anticipativeness is a minimal requirement for past-representability. Importantly,

notice that a single non-anticipative latent moving average is enough to render the aggregated process not past-representable, regardless of the other latent components. Also, for $\alpha \neq 1$, the past-representability of an aggregated process is equivalent to that of its latent moving averages, but this does not seem to hold in general for $\alpha = 1$. In the latter case however, if all the latent moving averages are symmetric, that is, $\beta_1 = \ldots = \beta_J = 0$, then the paths $\boldsymbol{X}_t$ are $\mathcal{S}1\mathcal{S}$ for any $m \geq 0$, $h \geq 1$ and $(\iota)(b)$ collapses to $(\iota)(a)$.

The representability condition also simplifies in the case of aggregated ARMA processes and requires each latent ARMA process to be anticipative.

Corollary 3.1. *For any $j = 1, \ldots, J$, let $(X_{j,t})$ be the ARMA strictly stationary solution of $\Psi_j(F)\Phi_j(B)X_{j,t} = \Theta_j(F)H_j(B)\varepsilon_{j,t}$, with mutually independent sequences $\varepsilon_{j,t} \overset{i.i.d.}{\sim} \mathcal{S}(\alpha, \beta_j, 1, 0)$. Define $\mathcal{X}_t = \sigma \sum_{j=1}^{J} \pi_j X_{j,t}$ for any positive weights π_j summing to 1 and $\sigma > 0$. Then, for any $\alpha \in (0, 2)$, $(\beta_1, \ldots, \beta_J) \in [-1, 1]^J$, the following statements are equivalent:*

(ι) *$(\mathcal{X}_t)$ is past-representable,*

$(\iota\iota)$ $\inf_j \deg(\Psi_j) \geq 1$,

$(\iota\iota\iota)$ $\sup_j m_{0,j} < +\infty$,

with the $m_{0,j}$'s as in (3.7). Moreover, letting $m \geq 0$, $h \geq 1$, the aggregated process $(\mathcal{X}_t)$ is (m, h)-past-representable if and only if for any $j = 1, \ldots, J$, $m_{0,j} < +\infty$, and $m \geq \max_j m_{0,j}$.

3.2. Tail conditional distribution of stable aggregates

Now, we derive the tail conditional distribution of linear stable aggregates. The case of a general past-representable stable aggregate is considered. We also pay a particular attention to the anticipative $\mathcal{G}\alpha\mathcal{S}$ AR(1) because to the best of our knowledge, no deconvolution estimation techniques exists for stable aggregates as defined in 2.1, except for the anticipative $\mathcal{G}\alpha\mathcal{S}$ AR(1) discussed in Section 2. To be relevant for the prediction framework, the Borel set B appearing in Equation 3.2 has to be chosen such that the conditioning event $\{\|\boldsymbol{X_t}\| > x\} \cap \{\boldsymbol{X_t}/\|\boldsymbol{X_t}\| \in B\}$ is independent of the future realisations $\mathcal{X}_{t+1}, \ldots, \mathcal{X}_{t+h}$. For $\|\cdot\|$ a semi-norm on $\mathbb{R}^{m+h+1}$ satisfying (3.3), denote $S_{m+1}^{\|\cdot\|} = \{(s_{-m}, \ldots, s_0) \in \mathbb{R}^{m+1} : \quad \|(s_{-m}, \ldots, s_0, 0, \ldots, 0)\| = 1\}$.[6] Then, for any Borel set $V \subset S_{m+1}^{\|\cdot\|}$, define the Borel set $B(V) \subset C_{m+h+1}^{\|\cdot\|}$ as

$$B(V) = V \times \mathbb{R}^h.$$

Notice in particular that for $V = S_{m+1}^{\|\cdot\|}$, we have $B(V) = C_{m+1}^{\|\cdot\|}$. In the following, we will use Borel sets of the above form to condition the distribution of the complete vector $\boldsymbol{X_t}/\|\boldsymbol{X_t}\|$ on the observed shape of the past trajectory. The latter information is contained in the Borel set V, which we will typically assume to be some small neighbourhood on $S_{m+1}^{\|\cdot\|}$. It will be useful in the following to notice that

$$V \times \mathbb{R}^h = \left\{ \boldsymbol{s} \in C_{m+h+1}^{\|\cdot\|} : \quad f(\boldsymbol{s}) \in V \right\},$$

[6] The set $S_{m+1}^{\|\cdot\|}$ corresponds to the unit sphere of $\mathbb{R}^{m+1}$ relative to the restriction of $\|\cdot\|$ to the first $m+1$ dimensions.

where f the function defined by

$$f : \begin{array}{ccc} \mathbb{R}^{m+h+1} & \longrightarrow & \mathbb{R}^{m+1} \\ (x_{-m}, \ldots, x_0, x_1, \ldots, x_h) & \longmapsto & (x_{-m}, \ldots, x_0) \end{array}. \tag{3.11}$$

Let $\mathcal{X}_t$ an α-stable aggregate as in Definition 2.1. Assume $\mathcal{X}_t$ is (m, h)-past-representable, for some $m \geq 0$, $h \geq 1$. Also, we know by Proposition 3.1 $(\iota\iota)$, that $\Gamma^{\|\cdot\|}$ is of the form

$$\Gamma^{\|\cdot\|} = \sigma^\alpha \sum_{j=1}^{J} \sum_{\vartheta \in S_1} \sum_{k \in \mathbb{Z}} w_{j,\vartheta} \pi_j^\alpha \|\boldsymbol{d}_{j,k}\|^\alpha \delta_{\left\{ \frac{\vartheta \boldsymbol{d}_{j,k}}{\|\boldsymbol{d}_{j,k}\|} \right\}}. \tag{3.12}$$

Proposition 3.2. *Let $\mathcal{X}_t$ be an α-stable aggregate as in Definition 2.1. Assume $\mathcal{X}_t$ is (m, h)-past-representable, for some $m \geq 0$, $h \geq 1$. Also, we know by Proposition 3.1 $(\iota\iota)$, that $\Gamma^{\|\cdot\|}$ is of the form*

$$\Gamma^{\|\cdot\|} = \sigma^\alpha \sum_{j=1}^{J} \sum_{\vartheta \in S_1} \sum_{k \in \mathbb{Z}} w_{j,\vartheta} \pi_j^\alpha \|\boldsymbol{d}_{j,k}\|^\alpha \delta_{\left\{ \frac{\vartheta \boldsymbol{d}_{j,k}}{\|\boldsymbol{d}_{j,k}\|} \right\}}. \tag{3.13}$$

Under the above assumptions, we have

$$\mathbb{P}_x^{\|\cdot\|}\Big(\boldsymbol{X_t}, A \Big| B(V)\Big) \underset{x \to +\infty}{\longrightarrow} \frac{\Gamma^{\|\cdot\|}\left(\left\{ \frac{\vartheta \boldsymbol{d}_{j,k}}{\|\boldsymbol{d}_{j,k}\|} \in A : \ \frac{\vartheta f(\boldsymbol{d}_{j,k})}{\|\boldsymbol{d}_{j,k}\|} \in V \right\} \right)}{\Gamma^{\|\cdot\|}\left(\left\{ \frac{\vartheta \boldsymbol{d}_{j,k}}{\|\boldsymbol{d}_{j,k}\|} \in C_{m+h+1}^{\|\cdot\|} : \ \frac{\vartheta f(\boldsymbol{d}_{j,k})}{\|\boldsymbol{d}_{j,k}\|} \in V \right\} \right)}, \tag{3.14}$$

for any Borel sets $A \subset C_{m+h+1}^{\|\cdot\|}$, $V \subset S_{m+1}^{\|\cdot\|}$ such that $\left\{ \frac{\vartheta \boldsymbol{d}_{j,k}}{\|\boldsymbol{d}_{j,k}\|} \in C_{m+h+1}^{\|\cdot\|} : \ \frac{\vartheta f(\boldsymbol{d}_{j,k})}{\|\boldsymbol{d}_{j,k}\|} \in V \right\} \neq \emptyset$, $\Gamma^{\|\cdot\|}\Big(\partial(A \cap B(V))\Big) = \Gamma^{\|\cdot\|}(\partial B(V)) = 0$, where $B(V) = V \times \mathbb{R}^h$ and f is as in (3.11).

Observe that setting $V = S_{m+1}^{\|\cdot\|}$, and A an arbitrarily small closed neighbourhood of all the points $(\vartheta \boldsymbol{d}_{j,k}/\|\boldsymbol{d}_{j,k}\|)_{\vartheta,j,k}$, as in the single-component case we have $\lim_{x \to +\infty} \mathbb{P}\Big(\boldsymbol{X_t}/\|\boldsymbol{X_t}\| \in A \Big| \|\boldsymbol{X_t}\| > x\Big) = 1$. In other terms, when far from central values, the trajectory of process (X_t) necessarily features patterns of the same shape as some $\vartheta \boldsymbol{d}_{j,k}/\|\boldsymbol{d}_{j,k}\|$, which is a finite piece of a moving average's coefficient sequence. The index j indicates from which of the J underlying moving averages the pattern stems from, the index k points to which piece $(d_{j,k+m}, \ldots, d_{j,k}, d_{j,k-1}, \ldots, d_{j,k-h})$ of this moving average it corresponds, and $\vartheta \in \{-1, +1\}$ indicates whether the pattern is flipped upside down (in case the extreme event is driven by a negative value of an error $(\varepsilon_{j,\tau})$). The likelihood of a pattern $\vartheta \boldsymbol{d}_{j,k}/\|\boldsymbol{d}_{j,k}\|$ can be evaluated by setting A to be a small neighbourhood of that point. In particular, only one pattern $\boldsymbol{d}_k/\|\boldsymbol{d}_k\|$ can appear through time for $J = 1$ (up to a time shift and sign flipping). This is no longer the case in general for $J \geq 2$, where the shape of each extreme event appears as if being drawn from a collection of patterns.

Interestingly, as in de Truchis et al. (2025a) in the non-aggregated case, the observed path $(\mathcal{X}_{t-m}, \ldots, \mathcal{X}_{t-1}, \mathcal{X}_t)/\|\boldsymbol{X_t}\|$ will *a fortiori* be of the same shape as some $\vartheta(d_{j,k+m}, \ldots, d_{j,k+1}, d_{j,k})/\|\boldsymbol{d}_{j,k}\|$

when an extreme event will approach in time. Observing the initial part of the pattern can give information about the remaining unobserved piece: the conditional likelihood of the latter can be assessed by setting V to be a small neighbourhood of the observed pattern. In practice, we anticipate that matching an observed path to a particular pattern j among the collection of J patterns will be challenging, even for a small number of latent components.

3.3. Example: stable aggregation of AR(1)

We now consider the aggregation of stable anticipative AR(1) processes discussed in Section 2. We assume without loss of generality that the ρ_j's are distinct. For each anticipative AR(1) with parameter ρ_j, the moving average coefficients are of the form $(\rho_j^k \mathbb{1}_{\{k\geq 0\}})_k$, and thus, $m_{0,j} = 0$ for all j, where the $m_{0,j}$'s are given in (3.7). By Corollary (3.1), we know for any $m \geq 0$, $h \geq 1$, the aggregated process $\mathcal{X}_t$ is (m,h)-past-representable. The spectral measures of paths $\boldsymbol{X}_t$ simplify and charge finitely many points. Their forms are given in the next lemma.

Lemma 3.3. *Let $\mathcal{X}_t$ be an aggregation of α-stable anticipative AR(1) processes as in Definition 2.1 with $d_{j,k} = \rho_j^k$ and general scale parameter $\sigma > 0$.*

Letting $\boldsymbol{X_t} = (\mathcal{X}_{t-m}, \dots, \mathcal{X}_t, \mathcal{X}_{t+1}, \dots, \mathcal{X}_{t+h})$ for $m \geq 0$, $h \geq 1$, its spectral measure on $C_{m+h+1}^{\|\cdot\|}$ for a seminorm satisfying (3.3) is given by

$$\Gamma^{\|\cdot\|} = \sum_{\vartheta\in S_1} \left[w_\vartheta \delta_{\{(\vartheta,0,\dots,0)\}} + \sum_{j=1}^{J} \sigma^\alpha \pi_j^\alpha \left(w_{j,\vartheta} \sum_{k=-m+1}^{h-1} \|\boldsymbol{d}_{j,k}\|^\alpha \delta_{\left\{\frac{\vartheta \boldsymbol{d}_{j,k}}{\|\boldsymbol{d}_{j,k}\|}\right\}} + \frac{\bar{w}_{j,\vartheta}}{1-|\rho_j|^\alpha} \|\boldsymbol{d}_{j,h}\|^\alpha \delta_{\left\{\frac{\vartheta\, \boldsymbol{d}_{j,h}}{\|\boldsymbol{d}_{j,h}\|}\right\}} \right) \right], \tag{3.15}$$

where for all $\vartheta \in S_1$, $j \in \{1,\dots,J\}$ and $-m+1 \leq k \leq h$,

$$\begin{aligned}
\boldsymbol{d}_{j,k} &= (\rho_j^{k+m}\mathbb{1}_{\{k\geq -m\}}, \dots, \rho_j^k \mathbb{1}_{\{k\geq 0\}}, \rho_j^{k-1}\mathbb{1}_{\{k\geq 1\}}, \dots, \rho_j^{k-h}\mathbb{1}_{\{k\geq h\}}),\\
w_{j,\vartheta} &= (1+\vartheta\beta_j)/2,\\
w_\vartheta &= \sum_{j=1}^{J} \sigma^\alpha \pi_j^\alpha w_{j,\vartheta},\\
\bar{w}_{j,\vartheta} &= (1+\vartheta\bar{\beta}_j)/2,\\
\bar{\beta}_j &= \beta_j \frac{1-\rho_j^{<\alpha>}}{1-|\rho_j|^\alpha},
\end{aligned}$$

and if $h = 1$ and $m = 0$, the sum $\sum_{k=-m+1}^{h-1}$ vanishes by convention.

The next proposition provides the tail conditional distribution of future paths in the case where the ρ_j's are positive. Let us first introduce useful neighbourhoods of the distinct charged points of $\Gamma^{\|\cdot\|}$. Denote $\boldsymbol{d}_{0,-m} = (\overbrace{1,0,\dots,0}^{m+h+1})$ so that the charged points of $\Gamma^{\|\cdot\|}$ are all of the form $\vartheta \boldsymbol{d}_{j,k}/\|\boldsymbol{d}_{j,k}\|$ with indexes (ϑ, j, k)

in the set $\mathcal{I} := S_1 \times \Big(\{1,\dots,J\}\times\{-m,h\}\cup\{(0,-m)\}\Big)$. With f as in (3.11), define for any $(\vartheta_0,j_0,k_0)\in\mathcal{I}$, the set V_0 as any closed neighbourhood of $\vartheta_0 f(\boldsymbol{d}_{j_0,k_0})/\|\boldsymbol{d}_{j_0,k_0}\|$ such that

$$\forall(\vartheta',j',k')\in\mathcal{I},\qquad \frac{\vartheta' f(\boldsymbol{d}_{j',k'})}{\|\boldsymbol{d}_{j',k'}\|}\in V_0 \quad\Longrightarrow\quad \frac{\vartheta' f(\boldsymbol{d}_{j',k'})}{\|\boldsymbol{d}_{j',k'}\|}=\frac{\vartheta_0 f(\boldsymbol{d}_{j_0,k_0})}{\|\boldsymbol{d}_{j_0,k_0}\|}, \tag{3.16}$$

In other terms, $V_0\times\mathbb{R}^d$ is a subset of $C^{\|\cdot\|}_{m+h+1}$ in which the only points charged by $\Gamma^{\|\cdot\|}$ all have the first $(m+1)^{\text{th}}$ coinciding with $\vartheta_0 f(\boldsymbol{d}_{j_0,k_0})/\|\boldsymbol{d}_{j_0,k_0}\|$. Define also $A_{\vartheta,j,k}$ for any (ϑ,j,k) as any closed neighbourhood of $\vartheta\boldsymbol{d}_{j,k}/\|\boldsymbol{d}_{j,k}\|$ which does not contain any other charged point of $\Gamma^{\|\cdot\|}$, that is,

$$\forall(\vartheta',j',k')\in\mathcal{I},\qquad \frac{\vartheta'\boldsymbol{d}_{j',k'}}{\|\boldsymbol{d}_{j',k'}\|}\in A_{\vartheta,j,k} \quad\Longrightarrow\quad (\vartheta',j',k')=(\vartheta,j,k). \tag{3.17}$$

Proposition 3.3. *Let $\mathcal{X}_t$ be an aggregation of α-stable anticipative AR(1) processes as in Definition 2.1 with $d_{j,k}=\rho_j^k\in(0,1)$ for all j's.,Let $\boldsymbol{X_t}$, the $\boldsymbol{d}_{j,k}$'s and the spectral measure of $\boldsymbol{X_t}$ be as given in Lemma 3.3, for any $m\geq 0$, $h\geq 1$. Let V_0 be any small closed neighbourhood of $\vartheta_0 f(\boldsymbol{d}_{j_0,k_0})/\|\boldsymbol{d}_{j_0,k_0}\|$ in the sense of (3.16) for some $(\vartheta_0,j_0,k_0)\in\mathcal{I}$ and let $B(V_0)=V_0\times\mathbb{R}^h$. Then, with $A_{\vartheta,j,k}$ an arbitrarily small neighbourhood of some $\vartheta\boldsymbol{d}_{j,k}/\|\boldsymbol{d}_{j,k}\|$ as in (3.17), the following hold.*

(ι) ***Case** $m\geq 1$.*

(a) *If $0\leq k_0\leq h$:*

$$\mathbb{P}_x^{\|\cdot\|}\Big(\boldsymbol{X_t},A_{\vartheta,j,k}\Big|B(V_0)\Big)\underset{x\to\infty}{\longrightarrow}\begin{cases}|\rho_{j_0}|^{\alpha k}(1-|\rho_{j_0}|^\alpha)\delta_{\vartheta_0}(\vartheta)\delta_{j_0}(j), & 0\leq k\leq h-1,\\ |\rho_{j_0}|^{\alpha h}\delta_{\vartheta_0}(\vartheta)\delta_{j_0}(j), & k=h.\end{cases}$$

(b) *If $-m\leq k_0\leq -1$:*

$$\mathbb{P}_x^{\|\cdot\|}\Big(\boldsymbol{X_t},A_{\vartheta,j,k}\Big|B(V_0)\Big)\underset{x\to\infty}{\longrightarrow}\delta_{\vartheta_0}(\vartheta)\delta_{j_0}(j)\delta_{k_0}(k).$$

($\iota\iota$) ***Case** $m=0$.*

$$\mathbb{P}_x^{\|\cdot\|}\Big(\boldsymbol{X_t},A_{\vartheta,j,k}\Big|B(V_0)\Big)\underset{x\to\infty}{\longrightarrow}\begin{cases}\dfrac{\sum_{i=1}^J\pi_i^\alpha w_{i,\vartheta_0}}{\sum_{i=1}^J p_{i,\vartheta_0}}\delta_{\{\vartheta_0\}}(\vartheta), & k=0\\ \dfrac{p_{j,\vartheta_0}}{\sum_{i=1}^J p_{i,\vartheta_0}}|\rho_j|^{\alpha k}(1-|\rho_j|^\alpha)\delta_{\{\vartheta_0\}}(\vartheta), & 1\leq k\leq h-1,\\ \dfrac{p_{j,\vartheta_0}}{\sum_{i=1}^J p_{i,\vartheta_0}}|\rho_j|^{\alpha h}\delta_{\{\vartheta_0\}}(\vartheta), & k=h,\end{cases}$$

with $p_{j,\vartheta_0}=\pi_j^\alpha w_{j,\vartheta_0}/(1-|\rho_j|^\alpha)$.

For $m\geq 1$, that is, if the observed path is assumed to be of length at least 2, there is a significant difference between whether $k_0\in\{0,\dots,h\}$ or $k_0\in\{-m,\dots,-1\}$. For the latter, the asymptotic probability of the

whole path $\boldsymbol{X_t}/\|\boldsymbol{X_t}\|$ being in an arbitrarily small neighbourhood of $\vartheta \boldsymbol{d}_{j,k}/\|\boldsymbol{d}_{j,k}\|$ is 1 if and only if $\vartheta = \vartheta_0$, $j = j_0$, $k = k_0$: given the observed path, the shape of the future trajectory is fully determined. For the former, this probability is strictly positive if and only if $\vartheta = \vartheta_0$ and $j = j_0$, but the observed pattern is compatible with several distinct future paths. One can see why this is the case from the form of the sequences $\boldsymbol{d}_{j,k}/\|\boldsymbol{d}_{j,k}\|$ and of their restrictions to the first $m+1$ components $f(\boldsymbol{d}_{j,k})/\|\boldsymbol{d}_{j,k}\|$. On the one hand (omitting ϑ),

$$\frac{\boldsymbol{d}_{j,k}}{\|\boldsymbol{d}_{j,k}\|} = \begin{cases} \dfrac{(\overbrace{\rho_j^{k+m}, \ldots, \rho_j^{k}}^{m+1}, \overbrace{\rho_j^{k-1}, \ldots, \rho_j, 1, 0, \ldots, 0}^{h})}{\|(\rho_j^{k+m}, \ldots, \rho_j^{k}, \rho_j^{k-1}, \ldots, \rho_j, 1, 0, \ldots, 0)\|}, & \text{for} \qquad k \in \{0, \ldots, h\}, \\ \dfrac{(\rho_j^{k+m}, \ldots, \rho_j, 1, 0, \ldots, 0, 0, \ldots, 0)}{\|(\underbrace{\rho_j^{k+m}, \ldots, \rho_j, 1, 0, \ldots, 0}_{m+1}, \underbrace{0, \ldots, 0}_{h})\|}, & \text{for} \qquad k \in \{-m, \ldots, -1\}. \end{cases}$$

We can notice that all the above sequences are pieces of explosive exponentials, terminated at some coordinate. For $k \in \{0, \ldots, h\}$, the first zero component, i.e. the crash of the bubble, is situated at or after the $(m+2)^{\text{th}}$ component, whereas for $k \in \{-m, \ldots, -1\}$, it is situated at or before the $(m+1)^{\text{th}}$. Using the homogeneity of the semi-norm, we have on the other hand that

$$\frac{f(\boldsymbol{d}_{j,k})}{\|\boldsymbol{d}_{j,k}\|} = \begin{cases} \dfrac{(\overbrace{\rho_j^{m}, \ldots, \rho_j, 1}^{m+1})}{\|(\underbrace{\rho_j^{m}, \ldots, \rho_j, 1}_{m+1}, \underbrace{0, \ldots, 0, 0, \ldots, 0}_{h})\|}, & \text{for} \qquad k \in \{0, \ldots, h\}, \\ \dfrac{(\overbrace{\rho_j^{k+m}, \ldots, \rho_j, 1, 0, \ldots, 0}^{m+1})}{\|(\underbrace{\rho_j^{k+m}, \ldots, \rho_j, 1, 0, \ldots, 0}_{m+1}, \underbrace{0, \ldots, 0}_{h})\|}, & \text{for} \qquad k \in \{-m, \ldots, -1\}. \end{cases}$$

Thus, conditioning the trajectory on the event $\{f(\boldsymbol{X_t})/\|\boldsymbol{X_t}\| \approx f(\boldsymbol{d}_{j_0,k_0})/\|\boldsymbol{d}_{j_0,k_0}\|\}$ for some $k_0 \in \{-m, \ldots, -1\}$ amounts to condition on the burst of a bubble being observed in the past trajectory with no new bubble forming yet, which allows to identify exactly the position of the pattern on the j^{th} moving average's coefficient sequence.

When conditioning with $k_0 \in \{0, \ldots, h\}$ however, the crash date is not observed and can happen either in the next $h-1$ periods, or after the h^{th}. However, the shape of the observed path is that of a piece of exponential with growth rate ρ_j^{-1} regardless of the remaining time before the burst, which leaves several future paths possible. One can quantify the likelihood of each potential scenario: the quantity $|\rho_j|^{\alpha k}(1-|\rho_j|^{\alpha})$ corresponds to the probability that the bubble will peak in exactly k periods ($0 \leq k < h$), and $|\rho_j|^{\alpha h}$ corresponds to the probability that the bubble will last at least h more periods.

The previous statement confirms the interpretation of the conditional moments proposed in Fries (2022) for the stable anticipative AR(1) case ($J = 1$). It also extends it in two ways:

(ι) by accounting for paths rather than point prediction,

($\iota\iota$) by showing that the aggregation of AR(1) processes also features killed exponential explosive episodes but with various growth rates and crash probabilities.

Proposition 3.3 furthermore shows that asymptotically, as few as two observations are sufficient to identify the growth rate ρ_j^{-1} of an ongoing extreme episode,[7] and the conditional dynamics within this given event will be similar to that of a simple AR(1) with corresponding parameter. An identification of the growth rate in the early developments of the bubble appears possible, allowing to infer in advance the odds of crashes.

4. Monte-Carlo Simulation

This section presents Monte Carlo evidence on the performance of the estimation method for α-stable moving average aggregates introduced in Section 2. We evaluate the estimator's ability to recover the true parameters under various specifications, focusing on the case where the observed process is generated by the aggregation of two independent α-stable AR(1) processes. We generate samples according to the model

$$\mathcal{X}_t = \pi_1 X_{1,t} + \pi_2 X_{2,t} \tag{4.1}$$

$$X_{j,t} = \rho_j X_{j,t-1} + \varepsilon_{j,t}, \quad \varepsilon_{j,t} \overset{i.i.d.}{\sim} \mathcal{S}(\alpha, \beta, 1, 0) \tag{4.2}$$

where $j \in \{1, 2\}$ and $\rho_j \in (0, 1)$. We fix $\sigma = 1.6$, $\pi_1 = 7/16$ and $\pi_2 = 9/16$ for the weights of the mixture in all scenarios. Recall that we alleviate the optimization problem by estimating the combined parameters $\varsigma_j = \sigma \times \pi_j$ for $j = 1, \ldots, J$, thereby leading to $\varsigma_1 = \sigma \times \pi_1 = 0.7$ and $\varsigma_2 = \sigma \times \pi_2 = 0.9$. We examine three specific cases:

1. Cauchy distribution ($\mathcal{S}1\mathcal{S}$): $\alpha = 1$ and $\beta = 0$
2. Symmetric α-stable ($\mathcal{S}\alpha\mathcal{S}$) distribution: general α with $\beta = 0$
3. General α-stable ($\mathcal{G}\alpha\mathcal{S}$) distribution: general α with $\beta \neq 0$

For each case, we perform simulations with sample sizes of $T = \{250, 500, 1000\}$, each with 1,000 replications. The parameters are estimated using the minimum distance estimator based on the empirical characteristic function as described in Section 2, uniform weights and grids for u and v defined as 10 equally spaced points in $[-0.5, 0.5]$. One could achieve higher efficiency by computing optimal weights but we do not explore further this issue.

[7] This holds asymptotically in the (semi-)norm of the observed path, but in practice it can be expected that the noise surrounding the trajectory will make this identification difficult with only two observations. Longer path lengths (higher m) may provide robustness to the identification, but could also incorporate some bias by taking into account past extreme events, such as now-collapsed bubbles. One can suspect a bias-variance trade-off when searching for an optimal choice of m.

In the $\mathcal{S}1\mathcal{S}$ scenario, both components share the Cauchy distribution restrictions. Table 1 presents the bias, the root mean square error (RMSE) and the mean relative error (MRE) for this scenario.

Table 1: Monte Carlo Results for $\mathcal{S}1\mathcal{S}$ AR(1) Aggregates

		$T = 250$			$T = 500$			$T = 1000$		
θ	True Value	Bias	RMSE	MRE	Bias	RMSE	MRE	Bias	RMSE	MRE
ρ_1	0.800	-0.008	0.050	0.046	-0.004	0.030	0.029	-0.002	0.020	0.019
ς_1	0.700	-0.023	0.322	0.368	0.002	0.249	0.275	-0.002	0.179	0.196
ρ_2	0.300	-0.035	0.169	0.455	-0.025	0.128	0.333	-0.012	0.089	0.223
ς_2	0.900	-0.035	0.279	0.249	-0.015	0.193	0.171	-0.007	0.134	0.119

The estimation of $\mathcal{S}1\mathcal{S}$ AR(1) aggregates demonstrates promising results across all parameters. For smaller sample sizes of $T = 250$, the estimator already shows good performance with a moderate bias (-0.008) and RMSE (0.050) for ρ_1, though the MRE is slightly higher at 4.6%. For the largest coefficient ρ_1, the results figures out negligible bias (-0.001), low RMSE (0.035), and MRE of only 3.5% for $T = 500$. These results further improve with the larger sample size, where the MRE decreases to 2.6% for $T = 1000$. The combined parameter ς_1 exhibits higher estimation uncertainty with an RMSE of 0.322 and MRE of 36.8% for $T = 250$, which improves to an RMSE of 0.201 and MRE of 22.7% for $T = 500$, and further to 0.147 and 16.9%, respectively, for $T = 1000$. The smallest autoregressive coefficient ρ_2 appears slightly more challenging to estimate, showing the highest mean relative error among all parameters (45.5% for $T = 250$, 34.8% for $T = 500$ and 26.6% for $T = 1000$). Importantly, the consistent reduction in RMSE and MRE from $T = 250$ to $T = 500$ to $T = 1000$ across all parameters confirms that the estimator behaves well in finite sample.

We now consider the $\mathcal{S}\alpha\mathcal{S}$ case with $\beta = 0$ and $\alpha = 1.5$. The true autoregressive and scale parameters remain the same as in the Cauchy case. The results are reported in Table 2. The results for $\mathcal{S}\alpha\mathcal{S}$ AR(1) aggregates reveal interesting patterns. Compared to the Cauchy case, all parameters show higher RMSE and mean relative errors, suggesting that estimation becomes more challenging when adding the identification of α. With small samples of $T = 250$, we observe a notable positive bias (0.013) for ρ_1 with RMSE of 0.081 and MRE of 7.3%, while ρ_2 shows substantial bias (-0.127) and MRE (60.0%). For the autoregressive coefficient ρ_1, the RMSE improves to 0.079 (compared to 0.035 in the Cauchy case) for $T = 500$, with a MRE of 7.8%. Similarly, ς_1 shows a substantial increase in estimation uncertainty, with RMSE of 0.276 and MRE of 33.0%. The parameter ρ_2 continues to exhibit the highest MRE (47.4%), indicating persistent challenges in its estimation. A notable result is the high precision in estimating the tail index α, with a small bias (-0.037) and MRE of 8.6% even at $T = 250$, improving to a bias of 0.015, relatively low RMSE (0.123), and

MRE of only 6.6% for $T = 500$. This improves further for $T = 1000$, with the MRE decreasing to 5.0%. The accurate estimation of α is crucial for practical applications, as it characterizes the heaviness of the tails of the distribution and it impact the identification of all other parameters. The increase in sample size from $T = 250$ to $T = 500$ to $T = 1000$ leads to consistent improvements in all estimation metrics for most parameters, though the magnitude of improvement varies across parameters. This confirms the good finite sample properties of the estimator when departing from the Cauchy and extending Gouriéroux and Zakoian (2017).

Table 2: Monte Carlo Results for $\mathcal{S}\alpha\mathcal{S}$ AR(1) Aggregates with $\alpha = 1.5$

		$T = 250$			$T = 500$			$T = 1000$		
θ	True Value	Bias	RMSE	MRE	Bias	RMSE	MRE	Bias	RMSE	MRE
ρ_1	0.800	0.013	0.081	0.073	0.000	0.062	0.057	-0.005	0.046	0.044
ς_1	0.700	-0.101	0.276	0.325	-0.021	0.216	0.247	0.019	0.168	0.195
ρ_2	0.300	-0.127	0.209	0.600	-0.096	0.190	0.529	-0.072	0.148	0.391
ς_2	0.900	-0.124	0.235	0.212	-0.098	0.197	0.175	-0.071	0.153	0.135
α	1.500	-0.037	0.173	0.086	-0.014	0.127	0.065	-0.004	0.088	0.046

Finally, Table 3 presents the estimation results for the $\mathcal{G}\alpha\mathcal{S}$ AR(1) aggregates with both $\alpha = 1.5$ and $\beta = 0.3$. The estimation of $\mathcal{G}\alpha\mathcal{S}$ AR(1) aggregates introduces additional challenges due to the non-zero asymmetry parameter β. At the smallest sample size of $T = 250$, the estimator already displays some stability with a slight negative bias (-0.005) for ρ_1, though with higher RMSE (0.091) and MRE (8.4%) compared to simpler specifications. The autoregressive coefficient ρ_1 shows a positive bias (0.006) for $T = 500$, unlike the negative biases observed in the previous cases. Its RMSE (0.097) and MRE (9.6%) are higher than both the Cauchy and SαS cases, indicating increased estimation difficulty. The parameter ρ_2 continues to be the most challenging among the autoregressive and scale parameters, with a substantial negative bias (-0.089) and high mean relative error (59.4%) for $T = 250$, improving slightly with a negative bias (-0.075), high RMSE (0.193), and MRE of 53.6% for $T = 500$. The combined parameters ς_1 and ς_2 also exhibit considerable estimation uncertainty. Despite these challenges, the tail index α is estimated with remarkable precision even at $T = 250$ with a small bias (-0.026), RMSE of 0.164, and MRE of 8.3%, improving to a minimal bias (-0.006), RMSE of 0.116, and MRE of just 6.2% for $T = 500$. This reinforces the robustness of the estimator in recovering the tail behavior even in more complex settings. As expected, the asymmetry parameter β proves to be the most difficult to estimate, with a MRE of 62.8% for $T = 250$ and 56.3% for $T = 500$. While this improves to 37.4% for $T = 1000$, it remains substantially higher than the other parameters, highlighting the intrinsic difficulty in capturing the asymmetry in stable distributions.

Fortunately, identification of AR and scales parameters do not depend on β meaning that this lack of precision is not detrimental if one is not crucially interested in measuring accurately the asymmetry.

Table 3: Monte Carlo Results for $\mathcal{G}\alpha\mathcal{S}$ AR(1) Aggregates with $\alpha = 1.5$, $\beta = 0.3$

		$T = 250$			$T = 500$			$T = 1000$		
θ	True Value	Bias	RMSE	MRE	Bias	RMSE	MRE	Bias	RMSE	MRE
ρ_1	0.800	-0.005	0.091	0.084	-0.015	0.073	0.069	-0.013	0.057	0.055
ς_1	0.700	-0.054	0.285	0.335	0.013	0.234	0.278	0.026	0.200	0.236
ρ_2	0.300	-0.089	0.208	0.594	-0.068	0.186	0.510	-0.052	0.146	0.388
ς_2	0.900	-0.124	0.234	0.211	-0.115	0.205	0.179	-0.092	0.178	0.154
α	1.500	-0.026	0.164	0.083	-0.009	0.120	0.060	-0.003	0.082	0.042
β	0.300	-0.007	0.262	0.628	-0.003	0.186	0.457	-0.001	0.132	0.328

5. Application to financial markets

To illustrate the empirical relevance of our estimator and forecasting theoretical results, we apply them to financial data. In particular, we focus on the CBOE Crude Oil ETF Volatility Index (OVX) as it reflects, by essence, the market's anticipation regarding the volatility of crude oil ETF prices over the next 30 days. In that sense, it aggregates all sources of investors' expectations and this explains why VIX indexes are often referred to as *fear indices*. In the traditional theoretical foundation of the efficient markets hypothesis, agents are homogeneous and make rational use of all relevant information in their trading decisions, thereby leading to perfectly random movement of prices. However, a large body of the financial literature has identified various anomalies calling for heterogeneous agent models and in particular the so-called fundamentalist/chartist dichotomy (e.g. Agliari et al. , 2018). These two types of agents are likely to generate distinct dynamics in the crude oil volatility index, in particular when market fear is growing.

We collect the CBOE OVX index retrieved from the FRED (Federal Reserve Bank of St. Louis) website. The dataset, ranging from 23/05/2015 to 23/05/2025, is sampled at weekly frequency ($T = 522$) and linearly detrended to avoid high-frequency noise contamination (see Hecq and Voisin , 2021, for a discussion on the pre-treatment of data). We estimate three different models as described in Section 4, with initial guess obtained from the sequential estimation approach proposed by de Truchis et al. (2025b): a general α-stable model with asymmetry ($\mathcal{G}\alpha\mathcal{S}$), a symmetric α-stable model ($\mathcal{S}\alpha\mathcal{S}$), and a symmetric Cauchy model ($\mathcal{S}1\mathcal{S}$).

The results in Table 4 reveal several compelling patterns about the dynamics of the OVX index. First, the $\mathcal{G}\alpha\mathcal{S}$ specification provides strong evidence of anticipative dynamics, as demonstrated by the highly significant AR coefficients (with estimated values of $\rho_1 = 0.80$ and $\rho_2 = 0.85$). We observe a clear distinction

Table 4: Estimation results for OVX index with three different specifications

	$\mathcal{G}\alpha\mathcal{S}$			$\mathcal{S}\alpha\mathcal{S}$			$\mathcal{S}1\mathcal{S}$		
$\widehat{\theta}$	Estimate	Std.	t-stats	Estimate	Std.	t-stats	Estimate	Std.	t-stats
ρ_1	0.7989	0.0673	11.862	0.2507	0.0077	32.477	0.9226	0.0082	112.824
ρ_2	0.8470	0.0668	12.678	0.9865	0.0040	244.560	0.9346	0.0074	126.404
α	1.4686	0.0995	14.764	1.2405	0.0084	147.613	–	–	–
β	-0.1275	0.0684	-1.863	–	–	–	–	–	–
σ	2.0932	0.2400	8.723	0.8964	0.0212	42.226	0.1966	0.0294	6.692
π_1	0.2790	0.0403	6.930	0.8915	0.0052	171.084	0.5029	0.0511	9.833
π_2	0.7210	0.0409	17.622	0.1085	0.0182	5.957	0.4971	0.0545	9.121

between the two latent components: the first component ($\rho_1 = 0.80$) exhibits a slightly less persistent but still strong bubble pattern, while the second component ($\rho_2 = 0.85$) captures more persistent explosive episodes. The weights associated with each component show an asymmetric pattern, with $\pi_1 = 0.28$ and $\pi_2 = 0.72$, indicating a strong dominance of the second, more persistent component in the overall dynamics of crude oil volatility expectations.

Second, the estimated tail index parameter $\alpha = 1.47$ confirms the presence of heavy tails that significantly exceed what a Gaussian distribution would accommodate, reflecting the extreme nature of oil market volatility. The asymmetry parameter in the $\mathcal{G}\alpha\mathcal{S}$ specification is estimated at $\beta = -0.13$, with a t-statistic of -1.86, suggesting a lack of significance at 5% risk level.

Third, while the $\mathcal{S}\alpha\mathcal{S}$ model yields statistically significant parameter estimates, it shows a markedly different parameter structure with $\alpha = 1.24$ and very different AR coefficients ($\rho_1 = 0.25$, $\rho_2 = 0.99$), suggesting that the asymmetry, albeit probably not really significant, numerically plays a non-negligible role in the model specification. The $\mathcal{S}1\mathcal{S}$ (Cauchy) model, with its restriction of $\alpha = 1$, appears overly restrictive given the estimated α values in the more flexible models, though it still yields highly significant parameter estimates with $\rho_1 = 0.92$ and $\rho_2 = 0.93$.

To better visualize how each component captures distinct anticipative dynamics, we implement the deconvolution methodology proposed in de Truchis et al. (2025b) designed for extracting stable latent components. Our implementation employs a dual Markov-chain Monte-Carlo filtering approach with 2,000 particles over a 5-period rolling window. Figure 2 presents the results, revealing a clear demarcation in the roles of the two latent components. The dramatic spikes observed during periods of oil market turbulence are captured by both components, with the first component (middle panel), characterized by its slightly lower persistence coefficient ($\widehat{\rho}_1 = 0.80$), capturing more abrupt movements, while the second component

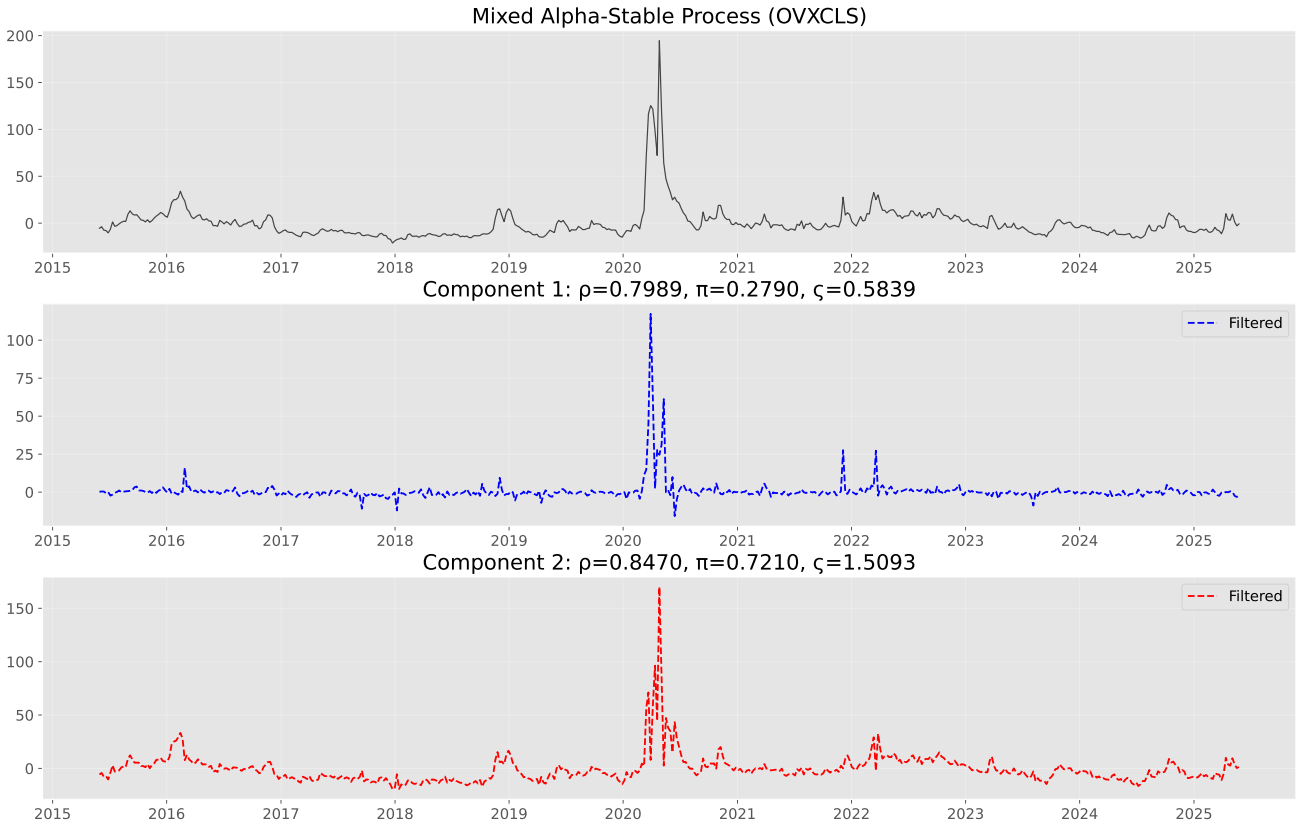

Figure 2: Deconvolution of the OVX index from the $\mathcal{G}\alpha\mathcal{S}$ two components model filtrated using de Truchis et al. (2025b)

(bottom panel), with its higher persistence ($\widehat{\rho}_2 = 0.85$), tracks the more sustained explosive patterns that characterize prolonged periods of oil market uncertainty.

Notably, the visualization reveals that periods of high oil market volatility can occasionally feature a superposition of two distinct bubble dynamics working simultaneously, with their combined effect visible in the observed index (top panel). The recent volatility episodes visible in the sample demonstrate how both components contribute to different aspects of oil market fear, with the first component providing rapid responses to immediate shocks and the second component maintaining longer-term market anxiety. This filtration-based visualization proves invaluable for matching observed market trajectories to specific $\mathbf{d}_{j,k}$ patterns among the collection generated by the latent components, thereby enhancing our ability to apply the forecasting theory developed in Section 3.

To illustrate our forecasting framework in practice, we conduct an in-sample prediction exercise for the 2020 oil market disruption event characterized by the significant volatility spike observed in the OVX index during the COVID-19 pandemic and the oil price war. Setting January 2020 as our cutoff point, we apply our methodology to forecast the subsequent crash dates for each of the identified latent components. Our approach is fundamentally based on pattern recognition, exploiting the theoretical finding that during extreme events, trajectories adhere to specific patterns characterized by the normalized form $\vartheta\mathbf{d}_{j,k}/|\mathbf{d}_{j,k}|$. These pattern structures are defined by four essential elements: the shape derived from the coefficient sequence $\mathbf{d}_{j,k}$; the component index $j \in \{1, \ldots, J\}$ identifying which latent process is driving the event; the time shift $k_0 \in \mathbb{Z}$ indicating the position within the pattern; and the sign $\vartheta \in \{-1, +1\}$ reflecting upward or downward movements. Our prediction strategy implements a systematic four-step algorithm. First, we observe the initial segment of an emerging extreme event. Second, we match this observed trajectory to the collection of theoretical patterns derived from our estimated stable aggregate model, conditioning on an $m + 1$ length of observed trajectory, thereby determining k_0. Third, we compute conditional probabilities for future trajectories using Proposition 3.2, which provides the mathematical foundation for calculating tail conditional distributions. Finally, we generate forecasts for the remaining trajectory based on these probabilistic assessments.

Table 5 presents the in-sample bubble forecast prediction probabilities derived from our empirical application. Each component generates a finite collection of potential patterns that an extreme event might follow. Proposition 3.3 provides explicit formulas for calculating the conditional probabilities of future trajectories given an observed pattern. The length of the trajectory segment that we use for pattern matching for each component is $m = 20$. For a bubble identified as originating from component j_0 (see Figure 2), our model provides precise probabilistic forecasts of its future trajectory. The probability of the bubble crashing in exactly k periods is given by $|\rho_{j_0}|^{\alpha k}(1 - |\rho_{j_0}|^{\alpha})$, while the probability of the bubble surviving at least h periods is $|\rho_{j_0}|^{\alpha h}$. These probabilities correspond directly to the columns labeled "Crash at h" and "Survive at h" in Table 5 for each component. Furthermore, the growth rate of the bubble is determined by

$\rho_{j_0}^{-1}$, which allows for trajectory forecasting once the component is identified. These forecasted values are presented in the "Forecast" column of Table 5.

As shown in Table 5, for $j_0 = 1$, we identify $k_0 = 3$, which means that from the start date through the third period, the crash has not yet occurred with certainty. Consequently, computing crash and survival probabilities for these early periods is not meaningful as the probability of a crash during this period is effectively zero. Only beginning in the fourth period do the crash probabilities become relevant, as this represents the earliest possible point at which the bubble could collapse according to our identified pattern structure. For $j_0 = 2$, with $k_0 = 1$, we observe that crash probabilities become relevant immediately in the second period, reflecting the more immediate nature of bubbles generated by this component despite its higher persistence.

A critical element in our forecasting framework is the risk threshold parameter (set to 99% in Table 5), which allows practitioners to customize predictions according to their risk tolerance. Specifically, analysts using our procedure can select an acceptable probability threshold, such as 90%, to determine when a bubble is likely to crash. When the cumulative crash probability $P(\text{crash within } k \text{ periods}) = 1 - |\rho_{j_0}|^{\alpha k}$ exceeds this threshold, the model predicts a crash; otherwise, it anticipates continued growth. This flexibility in threshold selection creates a natural trade-off: higher thresholds (e.g., 99%) generate more extreme bubble projections before predicting a crash, while lower thresholds (e.g., 90%) produce more conservative forecasts with earlier predicted crash points. Figures 3 and 4 illustrate how this risk threshold impact the forecast accuracy. For a comprehensive Monte Carlo study of the performance of this approach and its sensitivity to the four key parameters, we direct the reader to the Monte Carlo simulation section of de Truchis et al. (2025a).

In Table 5, we observe distinct predicted dynamics between the two latent components. The first component ($k_0 = 3$) suggests a gradual bubble formation with forecast values escalating from 11.27 at the start to 208.73. However, with a relatively higher growth rate, this bubble collapses in the 14th period (when using a 99% acceptable probability risk threshold). Conversely, the second component ($k_0 = 1$) suggests rapid build-up in crash probabilities. But with a relatively lower growth rate and probabilities reaching 0.22 by the second period and exceeding 0.99 by the 19th period, this bubble exhibits a more sustained but ultimately explosive episode that reaches higher absolute forecast values before crashing.

Finally, Figure 5 presents the combined forecast results at the 99% risk threshold, demonstrating the practical implementation of our stable aggregate forecasting framework on the OVX index. The methodology successfully captures the explosive trajectory leading to the March 2020 volatility spike, with the combined forecast (red dashed line) closely tracking the realized path during the critical period. The identification of the historical theoretical pattern (green line) starting in late 2019 provides the foundation for the forecast, which accurately predicts both the timing and magnitude of the subsequent market disruption. Notably, the combined forecast from both components generates a trajectory that reaches approximately 220 before the

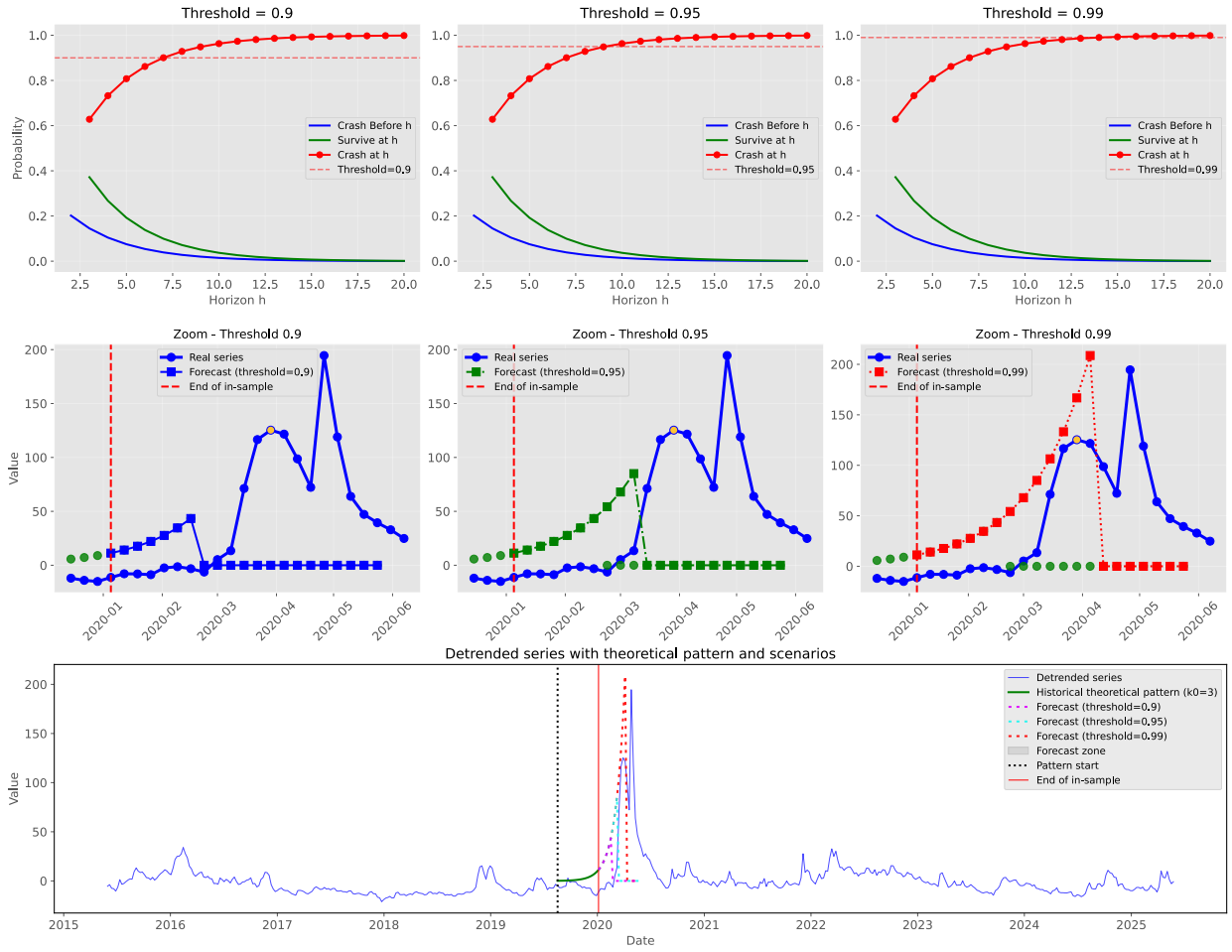

Figure 3: Forecast of the 2020 oil market bubble using the first component ($\hat{\rho}_1 = 0.7989$) from the OVX index filtration. The top row displays crash probability profiles across three different acceptable probability risk thresholds: 0.9 (left), 0.95 (center), and 0.99 (right). Each panel shows the probability of crashing at a given date (red line with circles), surviving beyond that date (green line), the cumulative crash probability up to that date (blue line), and the respective threshold value (horizontal dashed red line). The middle row presents zoomed-in forecasts for each threshold value, showing the real time series (blue line with circles) and the forecasted values (colored squares) that continue until the crash is predicted to occur according to each threshold. The vertical dashed red line indicates the end of the in-sample period (January 2020). The bottom panel situates these forecasts within the complete time series (blue line), with the historical theoretical pattern ($k_0 = 3$) shown in green. The colored lines represent forecasts for different threshold values: 0.9 (yellow), 0.95 (green dashed), and 0.99 (red dashed). The vertical black dotted line marks the pattern start, the vertical red dotted line indicates the end of the in-sample period, and the shaded gray area represents the forecast zone. The length of the trajectory segment used for pattern matching is $m = 20$.

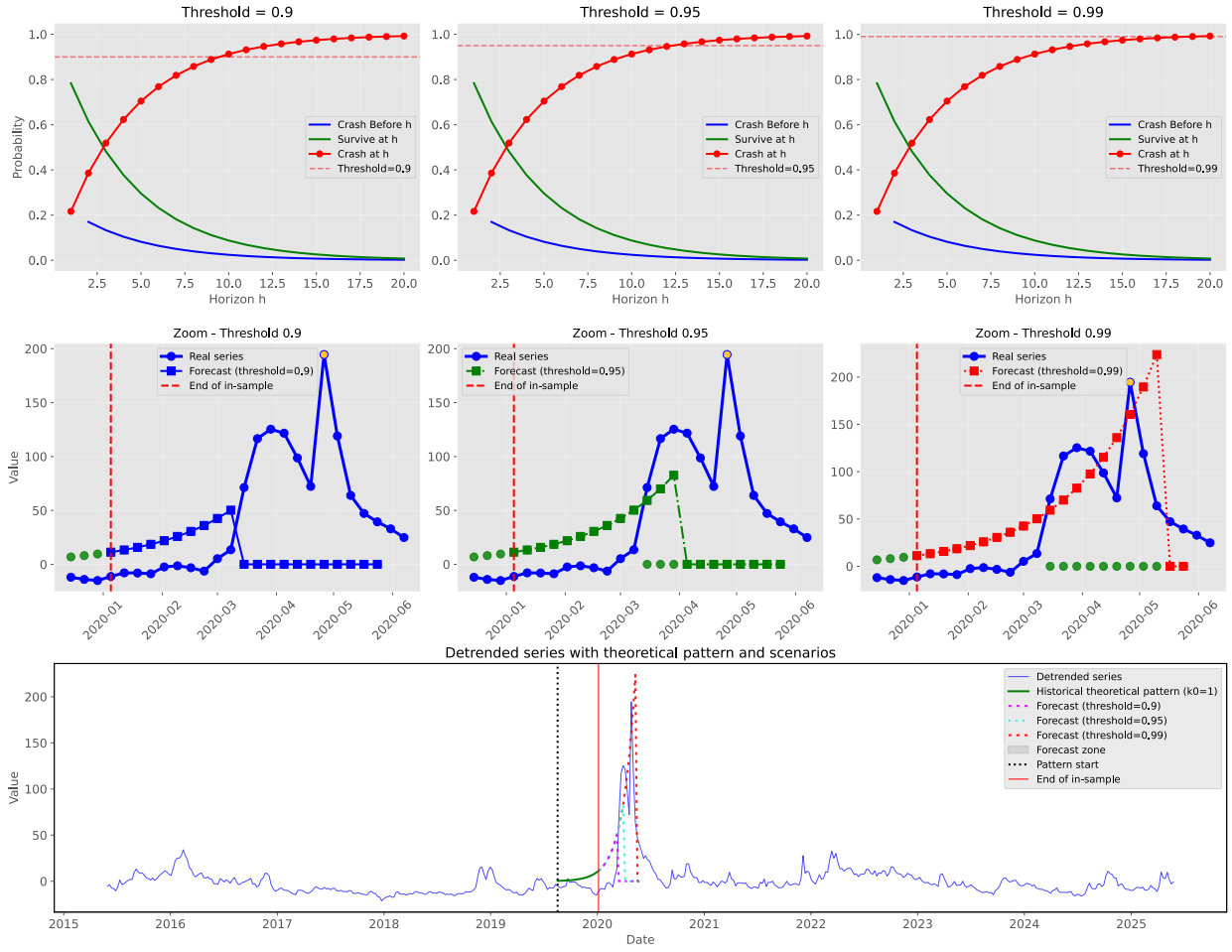

Figure 4: Forecast of the 2020 oil market bubble using the second component ($\hat{\rho}_2 = 0.8470$) from the OVX index filtration. The top row presents crash probability profiles for three different acceptable probability risk thresholds: 0.9 (left), 0.95 (center), and 0.99 (right). Each panel shows the probability of crashing at a given date (red line with circles), surviving beyond that date (green line), the cumulative crash probability up to that date (blue line), and the corresponding threshold value (horizontal dashed red line). The middle row displays zoomed-in forecasts for each threshold scenario, with the real time series (blue line with circles) and forecasted values (colored squares). The vertical dashed red line marks the end of the in-sample period (January 2020). The bottom panel places these forecasts in context of the complete time series (blue line), with the historical theoretical pattern ($k_0 = 1$) shown in green. The colored lines represent forecasts under different threshold values: 0.9 (yellow), 0.95 (green dashed), and 0.99 (red dashed). The black vertical dotted line indicates the pattern start, the red vertical dotted line shows the end of the in-sample period, and the gray shaded area represents the forecast zone. The second component exhibits different growth dynamics and crash patterns compared to the first component, reflecting the heterogeneous nature of oil market volatility expectations. The length of the trajectory segment used for pattern matching is $m = 20$.

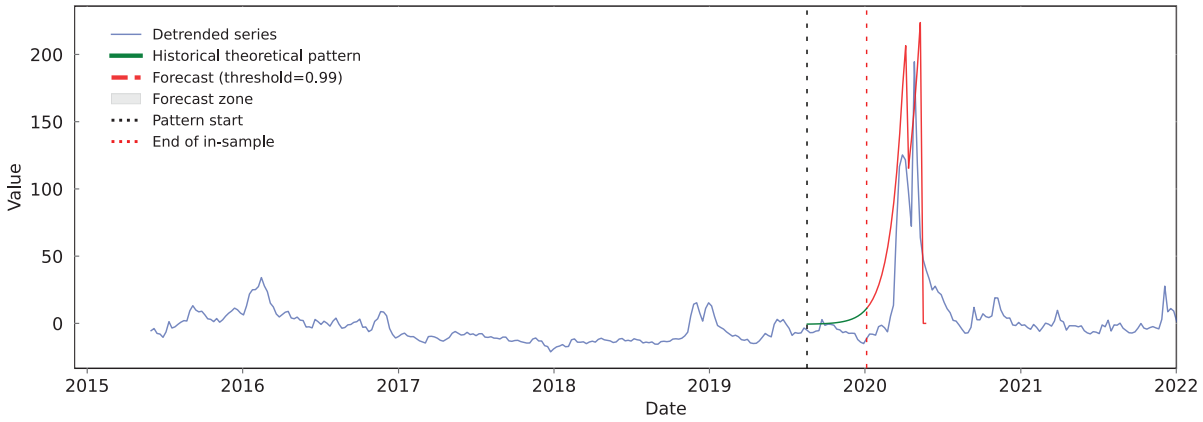

Figure 5: To be commented

predicted crash, remarkably close to the observed peak of around 230 in the actual OVX series. This strong forecasting performance validates our theoretical framework's ability to provide early warning signals for extreme volatility events in commodity markets, offering practitioners a quantitative tool for anticipating and preparing for periods of exceptional market stress in the oil sector.

6. Conclusion

This paper addresses a fundamental limitation in the modeling of speculative bubbles in financial markets by introducing a novel framework based on α-stable moving average aggregates. Traditional approaches to bubble modeling face two critical shortcomings: Gaussian linear models fail to capture the extreme events and heavy-tailed characteristics inherent in financial markets, while existing anticipative heavy-tailed processes impose uniform bubble patterns across different episodes, contradicting the observed heterogeneity in market dynamics.

Our contribution is both theoretical and methodological. Theoretically, we develop a flexible model built on α-stable moving average aggregates that accommodates diverse bubble growth patterns and crash dynamics. We establish that this model admits a semi-norm representation on a unit cylinder, similar to non-aggregated moving averages, thereby enabling the forecasting of bubble episodes with heterogeneous growth trajectories. We extend the spectral representation of stable processes to aggregated components and derive conditions under which the tail conditional distribution can be used for prediction, showing that anticipativeness remains a necessary condition for past-representability even in the aggregated case.

Methodologically, we develop a minimum distance estimation procedure based on the joint characteristic function that effectively identifies the parameters of stable aggregates. Unlike existing approaches limited to the Cauchy case with continuous support distributions, our framework extends to the general α-stable family

with discrete support, making it more suitable for empirical applications. Our Monte Carlo simulations demonstrate robust finite-sample performance across various specifications.

An empirical application to the CBOE OVX index reveals the presence of multiple anticipative components with distinct persistence properties and asymmetric weights. The deconvolution analysis demonstrates that what appears as a single volatility episode during the 2020 oil market disruption actually comprises multiple superimposed processes with heterogeneous growth rates and crash probabilities. Our forecasting framework successfully anticipates both the timing and magnitude of the March 2020 volatility spikes.

The pattern recognition approach underlying our forecasting methodology proves particularly valuable, allowing practitioners to distinguish between different sources of market stress—rapid panic responses versus slow-building fundamental concerns—and tailor their risk management strategies accordingly. The flexibility in risk threshold selection creates a natural trade-off between conservative and aggressive forecasting strategies, accommodating different risk tolerance levels in practical applications.

Table 5: In-sample bubble forecast: prediction probabilities

		First component ($k_0 = 3$)			Second component ($k_0 = 1$)		
Date	h	Forecast	Crash at h	Survive at h	Forecast	Crash at h	Survive at h
2020-01-05	0	11.2714	–	–	11.2714	–	–
2020-01-12	1	14.1087	–	–	13.3068	0.2164	0.7836
2020-01-19	2	17.6601	–	–	15.7098	0.3859	0.6141
2020-01-26	3	22.1056	0.6281	0.3719	18.5467	0.5188	0.4812
2020-02-02	4	27.6701	0.7326	0.2674	21.8958	0.6229	0.3771
2020-02-09	5	34.6325	0.8077	0.1923	25.8498	0.7045	0.2955
2020-02-16	6	43.3537	0.8617	0.1383	30.5178	0.7684	0.2316
2020-02-23	7	54.2668	0.9006	0.0994	36.0288	0.8185	0.1815
2020-03-01	8	67.9270	0.9285	0.0715	42.5349	0.8578	0.1422
2020-03-08	9	85.0258	0.9486	0.0514	50.2159	0.8886	0.1114
2020-03-15	10	106.4287	0.9630	0.0370	59.2839	0.9127	0.0873
2020-03-22	11	133.2193	0.9734	0.0266	69.9890	0.9316	0.0684
2020-03-29	12	166.7534	0.9810	0.0190	82.6283	0.9464	0.0536
2020-04-05	13	208.7292	0.9865	0.0135	97.5494	0.9580	0.0420
2020-04-12	14	0.0000	0.9901	0.0099	115.1651	0.9671	0.0329
2020-04-19	15	0.0000	0.9929	0.0071	135.9617	0.9742	0.0258
2020-04-26	16	0.0000	0.9949	0.0051	160.5139	0.9798	0.0202
2020-05-03	17	0.0000	0.9963	0.0037	189.4997	0.9842	0.0158
2020-05-10	18	0.0000	0.9974	0.0026	223.7200	0.9876	0.0124
2020-05-17	19	0.0000	0.9981	0.0019	0.0000	0.9903	0.0097

7. Proofs

7.1. Proof of Lemma 2.1

We first establish the $C^k(\Theta)$ regularity of (2.11), the MDE objective function. The proof proceeds by analyzing the theoretical characteristic function structure and establishing precise control over its derivatives. We then show that under the condition obtained to insure that (2.11) belongs to the $C^2(\Theta)$ class, Assumptions 3, 6, 7 and 8 are satisfied.

7.1.1. First order derivatives analysis

For α-stable AR(1) aggregates, let rewrite (2.5) as $\log \varphi_{X_j}(u,v;\theta) = -\sigma^\alpha \left[\frac{|\rho_j u+v|^\alpha}{1-|\rho_j|^\alpha} + |u|^\alpha\right] \Phi_j(u,v;\alpha,\beta)$ with the asymmetry term

$$\Phi_j(u,v;\alpha,\beta) = \begin{cases} 1 - \beta i \left[\operatorname{sign}(\rho_j u+v) + \operatorname{sign}(u)\right] \tan\left(\frac{\pi\alpha}{2}\right) & \text{if } \alpha \neq 1 \\ 1 + \beta i \left[\frac{2\operatorname{sign}(\rho_j u+v)}{\pi} \ln|\rho_j u+v| + \frac{2\operatorname{sign}(u)}{\pi} \ln|u|\right] & \text{if } \alpha = 1 \end{cases}$$

Let $K \subset \Theta$ be any compact subset satisfying the uniform bounds $\inf_{j,\theta\in K}(1-|\rho_j|) \geq \delta > 0$, $\inf_{\theta\in K} \alpha \geq \alpha_0 > 0$, $\sup_{\theta\in K} \sigma \leq M < \infty$, and $\sup_{\theta\in K} |\beta| \leq B < \infty$. We analyze the first derivatives with respect to all parameters $\theta = (\sigma, \rho_1, \ldots, \rho_J, \pi_1, \ldots, \pi_J, \alpha, \beta)$ and derive the following bounds.

(ι) The derivative with respect to π_k is

$$\frac{\partial \varphi}{\partial \pi_k}(u,v;\theta) = \varphi(u,v;\theta) \cdot \alpha \pi_k^{\alpha-1} \log \varphi_{X_k}(u,v;\theta)$$

thereby leading to

$$\begin{aligned} \left|\frac{\partial \varphi}{\partial \pi_k}(u,v;\theta)\right| &\leq |\varphi(u,v;\theta)| \cdot \alpha \pi_k^{\alpha-1} \sigma^\alpha \left[\frac{|\rho_k u+v|^\alpha}{1-|\rho_k|^\alpha} + |u|^\alpha\right] (1 + B\tan(\pi\alpha/2)) \\ &\leq C_\pi |\varphi(u,v;\theta)| \left[\frac{|\rho_k u+v|^\alpha}{\delta} + |u|^\alpha\right] \end{aligned}$$

where $C_\pi = \alpha M^\alpha (1 + B\tan(\pi\alpha_{\max}/2))$ with $\alpha_{\max} = \sup_{\theta\in K} \alpha$.

($\iota\iota$) The derivative with respect to α is given by

$$\begin{aligned} \frac{\partial \log \varphi_{X_j}}{\partial \alpha} &= -\sigma^\alpha \ln\sigma \left[\frac{|\rho_j u+v|^\alpha}{1-|\rho_j|^\alpha} + |u|^\alpha\right] \Phi_j \\ &\quad - \sigma^\alpha \left[\frac{|\rho_j u+v|^\alpha \ln|\rho_j u+v|}{1-|\rho_j|^\alpha} + |u|^\alpha \ln|u|\right] \Phi_j \\ &\quad + \sigma^\alpha \left[\frac{|\rho_j u+v|^\alpha |\rho_j|^\alpha \ln|\rho_j|}{(1-|\rho_j|^\alpha)^2}\right] \Phi_j + \sigma^\alpha \left[\frac{|\rho_j u+v|^\alpha}{1-|\rho_j|^\alpha} + |u|^\alpha\right] \frac{\partial \Phi_j}{\partial \alpha} \end{aligned}$$

and leads the following bound

$$\left|\frac{\partial \log \varphi_{X_j}}{\partial \alpha}\right| \leq M^\alpha |\ln M| \left[\frac{|\rho_j u+v|^\alpha}{\delta}+|u|^\alpha\right](1+B\tan(\pi\alpha_{\max}/2))$$
$$+M^\alpha\left[\frac{|\rho_j u+v|^\alpha(|\ln|\rho_j u+v||+|\ln|\rho_j||)}{\delta}+|u|^\alpha|\ln|u||\right](1+B\tan(\pi\alpha_{\max}/2))$$
$$+M^\alpha\left[\frac{|\rho_j u+v|^\alpha}{\delta}+|u|^\alpha\right]\frac{\pi B}{2\cos^2(\pi\alpha_{\max}/2)}$$

Since logarithmic terms grow slower than any positive power, we have

$$|\ln|\rho_j u+v||+|\ln|u||=O((|\rho_j u+v|^\epsilon+|u|^\epsilon)) \quad \text{for any } \epsilon>0$$

and hence

$$\left|\frac{\partial\varphi}{\partial\alpha}(u,v;\theta)\right| \leq C_\alpha|\varphi(u,v;\theta)|\left[\frac{|\rho_j u+v|^{\alpha+\epsilon}}{\delta}+|u|^{\alpha+\epsilon}\right]$$

for some constant C_α depending on the compact set K.

($\iota\iota$) The derivative with respect to σ is

$$\frac{\partial \log\varphi_{X_j}}{\partial\sigma}(u,v;\theta)=-\alpha\sigma^{\alpha-1}\left[\frac{|\rho_j u+v|^\alpha}{1-|\rho_j|^\alpha}+|u|^\alpha\right]\Phi_j(u,v;\alpha,\beta)$$

and implies the following bound

$$\left|\frac{\partial\varphi}{\partial\sigma}(u,v;\theta)\right| \leq |\varphi(u,v;\theta)|\cdot\alpha M^{\alpha-1}\sum_{j=1}^J\pi_j^\alpha\left[\frac{|\rho_j u+v|^\alpha}{1-|\rho_j|^\alpha}+|u|^\alpha\right](1+B\tan(\pi\alpha_{\max}/2))$$
$$\leq C_\sigma|\varphi(u,v;\theta)|\left[\sum_{j=1}^J\frac{|\rho_j u+v|^\alpha}{\delta}+J|u|^\alpha\right]$$

where $C_\sigma=\alpha M^{\alpha-1}(1+B\tan(\pi\alpha_{\max}/2))$.

($\iota\nu$) We now turn to the most critical case, the derivative with respect to ρ_k, given by

$$\frac{\partial\log\varphi_{X_k}}{\partial\rho_k}=-\sigma^\alpha\frac{\partial}{\partial\rho_k}\left[\frac{|\rho_k u+v|^\alpha}{1-|\rho_k|^\alpha}\right]\Phi_k-\sigma^\alpha\left[\frac{|\rho_k u+v|^\alpha}{1-|\rho_k|^\alpha}+|u|^\alpha\right]\frac{\partial\Phi_k}{\partial\rho_k}$$

The first term on the right hand side is

$$\frac{\partial}{\partial\rho_k}\left[\frac{|\rho_k u+v|^\alpha}{1-|\rho_k|^\alpha}\right]=\frac{\alpha|\rho_k u+v|^{\alpha-1}\text{sign}(\rho_k u+v)u}{1-|\rho_k|^\alpha}+\frac{|\rho_k u+v|^\alpha\alpha|\rho_k|^{\alpha-1}\text{sign}(\rho_k)}{(1-|\rho_k|^\alpha)^2}$$

and we define the corresponding bound

$$T_1(u,v)=\frac{\alpha|u||\rho_k u+v|^{\alpha-1}}{1-|\rho_k|^\alpha}\leq\frac{\alpha|u||\rho_k u+v|^{\alpha-1}}{\delta}$$

This term is problematic in view of the integrability requirement. At this stage we introduce $w(u,v)=\exp(-\kappa(u^2+v^2))$ with κ a positive constant and prove convergence using polar coordinates of

$$I_1=\int_{-\infty}^{+\infty}\int_{-\infty}^{+\infty}\frac{|u||\rho_k u+v|^{\alpha-1}}{\delta}\exp(-\kappa(u^2+v^2))\,du\,dv$$

Defining $u = r\cos\theta$, $v = r\sin\theta$, I_1 becomes

$$\begin{aligned} I_1 &= \frac{1}{\delta}\int_0^{2\pi}\int_0^{\infty} r|\cos\theta|\cdot r^{\alpha-1}|\rho_k\cos\theta+\sin\theta|^{\alpha-1}e^{-\kappa r^2}\,r\,dr\,d\theta \\ &= \frac{1}{\delta}\int_0^{2\pi}|\cos\theta||\rho_k\cos\theta+\sin\theta|^{\alpha-1}\left[\int_0^{\infty} r^{\alpha+1}e^{-\kappa r^2}\,dr\right]d\theta \end{aligned}$$

where the radial integral converges for $\alpha > -2$

$$\int_0^{\infty} r^{\alpha+1}e^{-\kappa r^2}\,dr = \frac{\Gamma((\alpha+2)/2)}{2\kappa^{(\alpha+2)/2}}$$

and the angular integral, near singularities where $\rho_k\cos\theta+\sin\theta = 0$, converges for $\alpha > 0$

$$\int_{\theta_0-\epsilon}^{\theta_0+\epsilon}|\rho_k\cos\theta+\sin\theta|^{\alpha-1}d\theta = \frac{2(\sqrt{1+\rho_k^2})^{\alpha-1}\epsilon^{\alpha}}{\alpha} < \infty$$

Therefore for any $\alpha \in (0,2)$,

$$\left|\frac{\partial\varphi}{\partial\rho_k}(u,v;\theta)\right| \le C_\rho|\varphi(u,v;\theta)|\left[\frac{|u||\rho_k u+v|^{\alpha-1}}{\delta}+\frac{|\rho_k u+v|^{\alpha}}{\delta^2}+|u|^{\alpha}\right] \tag{7.1}$$

where $C_\rho = \sigma^\alpha(1+B\tan(\pi\alpha_{\max}/2))$, all terms being integrable for $\alpha > 0$. This completes the first-order derivative analysis with precise bounds, establishing uniform integrability that enables application of the dominated convergence theorem for C^1 regularity when $\alpha > 0$.

7.1.2. Second-order derivatives analysis

Establishing C^2 regularity lies in proving that second derivatives exist and are bounded. As revealed by the first-order analysis, the most critical case is related to the ρ_j parameters. Hence, we only detailed our analysis for $\partial^2\varphi/(\partial\rho_k\partial\rho_\ell)$, using the same polar coordinate approach. Starting the expression in $(\iota\nu)$ we have

$$\frac{\partial^2\varphi}{\partial\rho_k^2} = \left(\frac{\partial\varphi}{\partial\rho_k}\right)\cdot\pi_k^{\alpha}\frac{\partial\log\varphi_{X_k}}{\partial\rho_k}+\varphi(u,v;\theta)\cdot\pi_k^{\alpha}\frac{\partial^2\log\varphi_{X_k}}{\partial\rho_k^2}$$

The first term on the right hand side is bounded by the product of first-order bounds established in (7.1). The second term is

$$\begin{aligned} \frac{\partial^2\log\varphi_{X_k}}{\partial\rho_k^2} = &-\sigma^{\alpha}\frac{\partial^2}{\partial\rho_k^2}\left[\frac{|\rho_k u+v|^{\alpha}}{1-|\rho_k|^{\alpha}}\right]\Phi_k \\ &-2\sigma^{\alpha}\frac{\partial}{\partial\rho_k}\left[\frac{|\rho_k u+v|^{\alpha}}{1-|\rho_k|^{\alpha}}\right]\frac{\partial\Phi_k}{\partial\rho_k} \\ &-\sigma^{\alpha}\left[\frac{|\rho_k u+v|^{\alpha}}{1-|\rho_k|^{\alpha}}+|u|^{\alpha}\right]\frac{\partial^2\Phi_k}{\partial\rho_k^2} \end{aligned}$$

and involves

$$\begin{aligned} \frac{\partial^2}{\partial\rho_k^2}\left[\frac{|\rho_k u+v|^{\alpha}}{1-|\rho_k|^{\alpha}}\right] = &\frac{1}{1-|\rho_k|^{\alpha}}\frac{\partial^2}{\partial\rho_k^2}|\rho_k u+v|^{\alpha} \\ &+\frac{2\alpha|\rho_k|^{\alpha-1}\mathrm{sign}(\rho_k)}{(1-|\rho_k|^{\alpha})^2}\frac{\partial}{\partial\rho_k}|\rho_k u+v|^{\alpha} \\ &+|\rho_k u+v|^{\alpha}\frac{\alpha(\alpha-1)|\rho_k|^{\alpha-2}+2\alpha^2|\rho_k|^{2\alpha-1}/(1-|\rho_k|^{\alpha})}{(1-|\rho_k|^{\alpha})^2} \end{aligned}$$

showing that the most critical derivative is

$$\frac{\partial^2}{\partial \rho_k^2}|\rho_k u + v|^\alpha = \alpha(\alpha-1)u^2|\rho_k u + v|^{\alpha-2} \tag{7.2}$$

and the most singular terms are of form

$$T_2(u,v) = \frac{\alpha(\alpha-1)u^2|\rho_k u + v|^{\alpha-2}}{1-|\rho_k|^\alpha} \leq \frac{\alpha(\alpha-1)u^2|\rho_k u + v|^{\alpha-2}}{\delta}$$

Again, we invoke the weight function $w(u,v) = \exp(-\kappa(u^2+v^2))$ prove convergence using polar coordinates of

$$\begin{aligned} I_2 &= \int_{-\infty}^{+\infty}\int_{-\infty}^{+\infty} \frac{u^2|\rho_k u + v|^{\alpha-2}}{\delta} \exp(-\kappa(u^2+v^2))\, du\, dv \\ &= \frac{1}{\delta}\int_0^{2\pi}\int_0^{\infty} r^2\cos^2\theta \cdot r^{\alpha-2}|\rho_k\cos\theta + \sin\theta|^{\alpha-2} e^{-\kappa r^2} r\, dr\, d\theta \\ &= \frac{1}{\delta}\int_0^{2\pi} \cos^2\theta|\rho_k\cos\theta+\sin\theta|^{\alpha-2}\left[\int_0^\infty r^{\alpha+1}e^{-\kappa r^2}\, dr\right] d\theta \end{aligned}$$

The angular integral becomes

$$J_\alpha = \int_0^{2\pi} \cos^2\theta|\rho_k\cos\theta+\sin\theta|^{\alpha-2} d\theta$$

and the singularities occur when $\rho_k\cos\theta + \sin\theta = 0$, i.e., when $\tan\theta = -\rho_k$. Let $\theta_0 = \arctan(-\rho_k)$ be one such point. Near θ_0, using a local expansion

$$\rho_k\cos\theta + \sin\theta = \sqrt{1+\rho_k^2}\sin(\theta+\phi) \approx \sqrt{1+\rho_k^2}(\theta-\theta_0)$$

with $\phi = \arctan(\rho_k)$. Then, the local behavior near θ_0 is

$$\begin{aligned} \int_{\theta_0-\epsilon}^{\theta_0+\epsilon} \cos^2\theta|\rho_k\cos\theta+\sin\theta|^{\alpha-2} d\theta &\approx \cos^2\theta_0(\sqrt{1+\rho_k^2})^{\alpha-2}\int_{\theta_0-\epsilon}^{\theta_0+\epsilon}|\theta-\theta_0|^{\alpha-2}d\theta \\ &= \cos^2\theta_0(\sqrt{1+\rho_k^2})^{\alpha-2}\cdot 2\int_0^\epsilon t^{\alpha-2}dt \\ &= \cos^2\theta_0(\sqrt{1+\rho_k^2})^{\alpha-2}\cdot\frac{2\epsilon^{\alpha-1}}{\alpha-1} \end{aligned}$$

This local integral converges if and only if $\alpha - 2 > -1 \iff \alpha > 1$. We now can define an appropriate bound for J_α

$$J_\alpha \leq C(\alpha,\rho_k) = \frac{2\pi\max_\theta\cos^2\theta}{\alpha-1}(\sqrt{1+\rho_k^2})^{\alpha-2} + \int_{(0,2\pi)\setminus\bigcup_i B(\theta_{0,i},\epsilon)} \cos^2\theta|\rho_k\cos\theta+\sin\theta|^{\alpha-2}d\theta$$

where $\theta_{0,i} = \arctan(-\rho_k) + i\pi$ are the singularity points in $(0,2\pi)$, $B(\theta_{0,i},\epsilon) = (\theta_{0,i}-\epsilon, \theta_{0,i}+\epsilon)$ with $\epsilon > 0$ sufficiently small, and the integral I_2

$$I_2 \leq \frac{C(\alpha,\rho_k)}{\delta}\cdot\frac{\Gamma((\alpha+2)/2)}{2\kappa^{(\alpha+2)/2)}} < \infty$$

Notice that for $k \neq \ell$,

$$\frac{\partial^2 \varphi}{\partial \rho_k \partial \rho_\ell} = \left(\frac{\partial \varphi}{\partial \rho_\ell} \right) \cdot \pi_k^\alpha \frac{\partial \log \varphi_{X_k}}{\partial \rho_k},$$

the terms are products of first derivatives and therefore remain bounded when $\alpha > 0$. Following similar analysis, derivatives with respect to σ, π_j, α, and β do not involve singular terms.

7.1.3. Application of Dominated Convergence Theorem

Having established uniform bounds on derivatives, we now can apply the dominated convergence theorem to justify differentiation under the integral sign in (2.11). For any parameter $\theta_i \in \{\sigma, \rho_1, \ldots, \rho_J, \pi_1, \ldots, \pi_J, \alpha, \beta\}$, we have shown:

$$\left| \frac{\partial}{\partial \theta_i} |\varphi_n(u,v) - \varphi(u,v;\theta)|^2 \right| \leq 2|\varphi_n(u,v) - \varphi(u,v;\theta)| \left| \frac{\partial \varphi}{\partial \theta_i}(u,v;\theta) \right| \tag{7.3}$$

$$\leq 2(|\varphi_n(u,v)| + |\varphi(u,v;\theta)|) \left| \frac{\partial \varphi}{\partial \theta_i}(u,v;\theta) \right| \tag{7.4}$$

Since $|\varphi_n(u,v)| \leq 1$ and $|\varphi(u,v;\theta)| \leq 1$ and by the established uniform bounds

$$\left| \frac{\partial \varphi}{\partial \theta_i}(u,v;\theta) \right| \leq C_i(\theta) G_i(u,v) \tag{7.5}$$

where $G_i(u,v)$ are functions with

$$\int_{-\infty}^{+\infty} \int_{-\infty}^{+\infty} G_i(u,v) w(u,v)\, du\, dv < \infty, \tag{7.6}$$

the dominating function is

$$H_1(u,v) = 2 \max_i C_i(\theta) G_i(u,v) w(u,v) \tag{7.7}$$

Since $\int_{-\infty}^{+\infty} \int_{-\infty}^{+\infty} H_1(u,v)\, du\, dv < \infty$, the dominated convergence theorem applies, and

$$\frac{\partial D_{\mathcal{X}}}{\partial \theta_i}(\theta) = \int_{-\infty}^{+\infty} \int_{-\infty}^{+\infty} \frac{\partial}{\partial \theta_i} |\varphi_n(u,v) - \varphi(u,v;\theta)|^2 w(u,v)\, du\, dv,$$

showing that (2.11) is $C^1(\Theta)$ for any $\alpha \in (0,2)$ and the weight function as $w(u,v) = \exp(-\kappa(u^2+v^2))$ with κ a positive constant. Regarding the second derivatives, for $\alpha > 1$, we have established:

$$\left| \frac{\partial^2 \varphi}{\partial \rho_k^2}(u,v;\theta) \right| \leq C_2(\theta) G_2(u,v) \tag{7.8}$$

where $G_2(u,v)$ is

$$G_2(u,v) \sim |\varphi(u,v;\theta)| \cdot \left[u^2 |\rho_k u + v|^{\alpha-2} + O(|u|^\alpha + |v|^\alpha) \right] \tag{7.9}$$

For $\alpha > 1$, we proved

$$\int_{-\infty}^{+\infty} \int_{-\infty}^{+\infty} u^2 |\rho_k u + v|^{\alpha-2} e^{-\kappa(u^2+v^2)}\, du\, dv < \infty \tag{7.10}$$

the second derivative of (2.11) exists when

$$\left| \frac{\partial^2}{\partial\theta_i \partial\theta_j} |\varphi_n(u,v) - \varphi(u,v;\theta)|^2 \right| \leq H_2(u,v) \tag{7.11}$$

where $H_2(u,v)$ includes terms of form

$$H_2(u,v) \leq 2 \left| \frac{\partial^2 \varphi}{\partial\theta_i \partial\theta_j} \right| + 2 \left| \frac{\partial\varphi}{\partial\theta_i} \right| \left| \frac{\partial\varphi}{\partial\theta_j} \right| \tag{7.12}$$

multiplied by $w(u,v)$. For $\alpha > 1$, all these terms are integrable, so

$$\int_{-\infty}^{+\infty} \int_{-\infty}^{+\infty} H_2(u,v)\, du\, dv < \infty \tag{7.13}$$

Therefore, the dominated convergence theorem applies for second derivatives, showing that (2.11) is $C^2(\Theta)$ for any $\alpha \in (1,2)$ and appropriate exponential weights. This result is sufficient to prove that Assumption 3 holds.

7.1.4. Validation of Assumption 6

Having established the $C^2(\Theta)$ regularity of the MDE objective function in Lemma 2.1, we now proceed to verify that Assumption 6 holds for α-stable AR(1) aggregates under exponential weight regularization. This assumption requires that the random sequence $K(x;\theta)$ defined in (2.14) is measurable and bounded. From the $C^1(\Theta)$ analysis in Lemma 2.1, the boundedness of $K(x;\theta)$ follows from the natural bounds of trigonometric functions. Since $|\cos(ux_{j+1} + vx_j)| \leq 1$ and $|\sin(ux_{j+1} + vx_j)| \leq 1$ for all (u,v,x), we have:

$$\begin{aligned} |K(x;\theta)| &\leq \int_{-\infty}^{\infty} \int_{-\infty}^{\infty} \left[2 \left| \frac{\partial \text{Re } \varphi(u,v;\theta)}{\partial\theta} \right| + 2 \left| \frac{\partial \text{Im } \varphi(u,v;\theta)}{\partial\theta} \right| \right] w(u,v)\, du\, dv \\ &= 2 \int_{-\infty}^{\infty} \int_{-\infty}^{\infty} \left| \frac{\partial\varphi(u,v;\theta)}{\partial\theta} \right| w(u,v)\, du\, dv =: C(\theta) \end{aligned} \tag{7.14}$$

From Lemma 2.1, we established that for $\alpha > 1$, the most critical terms satisfy

$$\left| \frac{\partial\varphi}{\partial\rho_k}(u,v;\theta) \right| \leq C_1(\theta) |\varphi(u,v;\theta)| \left[\frac{|\rho_k u + v|^\alpha}{\delta} + |u|^\alpha \right]$$

where $\delta = \inf_{j,\theta}(1 - |\rho_j|) > 0$ and $C_1(\theta)$ is a constant depending only on the parameter bounds. More generally, for each parameter component $\theta_i \in \{\sigma, \rho_1, \ldots, \rho_J, \pi_1, \ldots, \pi_J, \alpha, \beta\}$, the derivative bounds established in Lemma 2.1 ensure

$$\int_{-\infty}^{\infty} \int_{-\infty}^{\infty} \left| \frac{\partial\varphi(u,v;\theta)}{\partial\theta_i} \right| w(u,v)\, du\, dv \leq C_i(\theta) < \infty$$

where $C_i(\theta)$ depends on the specific parameter and the bounds established for each case in the first-order analysis. □

7.1.5. Validation of Assumption 7

Having established the $C^2(\Theta)$ regularity of the MDE objective function in Lemma 2.1 and the uniform boundedness of second derivatives, we now demonstrate that Assumption 7 holds for $\alpha > 1$ and exponential weights. The uniform boundedness condition follows directly from our second-order derivatives analysis. From the explicit decomposition:

$$\frac{\partial^2 \varphi}{\partial \rho_k^2} = \left(\frac{\partial \varphi}{\partial \rho_k}\right) \cdot \pi_k^\alpha \frac{\partial \log \varphi_{X_k}}{\partial \rho_k} + \varphi(u, v; \theta) \cdot \pi_k^\alpha \frac{\partial^2 \log \varphi_{X_k}}{\partial \rho_k^2} \tag{7.15}$$

The first term contributes $O(C_\rho^2)$ where $C_\rho = \sigma^\alpha(1 + B\tan(\pi\alpha_{\max}/2))$ from (7.1). The second term involves the critical derivative $\frac{\partial^2}{\partial \rho_k^2}|\rho_k u + v|^\alpha = \alpha(\alpha-1)u^2|\rho_k u + v|^{\alpha-2}$, with asymmetry derivatives contributing $O\left(\frac{\pi^2 B}{\cos^3(\pi\alpha_{\max}/2)} u|\rho_k u + v|^{\alpha-2}\right)$. Therefore, the uniform bound constant is:

$$C_2(\theta) = \frac{\pi_k^\alpha \sigma^\alpha}{\delta}\left[\alpha(\alpha-1) + O\left(\frac{\sigma^{2\alpha}}{\delta}\right) + O\left(\frac{B^2\pi^2\sigma^\alpha}{\delta\cos^3(\pi\alpha_{\max}/2)}\right)\right] \tag{7.16}$$

For each parameter pair (θ_i, θ_j), we obtain explicit uniform constants:

$$C_{kk}(\theta) = \frac{\pi_k^\alpha \sigma^\alpha}{\delta}\left[\alpha(\alpha-1) + O(\sigma^{2\alpha}) + O\left(\frac{B^2\pi^2}{\cos^3(\pi\alpha_{\max}/2)}\right)\right] \tag{7.17}$$

$$C_{k\ell}(\theta) = \pi_k^\alpha \pi_\ell^\alpha \sigma^{2\alpha}\left[\frac{1}{\delta^2} + O\left(\frac{B\tan(\pi\alpha_{\max}/2)}{\delta}\right)\right] \quad (k \neq \ell) \tag{7.18}$$

$$C_{\sigma\sigma}(\theta) = \alpha^2 M^{2(\alpha-1)} J\left[1 + O(B\tan(\pi\alpha_{\max}/2))\right]^2 \tag{7.19}$$

$$C_{\pi_k\pi_\ell}(\theta) = \alpha^2 \pi_k^{\alpha-1}\pi_\ell^{\alpha-1} M^{2\alpha}\left[\frac{1}{\delta^2} + O(B^2\tan^2(\pi\alpha_{\max}/2))\right] \tag{7.20}$$

For any compact subset $K \subset \Theta$ with the established uniform bounds, these constants ensure:

$$\left|\frac{\partial^2 \varphi(u, v; \theta)}{\partial\theta_i \partial\theta_j}\right| \leq C_{ij}(\theta) \cdot H_{ij}(u, v) \tag{7.21}$$

where all $H_{ij}(u, v)$ are w-integrable for $\alpha > 1$.

Let's know proof the non-singularity of $\Sigma(\theta_0)$, since $\varphi(u, v; \theta)$ is real-valued, the Fisher Information Matrix is:

$$\Sigma_{ij}(\theta_0) = \int_{-\infty}^{+\infty}\int_{-\infty}^{+\infty} \frac{\partial \varphi(u, v; \theta_0)}{\partial\theta_i}\frac{\partial \varphi(u, v; \theta_0)}{\partial\theta_j} w(u, v)\, du\, dv \tag{7.22}$$

To establish non-singularity, we show that for any non-zero vector $c \neq 0$:

$$c^T\Sigma(\theta_0)c = \int_{-\infty}^{+\infty}\int_{-\infty}^{+\infty}\left|\sum_k c_k \frac{\partial \varphi(u, v; \theta_0)}{\partial\theta_k}\right|^2 w(u, v)\, du\, dv > 0 \tag{7.23}$$

From the aggregate structure $\varphi(u, v; \theta) = \prod_{j=1}^J \pi_j \varphi_{X_j}(u, v; \theta)$, we write:

$$\frac{\partial \varphi}{\partial\theta_k}(u, v; \theta) = \varphi(u, v; \theta) \cdot g_k(u, v; \theta) \tag{7.24}$$

where $g_k(u,v;\theta) = \frac{\partial \log \varphi}{\partial \theta_k}(u,v;\theta)$ are the logarithmic derivatives established in our first-order analysis. The condition reduces to proving linear independence:

$$\sum_k c_k g_k(u,v;\theta_0) = 0 \quad \text{a.e. w.r.t. } w(u,v)dudv \quad \Rightarrow \quad c = 0 \tag{7.25}$$

The key insight is that each parameter class affects the characteristic function through fundamentally different mechanisms: the AR parameters ρ_k create singularities along distinct lines $\rho_k u + v = 0$. From our polar coordinate analysis, near each singularity line $\theta_0 = \arctan(-\rho_k)$:

$$g_{\rho_k}(u,v;\theta) \sim \frac{\alpha|\rho_k u + v|^{\alpha-1}u}{1 - |\rho_k|^\alpha} \tag{7.26}$$

These singularities have different orientations for different ρ_k values, while g_σ, g_{π_j}, g_α, and g_β remain bounded near these lines. For large $|(u,v)|$, the established bounds reveal distinct growth patterns:

$$g_\sigma(u,v;\theta) \sim -\alpha\sigma^{\alpha-1}\sum_j \pi_j^\alpha |u|^\alpha \tag{7.27}$$

$$g_{\rho_k}(u,v;\theta) \sim \frac{\sigma^\alpha \pi_k^\alpha \alpha|\rho_k|^{\alpha-1}|\rho_k u + v|^\alpha}{(1 - |\rho_k|^\alpha)^2} \tag{7.28}$$

$$g_{\pi_k}(u,v;\theta) \sim \alpha\pi_k^{\alpha-1}\sigma^\alpha \left[\frac{|\rho_k u + v|^\alpha}{1 - |\rho_k|^\alpha} + |u|^\alpha\right] \tag{7.29}$$

From our analysis of derivatives with respect to α, we have:

$$g_\alpha(u,v;\theta) \sim -\sigma^\alpha \sum_j \pi_j^\alpha |u|^\alpha \ln|u| \tag{7.30}$$

where the logarithmic terms create functional independence from polynomial growth. For the asymmetry parameter, the established asymmetry term derivatives yield:

$$g_\beta(u,v;\theta) \sim i\sigma^\alpha \sum_j \pi_j^\alpha |u|^\alpha \tan(\pi\alpha/2) \tag{7.31}$$

where the imaginary component ensures independence from real-valued functions.

Suppose $\sum_k c_k g_k(u,v;\theta_0) = 0$ almost everywhere. If any $c_{\rho_k} \neq 0$, the singularity structure along $\rho_k u + v = 0$ dominates locally, contradicting the zero combination since other functions remain bounded. If $c_{\rho_k} = 0$ for all k but $c_\alpha \neq 0$, the logarithmic growth $|u|^\alpha \ln|u|$ in g_α differs fundamentally from the polynomial terms in g_σ and g_{π_k}. If $c_{\rho_k} = c_\alpha = 0$ but $c_\beta \neq 0$, the imaginary structure in g_β ensures independence from the remaining real-valued functions. The remaining case with only c_σ and c_{π_k} non-zero fails due to the different directional dependencies: $g_\sigma \sim |u|^\alpha$ versus $g_{\pi_k} \sim |\rho_k u + v|^\alpha + |u|^\alpha$. The exponential weight $w(u,v) = \exp(-\kappa(u^2 + v^2))$ assigns positive measure to every open set in $\mathbb{R}^2$. This ensures three facts: first, all singularity lines $\rho_k u + v = 0$ receive positive measure, second asymptotic behaviors as $|(u,v)| \to \infty$ contribute meaningfully and finnaly local functional differences are preserved in the L^2 norm. This functional independence is consistent with our identification analysis via the $g_n(\lambda)$ approach, where the

ability to identify parameters from different λ values relies on the same orthogonality properties. Therefore, $\Sigma(\theta_0)$ is non-singular for $\alpha > 1$, where the condition $\alpha > 1$ ensures convergence of all defining integrals from our integrability analysis.

7.1.6. Validation of Assumption 8

Having established the $C^2(\Theta)$ regularity and the boundedness of $K(x;\theta)$ in the verification of Assumption 6, we now demonstrate that Assumption 8 holds for $\alpha > 1$ and exponential weights. The proof relies on establishing the connection between empirical uncorrelatedness and α-mixing properties, which we detail in the following steps. From Gouriéroux and Zakoian (2017), each non-causal α-stable AR(1) component $X_{j,t} = \rho_j X_{j,t+1} + \varepsilon_{j,t}$ with $\alpha \geq 1$ admits a weak causal linear representation:

$$X_{j,t} = \rho_j X_{j,t-1} + u_{j,t} \tag{7.32}$$

where the $u_{j,t}$ are "empirically uncorrelated" variables satisfying:

$$\frac{1}{n}\sum_{t=\ell+1}^{n} u_{j,t}u_{j,t-\ell} \Big/ \frac{1}{n}\sum_{t=1}^{n} u_{j,t}^2 \to 0 \quad \text{in probability as } n \to \infty \tag{7.33}$$

for any $\ell > 0$. Unlike standard white noise where $\mathbb{E}[u_t u_{t-\ell}] = 0$ exactly, here we only have *asymptotic* sample uncorrelatedness. This weaker condition is sufficient for our purposes but requires careful analysis of its implications. The empirical uncorrelatedness condition (7.33) implies that the sample autocovariances of $\{u_{j,t}\}$ behave asymptotically like those of white noise. Specifically, for the process (7.32), we can establish:

Lemma 7.1. *If $X_{j,t} = \rho_j X_{j,t-1} + u_{j,t}$ where $\{u_{j,t}\}$ satisfies (7.33) and $|\rho_j| < 1$, then:*

$$\gamma_{X_j}(\ell) = \mathbb{E}[X_{j,t}X_{j,t-\ell}] = O(|\rho_j|^{\ell}) \quad \text{as } \ell \to \infty$$

Proof: From the causal representation, we have:

$$X_{j,t} = \sum_{k=0}^{\infty} \rho_j^k u_{j,t-k}$$

Therefore:

$$\gamma_{X_j}(\ell) = \mathbb{E}[X_{j,t}X_{j,t-\ell}] \tag{7.34}$$

$$= \mathbb{E}\left[\left(\sum_{k=0}^{\infty} \rho_j^k u_{j,t-k}\right)\left(\sum_{m=0}^{\infty} \rho_j^m u_{j,t-\ell-m}\right)\right] \tag{7.35}$$

$$= \sum_{k=0}^{\infty}\sum_{m=0}^{\infty} \rho_j^{k+m}\mathbb{E}[u_{j,t-k}u_{j,t-\ell-m}] \tag{7.36}$$

The empirical uncorrelatedness (7.33) implies that for large samples, $\mathbb{E}[u_{j,t-k}u_{j,t-\ell-m}] \approx 0$ unless $k = m+\ell$. When $k = m + \ell$:

$$\gamma_{X_j}(\ell) \approx \sum_{m=0}^{\infty} \rho_j^{m+\ell+m}\sigma_{u,j}^2 = \rho_j^{\ell} \sum_{m=0}^{\infty} \rho_j^{2m}\sigma_{u,j}^2 \tag{7.37}$$

$$= \rho_j^{\ell} \frac{\sigma_{u,j}^2}{1-\rho_j^2} \tag{7.38}$$

where $\sigma_{u,j}^2$ represents the "effective variance" of the $u_{j,t}$ process under the empirical uncorrelatedness assumption. □

The geometric decay of autocovariances established in Lemma 7.1 directly implies α-mixing with geometric rate. For a stationary process $\{X_{j,t}\}$ with autocovariance function satisfying $|\gamma_{X_j}(\ell)| \leq C|\rho_j|^{\ell}$ for some $C > 0$ and $|\rho_j| < 1$, the process is α-mixing with:

$$\alpha_{X_j}(h) \leq K|\rho_j|^h$$

for some constant $K > 0$. The empirical uncorrelatedness (7.33), combined with the AR(1) structure and $|\rho_j| < 1$, ensures that the asymptotic behavior mimics that of classical AR(1) processes, yielding geometric decay of temporal dependence and consequently α-mixing with geometric rate $|\rho_j|^h$. This follows from the general principle in mixing theory (see e.g., Doukhan (1994)) that geometric decay of temporal dependence implies geometric mixing rates, which applies to our setting due to the empirical uncorrelatedness property combined with the AR(1) structure. While the classical results in Doukhan (1994) apply to Markov processes with white noise innovations, the same geometric mixing conclusion holds in our case because the empirical uncorrelatedness (7.33) provides sufficient asymptotic independence to preserve the geometric decay structure inherent in AR(1) processes with $|\rho_j| < 1$.

Combining Lemma 7.1 with this α-mixing property, we obtain:

$$\alpha_{X_j}(h) = O(|\rho_j|^h)$$

For the aggregate process $\mathcal{X}_t = \sigma \sum_{j=1}^{J} \pi_j X_{j,t}$, since the components $X_{j,t}$ are independent across j:

$$\alpha_{\mathcal{X}}(h) \leq \max_{j=1,\ldots,J} \alpha_{X_j}(h) = O\left(\max_{j=1,\ldots,J} |\rho_j|^h\right) = O(\bar{\rho}^h) \tag{7.39}$$

where $\bar{\rho} = \max_{j=1,\ldots,J} |\rho_j| < 1$.

We define the natural filtration $\mathcal{F}_j = \sigma(K_0, K_1, \ldots, K_j)$ where $K_j = K(x_j; \theta)$. Under exponential weights with $\kappa > 0$ sufficiently large, the function K satisfies the Lipschitz property:

$$|K(x;\theta) - K(x';\theta)| \leq L_\kappa \|x - x'\| \tag{7.40}$$

where L_κ depends on κ and the parameter bounds, and decreases as κ increases.

Combined with the geometric mixing of $\mathcal{X}_t$, the Lipschitz property (7.40) implies that the K function sequence inherits the mixing structure:

$$\alpha_K(h) \leq L_\kappa \cdot \alpha_{\mathcal{X}}(h) = O(L_\kappa \bar{\rho}^h) \tag{7.41}$$

Finally, we verify the conditions of Assumption 8.

First condition: The geometric α-mixing property (7.41) ensures that the martingale differences $\nu_j = \mathbb{E}[K_0|\mathcal{F}_j] - \mathbb{E}[K_0|\mathcal{F}_{j-1}]$ satisfy:

$$|\nu_j| \leq 2L_\kappa \bar{\rho}^j C(\theta) \tag{7.42}$$

where $C(\theta)$ is the bound from (7.14).

The geometric mixing immediately yields:

$$\mathbb{E}[|\mathbb{E}[K_0|\mathcal{F}_{-m}]|^2] \leq \left(\frac{2L_\kappa C(\theta)\bar{\rho}^{m+1}}{1-\bar{\rho}}\right)^2 \to 0 \quad \text{as } m \to \infty \tag{7.43}$$

Second condition: The summability of martingale differences. The exponential decay of martingale differences ensures:

$$\sum_{j=0}^{\infty} \mathbb{E}[\nu_j'\nu_j]^{1/2} \leq \sum_{j=0}^{\infty} 2L_\kappa C(\theta)\bar{\rho}^j = \frac{2L_\kappa C(\theta)}{1-\bar{\rho}} < \infty \tag{7.44}$$

This demonstrates that Assumption 8 holds for $\alpha > 1$ under appropriate exponential weight regularization. □

7.2. Proof of Lemma 3.1

Denote $\boldsymbol{X}_{j,t} = (X_{j,t-m}, \ldots, X_{j,t}, X_{j,t+1}, \ldots, X_{j,t+h})$ the paths of the moving averages $(X_{j,t})$, for $j = 1, \ldots, J$. The $\boldsymbol{X}_{j,t}$'s are independent α-stable random vectors with spectral representations $(\Gamma_j, \boldsymbol{\mu}_j^0)$. We consider only the more delicate case $\alpha = 1$ and $\beta_j \in [-1, 1]$ for $j = 1, \ldots, J$. Because of the independence between $\boldsymbol{X}_{1,t}, \ldots, \boldsymbol{X}_{J,t}$, we have with $a = 2/\pi$

$$\begin{aligned}
\mathbb{E}\Big[e^{i\langle \boldsymbol{u}, \boldsymbol{X_t}\rangle}\Big] &= \mathbb{E}\Big[e^{i\langle \boldsymbol{u}, \sigma \sum_{j=1}^J \pi_j \boldsymbol{X}_{j,t}\rangle}\Big] = \prod_{j=1}^J \mathbb{E}\Big[e^{i\langle \sigma\pi_j \boldsymbol{u}, \boldsymbol{X}_{j,t}\rangle}\Big] \\
&= \prod_{j=1}^J \exp\left\{ -\int_{S_{m+h+1}} \Big(|\langle \sigma\pi_j \boldsymbol{u}, \boldsymbol{s}\rangle| + ia\langle \sigma\pi_j \boldsymbol{u}, \boldsymbol{s}\rangle \ln|\langle \sigma\pi_j \boldsymbol{u}, \boldsymbol{s}\rangle|\Big)\Gamma_j(d\boldsymbol{s}) + i\langle \sigma\pi_j \boldsymbol{u}, \boldsymbol{\mu_j}^0\rangle \right\} \\
&= \exp\left\{ -\int_{S_{m+h+1}} \Big(|\langle \boldsymbol{u}, \boldsymbol{s}\rangle| + ia\langle \boldsymbol{u}, \boldsymbol{s}\rangle \ln|\langle \boldsymbol{u}, \boldsymbol{s}\rangle|\Big) \sum_{j=1}^J \sigma^\alpha \pi_j^\alpha \Gamma_j(d\boldsymbol{s}) \right. \\
&\qquad \left. + i\sum_{j=1}^J \left(\langle \boldsymbol{u}, \sigma\pi_j \boldsymbol{\mu_j}^0\rangle - a\sigma\pi_j \ln(\sigma\pi_j) \int_{S_{m+h+1}} \langle \boldsymbol{u}, \boldsymbol{s}\rangle \Gamma_j(d\boldsymbol{s}) \right) \right\}.
\end{aligned}$$

Focusing on the shift vector, we have

$$\sum_{j=1}^{J}\left(\langle \boldsymbol{u}, \sigma\pi_j {\boldsymbol{\mu_j}}^0\rangle - a\sigma\pi_j \ln(\sigma\pi_j)\int_{S_{m+h+1}}\langle \boldsymbol{u},\boldsymbol{s}\rangle\Gamma_j(d\boldsymbol{s})\right) = \langle \boldsymbol{u}, \sum_{j=1}^{J}\sigma\pi_j(\boldsymbol{\mu}_j^0 - a\ln(\sigma\pi_j)\tilde{\boldsymbol{\mu}}_j)\rangle,$$

with $\tilde{\boldsymbol{\mu}}_j = (\tilde{\mu}_{j,\ell})$ and $\tilde{\mu}_{j,\ell} = \int_{S_{m+h+1}} s_\ell \Gamma_j(d\boldsymbol{s})$, $\ell = -m,\dots,0,1,\dots,h$. Using the form of Γ_j, i.e., $\Gamma_j = \sum_{\vartheta\in S_1}\sum_{k\in\mathbb{Z}} w_{j,\vartheta}\|\boldsymbol{d}_{j,k}\|_e \delta_{\left\{\frac{\vartheta \boldsymbol{d}_{j,k}}{|\boldsymbol{d}_{j,k}\|_e}\right\}}$, we get

$$\tilde{\mu}_{j,\ell} = \int_{S_{m+h+1}} s_\ell \Gamma_j(d\boldsymbol{s}) = \sum_{\vartheta\in S_1}\sum_{k\in\mathbb{Z}} w_{j,\vartheta}\|\boldsymbol{d}_{j,k}\|_e \frac{\vartheta d_{j,k+\ell}}{\|\boldsymbol{d}_{j,k}\|_e} = \beta_j \sum_{k\in\mathbb{Z}} d_{j,k+\ell}, \quad \ell = -m,\dots,h.$$

Hence, $\tilde{\boldsymbol{\mu}}_j = \beta_j \sum_{k\in\mathbb{Z}} \boldsymbol{d}_{j,k}$, and using the form of $\boldsymbol{\mu}_j^0$ as given in (3.5),

$$\begin{aligned}
\sum_{j=1}^{J}\sigma\pi_j(\boldsymbol{\mu}_j^0 - a\ln(\sigma\pi_j)\tilde{\boldsymbol{\mu}}_j) &= \sum_{j=1}^{J}\sigma\pi_j\Big(- a\beta_j\sum_{k\in\mathbb{Z}}\boldsymbol{d}_{j,k}\ln\|\boldsymbol{d}_{j,k}\|_e - a\ln(\sigma\pi_j)\beta_j\sum_{k\in\mathbb{Z}}\boldsymbol{d}_{j,k}\Big)\\
&= -a\sum_{j=1}^{J}\sum_{k\in\mathbb{Z}}\sigma\pi_j\beta_j\boldsymbol{d}_{j,k}\ln\|\sigma\pi_j\boldsymbol{d}_{j,k}\|_e\\
&:= \boldsymbol{\mu}^0.
\end{aligned}$$

Therefore,

$$\mathbb{E}\Big[e^{i\langle \boldsymbol{u},\boldsymbol{X_t}\rangle}\Big] = \exp\left\{ - \int_{S_{m+h+1}}\Big(|\langle \boldsymbol{u},\boldsymbol{s}\rangle| + ia\langle \boldsymbol{u},\boldsymbol{s}\rangle\ln|\langle \boldsymbol{u},\boldsymbol{s}\rangle|\Big)\sum_{j=1}^{J}\sigma^\alpha\pi_j^\alpha\Gamma_j(d\boldsymbol{s}) + i\langle \boldsymbol{u},\boldsymbol{\mu}^0\rangle\right\},$$

and the random vector $\boldsymbol{X}_t$ is 1-stable with spectral measure

$$\sum_{j=1}^{J}\sigma^\alpha\pi_j^\alpha\Gamma_j = \sigma^\alpha\sum_{j=1}^{J}\sum_{\vartheta\in S_1}\sum_{k\in\mathbb{Z}} w_{j,\vartheta}\pi_j^\alpha\|\boldsymbol{d}_{j,k}\|_e^\alpha\delta_{\left\{\frac{\vartheta\boldsymbol{d}_{j,k}}{\|\boldsymbol{d}_{j,k}\|_e}\right\}},$$

and shift vector as announced in the lemma.

7.3. Proof of Lemma 3.2

With the usual notations, let the $\boldsymbol{X}_{j,t}$'s be the paths of the moving averages $(X_{j,t})$'s and let Γ_j, $j = 1,\dots,J$, their spectral measures on the Euclidean unit sphere. Let Γ be the spectral measure of $\boldsymbol{X}_t$. By Lemma 3.1, we have:

$$\Gamma = \sigma^\alpha\sum_{j=1}^{J}\pi_j^\alpha\Gamma_j.$$

Thus, by Proposition 1 of DFT, in the cases where either $\alpha \neq 1$ or $\boldsymbol{X}_t$ is symmetric, the vector $\boldsymbol{X}_t$ is representable on $C_{m+h+1}^{\|\cdot\|}$ if and only if

$$\begin{aligned}
\Gamma(K^{\|\cdot\|}) = 0 \quad &\Longleftrightarrow \quad \sigma^\alpha\sum_{j=1}^{J}\pi_j^\alpha\Gamma_j(K^{\|\cdot\|}) = 0\\
&\Longleftrightarrow \quad \Gamma_j(K^{\|\cdot\|}) = 0, \ \ \forall\, j = 1,\dots,J,
\end{aligned}$$

where the last equivalence follows from the fact that $\sigma^\alpha > 0$ and $\pi_j^\alpha > 0$ for all $j = 1, \dots, J$. Given that the Γ_j's are the spectral measures of paths of non-aggregated moving averages, we can apply the arguments from the proof of Theorem 1 in DFT. Specifically, for each j, the condition $\Gamma_j(K^{\|\cdot\|}) = 0$ is equivalent to the representability condition (3.4) holding for the sequence $(d_{j,k})_k$ with parameter m. Therefore, $\boldsymbol{X}_t$ is representable on $C^{\|\cdot\|}_{m+h+1}$ if and only if (3.4) holds with m for all sequences $(d_{j,k})_k$, $j = 1, \dots, J$. For the case $\alpha = 1$ and $\boldsymbol{X}_t$ asymmetric, we need to consider the additional condition involving the shift vector $\boldsymbol{\mu}^0$. From Lemma 3.1, we have:

$$\boldsymbol{\mu}^0 = -\mathbb{1}_{\{\alpha=1\}} \frac{2\sigma}{\pi} \sum_{j=1}^{J} \sum_{k\in\mathbb{Z}} \pi_j \beta_j \boldsymbol{d}_{j,k} \ln \|\sigma \pi_j \boldsymbol{d}_{j,k}\|_e.$$

By Proposition 1 of DFT, when $\alpha = 1$ and $\boldsymbol{X}_t$ is asymmetric, representability on $C^{\|\cdot\|}_{m+h+1}$ requires both:

1. $\Gamma(K^{\|\cdot\|}) = 0$, which as shown above is equivalent to (3.4) holding for all sequences $(d_{j,k})_k$;
2. The additional condition (3.6) must hold.

To verify condition (3.6), we need to show:

$$\sum_{k\in\mathbb{Z}} \|\boldsymbol{d}_k\|_e \left| \ln\left(\|\boldsymbol{d}_k\| / \|\boldsymbol{d}_k\|_e \right) \right| < +\infty.$$

However, in the context of stable aggregates, this condition must be interpreted in terms of the aggregated coefficients. Since $\boldsymbol{X}_t = \sigma \sum_{j=1}^{J} \pi_j \boldsymbol{X}_{j,t}$, the effective coefficients are combinations of the individual sequences $(d_{j,k})_k$. The condition (3.6) in the aggregated case becomes:

$$\sum_{k\in\mathbb{Z}} \|\boldsymbol{d}_k\|_e \left| \ln\left(\|\boldsymbol{d}_k\| / \|\boldsymbol{d}_k\|_e \right) \right| < +\infty,$$

where $\boldsymbol{d}_k$ now refers to the k-th vector in the aggregated representation. Given the linearity of the aggregation and the fact that the condition must hold for each component individually (as each $\boldsymbol{X}_{j,t}$ must satisfy the representability conditions), the condition (3.6) for the aggregate is satisfied if and only if it holds for all sequences $(d_{j,k})_k$, $j = 1, \dots, J$, with the same parameters m and h.

7.4. Proof of Proposition 3.1

If $\alpha \neq 1$, we have by Theorem 1 and the proof of Proposition 3 of DFT,

$$\begin{aligned}
(\mathcal{X}_t) \text{ past-representable} &\iff \exists\, m \geq 0,\ (3.4) \text{ holds with } m \text{ for all sequences } (d_{j,k})_k \\
&\iff \forall\, j = 1, \dots, J,\ m_{0,j} < +\infty \\
&\iff \forall\, j = 1, \dots, J,\ (X_{j,t}) \text{ past-representable.}
\end{aligned}$$

For a given series $(d_{j,k})_k$, (3.4) holds with $m \geq m_{0,j}$ and does not hold with $m < m_{0,j}$. Regarding the last statement, we know that for $(\mathcal{X}_t)$ (m, h)-past-representable, (3.4) holds with the same m for all the sequences

$(d_{j,k})_k$, $j = 1, \ldots, J$. This holds if $m \geq \max_j m_{0,j}$ and cannot hold if $m < \max_j m_{0,j}$. In the case where $\alpha = 1$, again by Theorem 1 of DFT and denoting generically by $\boldsymbol{X}_t$ a vector $(\mathcal{X}_{t-m}, \ldots, \mathcal{X}_t, \mathcal{X}_{t+1}, \ldots, \mathcal{X}_{t+h})$ of size $m + h + 1$,

$$\begin{aligned}
&\mathcal{X}_t \text{ past-representable} \\
&\iff \exists\, m \geq 0, h \geq 1, \begin{cases} \boldsymbol{X}_t\ \mathcal{S}1\mathcal{S} \text{ and (3.4) holds with } m \text{ for all sequences } (d_{j,k})_k \\ \text{or} \\ \boldsymbol{X}_t \text{ asymmetric and (3.4)-(3.6) hold with } m, h \text{ for all sequences } (d_{j,k})_k \end{cases} \\
&\iff \forall\, j = 1, \ldots, J,\ m_{0,j} < +\infty, \text{ and } \exists\, m \geq 0, h \geq 1, \begin{cases} \boldsymbol{X}_t\ \mathcal{S}1\mathcal{S} \\ \text{or} \\ \boldsymbol{X}_t \text{ asymmetric and (3.6) hold} \\ \text{with } m, h \text{ for all sequences } (d_{j,k})_k \end{cases}
\end{aligned}$$

We conclude again by noting that the necessary condition (3.4) holds for $m \geq \max_j m_{0,j}$ and is violated for $m < \max_j m_{0,j}$. Now, for part $(\iota\iota)$, let $\|\cdot\|$ be a semi-norm satisfying (3.3) and assume that $\mathcal{X}_t$ is (m, h)-past-representable for some $m \geq 0$, $h \geq 1$. We need to establish the spectral representation of the vector $\boldsymbol{X_t} = (\mathcal{X}_{t-m}, \ldots, \mathcal{X}_t, \mathcal{X}_{t+1}, \ldots, \mathcal{X}_{t+h})$ on $C^{\|\cdot\|}_{m+h+1}$. From Lemma 3.1, we know that the spectral representation $(\Gamma, \boldsymbol{\mu}^0)$ of $\boldsymbol{X}_t$ on the Euclidean unit sphere S_{m+h+1} is given by:

$$\Gamma = \sigma^\alpha \sum_{j=1}^{J} \sum_{\vartheta \in S_1} \sum_{k \in \mathbb{Z}} w_{j,\vartheta} \pi_j^\alpha \|\boldsymbol{d}_{j,k}\|_e^\alpha \delta_{\left\{ \frac{\vartheta \boldsymbol{d}_{j,k}}{\|\boldsymbol{d}_{j,k}\|_e} \right\}} \tag{7.45}$$

$$\boldsymbol{\mu}^0 = \begin{cases} \mathbf{0}, & \text{if } \alpha \neq 1 \\ -\frac{2\sigma}{\pi} \sum_{j=1}^{J} \sum_{k \in \mathbb{Z}} \pi_j \beta_j \boldsymbol{d}_{j,k} \ln \|\sigma \pi_j \boldsymbol{d}_{j,k}\|_e, & \text{if } \alpha = 1 \end{cases}$$

To obtain the spectral representation on $C^{\|\cdot\|}_{m+h+1}$, we apply the transformation established in DFT for changing from Euclidean to semi-norm representations. By Lemma 3.2, since $\mathcal{X}_t$ is (m, h)-past-representable, the vector $\boldsymbol{X}_t$ is representable on $C^{\|\cdot\|}_{m+h+1}$. The transformation from the Euclidean representation to the semi-norm representation proceeds as follows. Let $K^{\|\cdot\|} := \{\boldsymbol{s} \in S_{m+h+1} : \|\boldsymbol{s}\| = 0\}$ be the kernel of the semi-norm on the Euclidean unit sphere. Since $\boldsymbol{X}_t$ is representable on $C^{\|\cdot\|}_{m+h+1}$, we have $\Gamma(K^{\|\cdot\|}) = 0$. Define the projection mapping $T_{\|\cdot\|} : S_{m+h+1} \setminus K^{\|\cdot\|} \to C^{\|\cdot\|}_{m+h+1}$ by:

$$T_{\|\cdot\|}(\boldsymbol{s}) = \frac{\boldsymbol{s}}{\|\boldsymbol{s}\|} \tag{7.46}$$

By Proposition 2 of DFT, the spectral measure on the semi-norm unit cylinder is given by:

$$\Gamma^{\|\cdot\|}(A) = \int_{T^{-1}_{\|\cdot\|}(A)} \|\boldsymbol{s}\|_e^{-\alpha} \Gamma(d\boldsymbol{s}) \tag{7.47}$$

for any Borel set $A \subset C^{\|\cdot\|}_{m+h+1}$. Since the original spectral measure Γ from (7.45) is concentrated on atoms of the form $\{\vartheta \boldsymbol{d}_{j,k}/\|\boldsymbol{d}_{j,k}\|_e\}$, and since $\|\vartheta \boldsymbol{d}_{j,k}/\|\boldsymbol{d}_{j,k}\|_e\|_e = 1$, the transformation yields:

$$\Gamma^{\|\cdot\|}(A) = \sum_{j=1}^{J} \sum_{\vartheta \in S_1} \sum_{k \in \mathbb{Z}} w_{j,\vartheta} \pi_j^{\alpha} \sigma^{\alpha} \|\boldsymbol{d}_{j,k}\|_e^{\alpha} \cdot 1^{-\alpha} \cdot \mathbb{1}_A \left(\frac{\vartheta \boldsymbol{d}_{j,k}}{\|\boldsymbol{d}_{j,k}\|} \right) \tag{7.48}$$

where we use the fact that $\|\vartheta \boldsymbol{d}_{j,k}/\|\boldsymbol{d}_{j,k}\|_e\|_e = 1$ and $T_{\|\cdot\|}(\vartheta \boldsymbol{d}_{j,k}/\|\boldsymbol{d}_{j,k}\|_e) = \vartheta \boldsymbol{d}_{j,k}/\|\boldsymbol{d}_{j,k}\|$. Applying this transformation to (7.45), we obtain:

$$\Gamma^{\|\cdot\|} = \sigma^{\alpha} \sum_{j=1}^{J} \sum_{\vartheta \in S_1} \sum_{k \in \mathbb{Z}} w_{j,\vartheta} \pi_j^{\alpha} \|\boldsymbol{d}_{j,k}\|^{\alpha} \delta \left\{ \frac{\vartheta \boldsymbol{d}_{j,k}}{\|\boldsymbol{d}_{j,k}\|} \right\} \tag{7.49}$$

For the shift vector in the case $\alpha = 1$, the transformation yields:

$$\boldsymbol{\mu}^{\|\cdot\|} = -\frac{2\sigma}{\pi} \sum_{j=1}^{J} \sum_{k \in \mathbb{Z}} \pi_j \beta_j \boldsymbol{d}_{j,k} \ln \|\sigma \pi_j \boldsymbol{d}_{j,k}\| \tag{7.50}$$

This completes the proof that the spectral representation $(\Gamma^{\|\cdot\|}, \boldsymbol{\mu}^{\|\cdot\|})$ of $\boldsymbol{X}_t$ on $C^{\|\cdot\|}_{m+h+1}$ is given by (3.5) with the Euclidean norm $\|\cdot\|_e$ replaced by the semi-norm $\|\cdot\|$, and with the scale parameter σ explicitly included in all relevant terms.

7.5. Proof of Corollary 3.1

The equivalence between $(\iota\iota)$ and $(\iota\iota\iota)$ follows from Corollary 2 of DFT. From the proof of the Corollary in DFT, we also know that, for any j, if $m_{0,j} < +\infty$, then (3.6) holds for the sequence $(d_{j,k})_k$ for any $m \geq m_{0,j}$. For the aggregated process $\mathcal{X}_t = \sigma \sum_{j=1}^{J} \pi_j X_{j,t}$ with $\sigma > 0$, the effective moving average coefficients for each component j become $\sigma \pi_j d_{j,k}$ rather than $d_{j,k}$. However, the past-representability conditions depend only on the pattern of zeros and non-zeros in the coefficient sequences, not on their scaling. Specifically, for condition (3.4), we require:

$$\forall k \in \mathbb{Z}, \quad \Big[(\sigma \pi_j d_{j,k+m}, \ldots, \sigma \pi_j d_{j,k}) = \mathbf{0} \quad \Longrightarrow \quad \forall \ell \leq k-1, \quad \sigma \pi_j d_{j,\ell} = 0 \Big].$$

Since $\sigma > 0$ and $\pi_j > 0$ for all j, this is equivalent to:

$$\forall k \in \mathbb{Z}, \quad \Big[(d_{j,k+m}, \ldots, d_{j,k}) = \mathbf{0} \quad \Longrightarrow \quad \forall \ell \leq k-1, \quad d_{j,\ell} = 0 \Big].$$

Thus, the past-representability condition for the aggregated process is unchanged by the scaling factor σ. For the additional condition (3.6) when $\alpha = 1$ and the process is asymmetric, we need:

$$\sum_{k \in \mathbb{Z}} \|\sigma \pi_j \boldsymbol{d}_{j,k}\|_e \left| \ln \left(\|\sigma \pi_j \boldsymbol{d}_{j,k}\| / \|\sigma \pi_j \boldsymbol{d}_{j,k}\|_e \right) \right| < +\infty.$$

Since $\|\sigma \pi_j \boldsymbol{d}_{j,k}\|_e = \sigma \pi_j \|\boldsymbol{d}_{j,k}\|_e$ and the norm scales homogeneously, this becomes:

$$\sum_{k \in \mathbb{Z}} \sigma \pi_j \|\boldsymbol{d}_{j,k}\|_e \left| \ln \left(\|\boldsymbol{d}_{j,k}\| / \|\boldsymbol{d}_{j,k}\|_e \right) \right| < +\infty.$$

Since $\sigma\pi_j > 0$ is a finite constant, this condition is equivalent to:

$$\sum_{k\in\mathbb{Z}} \|\boldsymbol{d}_{j,k}\|_e \left| \ln\left(\|\boldsymbol{d}_{j,k}\| / \|\boldsymbol{d}_{j,k}\|_e \right) \right| < +\infty,$$

which is precisely condition (3.6) for the unscaled sequences. Therefore:

$$\begin{aligned} \sup_j m_{0,j} < +\infty &\implies \text{(3.6) holds for any sequence } (d_{j,k})_k \text{ for any } m \geq m_{0,j} \\ &\implies \text{(3.6) holds for any sequence } (\sigma\pi_j d_{j,k})_k \text{ for any } m \geq \max_j m_{0,j}. \end{aligned}$$

Thus, $(\iota\iota\iota)$ implies (ι). The reciprocal is clear. Regarding the last statement, notice that if $\mathcal{X}_t$ is (m,h)-past-representable for some $m < \max_j m_{0,j}$, there would then exist some j such that $m < m_{0,j}$. Hence, (3.4) would not hold with m for the particular sequence $(\sigma\pi_j d_{j,k})_k$, which is impossible by Lemma 3.2, since the past-representability depends only on the zero pattern, not the scaling.

7.6. Proof of Proposition 3.2

By Proposition 2 of DFT, the asymptotic conditional tail property states that for any Borel sets $A, B \subset C_{m+h+1}^{\|\cdot\|}$ with $\Gamma^{\|\cdot\|}\Big(\partial(A\cap B)\Big) = \Gamma^{\|\cdot\|}\big(\partial B\big) = 0$, and $\Gamma^{\|\cdot\|}(B) > 0$,

$$\mathbb{P}_x^{\|\cdot\|}(\boldsymbol{X_t}, A|B) \underset{x\to+\infty}{\longrightarrow} \frac{\Gamma^{\|\cdot\|}(A\cap B)}{\Gamma^{\|\cdot\|}(B)}.$$

Setting $B = B(V) = V \times \mathbb{R}^h$, we have

$$\mathbb{P}_x^{\|\cdot\|}\Big(\boldsymbol{X_t}, A\Big|B(V)\Big) \underset{x\to+\infty}{\longrightarrow} \frac{\Gamma^{\|\cdot\|}(A\cap B(V))}{\Gamma^{\|\cdot\|}(B(V))}.$$

From Proposition 3.1 $(\iota\iota)$, the spectral representation $(\Gamma^{\|\cdot\|}, \boldsymbol{\mu}^{\|\cdot\|})$ of the vector $\boldsymbol{X_t} = (\mathcal{X}_{t-m}, \ldots, \mathcal{X}_t, \mathcal{X}_{t+1}, \ldots, \mathcal{X}_{t+h})$ on $C_{m+h+1}^{\|\cdot\|}$ is given by equation (3.5) with the Euclidean norm $\|\cdot\|_e$ replaced by the semi-norm $\|\cdot\|$. From Lemma 3.1, the spectral measure can be written as:

$$\Gamma^{\|\cdot\|} = \sigma^\alpha \sum_{j=1}^{J} \sum_{\vartheta\in S_1} \sum_{k\in\mathbb{Z}} w_{j,\vartheta}\pi_j^\alpha \|\boldsymbol{d}_{j,k}\|^\alpha \delta_{\left\{\frac{\vartheta \boldsymbol{d}_{j,k}}{\|\boldsymbol{d}_{j,k}\|}\right\}},$$

where $\boldsymbol{d}_{j,k} = (d_{j,k+m}, \ldots, d_{j,k}, d_{j,k-1}, \ldots, d_{j,k-h})$, $w_{j,\vartheta} = (1+\vartheta\beta_j)/2$, and if $\boldsymbol{d}_{j,k} = \boldsymbol{0}$, the term vanishes by convention from the sums.

Now, we compute the numerator and denominator separately, we start by the numerator: $\Gamma^{\|\cdot\|}(A\cap B(V))$ Since $B(V) = V \times \mathbb{R}^h = \Big\{\boldsymbol{s} \in C_{m+h+1}^{\|\cdot\|} : \quad f(\boldsymbol{s}) \in V\Big\}$, we have:

$$A \cap B(V) = \{\boldsymbol{s} \in A : \quad f(\boldsymbol{s}) \in V\}.$$

The spectral measure $\Gamma^{\|\cdot\|}$ charges only the points of the form $\dfrac{\vartheta \boldsymbol{d}_{j,k}}{\|\boldsymbol{d}_{j,k}\|}$ for $(\vartheta, j, k) \in S_1 \times \{1, \ldots, J\} \times \mathbb{Z}$. Therefore:

$$\begin{aligned}
\Gamma^{\|\cdot\|}(A \cap B(V)) &= \sigma^\alpha \sum_{j=1}^{J} \sum_{\vartheta \in S_1} \sum_{k \in \mathbb{Z}} w_{j,\vartheta} \pi_j^\alpha \|\boldsymbol{d}_{j,k}\|^\alpha \delta_{\left\{ \frac{\vartheta \boldsymbol{d}_{j,k}}{\|\boldsymbol{d}_{j,k}\|} \right\}} (A \cap B(V)) \\
&= \sigma^\alpha \sum_{\substack{(\vartheta,j,k): \\ \frac{\vartheta \boldsymbol{d}_{j,k}}{\|\boldsymbol{d}_{j,k}\|} \in A \cap B(V)}} w_{j,\vartheta} \pi_j^\alpha \|\boldsymbol{d}_{j,k}\|^\alpha \\
&= \sigma^\alpha \sum_{\substack{(\vartheta,j,k): \\ \frac{\vartheta \boldsymbol{d}_{j,k}}{\|\boldsymbol{d}_{j,k}\|} \in A \text{ and } \frac{\vartheta f(\boldsymbol{d}_{j,k})}{\|\boldsymbol{d}_{j,k}\|} \in V}} w_{j,\vartheta} \pi_j^\alpha \|\boldsymbol{d}_{j,k}\|^\alpha .
\end{aligned}$$

This can be written as:

$$\Gamma^{\|\cdot\|}(A \cap B(V)) = \Gamma^{\|\cdot\|}\left(\left\{ \frac{\vartheta \boldsymbol{d}_{j,k}}{\|\boldsymbol{d}_{j,k}\|} \in A : \ \frac{\vartheta f(\boldsymbol{d}_{j,k})}{\|\boldsymbol{d}_{j,k}\|} \in V \right\} \right).$$

For the denominator $\Gamma^{\|\cdot\|}(B(V))$, we proceed as follows:

$$\begin{aligned}
\Gamma^{\|\cdot\|}(B(V)) &= \sigma^\alpha \sum_{\substack{(\vartheta,j,k): \\ \frac{\vartheta \boldsymbol{d}_{j,k}}{\|\boldsymbol{d}_{j,k}\|} \in B(V)}} w_{j,\vartheta} \pi_j^\alpha \|\boldsymbol{d}_{j,k}\|^\alpha \\
&= \sigma^\alpha \sum_{\substack{(\vartheta,j,k): \\ \frac{\vartheta f(\boldsymbol{d}_{j,k})}{\|\boldsymbol{d}_{j,k}\|} \in V}} w_{j,\vartheta} \pi_j^\alpha \|\boldsymbol{d}_{j,k}\|^\alpha .
\end{aligned}$$

This can be written as:

$$\Gamma^{\|\cdot\|}(B(V)) = \Gamma^{\|\cdot\|}\left(\left\{ \frac{\vartheta \boldsymbol{d}_{j,k}}{\|\boldsymbol{d}_{j,k}\|} \in C_{m+h+1}^{\|\cdot\|} : \ \frac{\vartheta f(\boldsymbol{d}_{j,k})}{\|\boldsymbol{d}_{j,k}\|} \in V \right\} \right).$$

Note that the factor σ^α appears in both the numerator and denominator, and therefore cancels out in the ratio:

$$\begin{aligned}
\frac{\Gamma^{\|\cdot\|}(A \cap B(V))}{\Gamma^{\|\cdot\|}(B(V))} &= \frac{\sigma^\alpha \sum_{\substack{(\vartheta,j,k): \\ \frac{\vartheta \boldsymbol{d}_{j,k}}{\|\boldsymbol{d}_{j,k}\|} \in A \text{ and } \frac{\vartheta f(\boldsymbol{d}_{j,k})}{\|\boldsymbol{d}_{j,k}\|} \in V}} w_{j,\vartheta} \pi_j^\alpha \|\boldsymbol{d}_{j,k}\|^\alpha}{\sigma^\alpha \sum_{\substack{(\vartheta,j,k): \\ \frac{\vartheta f(\boldsymbol{d}_{j,k})}{\|\boldsymbol{d}_{j,k}\|} \in V}} w_{j,\vartheta} \pi_j^\alpha \|\boldsymbol{d}_{j,k}\|^\alpha} \\
&= \frac{\Gamma^{\|\cdot\|}\left(\left\{ \frac{\vartheta \boldsymbol{d}_{j,k}}{\|\boldsymbol{d}_{j,k}\|} \in A : \ \frac{\vartheta f(\boldsymbol{d}_{j,k})}{\|\boldsymbol{d}_{j,k}\|} \in V \right\} \right)}{\Gamma^{\|\cdot\|}\left(\left\{ \frac{\vartheta \boldsymbol{d}_{j,k}}{\|\boldsymbol{d}_{j,k}\|} \in C_{m+h+1}^{\|\cdot\|} : \ \frac{\vartheta f(\boldsymbol{d}_{j,k})}{\|\boldsymbol{d}_{j,k}\|} \in V \right\} \right)}.
\end{aligned}$$

This establishes the desired result. The conclusion follows by considering the points of $B(V)$ and $A \cap B(V)$ that are charged by the spectral measure $\Gamma^{\|\cdot\|}$ given in equation (3.13). The presence of the scale parameter σ^α does not affect the asymptotic conditional probabilities as it appears multiplicatively in both the numerator and denominator of the ratio, thus canceling out in the final expression.

7.7. Proof of Lemma 3.3

By Proposition 3.1 and setting general scale parameter $\sigma > 0$, we have

$$\Gamma^{\|\cdot\|} = \sum_{j=1}^{J} \sum_{\vartheta \in S_1} \sum_{k \in \mathbb{Z}} w_{j,\vartheta} \sigma^{\alpha} \pi_j^{\alpha} \|\boldsymbol{d}_{j,k}\|^{\alpha} \delta_{\left\{\frac{\vartheta \boldsymbol{d}_{j,k}}{\|\boldsymbol{d}_{j,k}\|}\right\}},$$

with $\boldsymbol{d}_{j,k} = (\rho_j^{k+m} \mathbb{1}_{\{k+m \geq 0\}}, \ldots, \rho_j^{k-h} \mathbb{1}_{\{k-h \geq 0\}})$ for any $j = 1, \ldots, J$ and $k \in \mathbb{Z}$. Thus, for any $j \in \{1, \ldots, J\}$

$$\boldsymbol{d}_{j,k} = \begin{cases} \mathbf{0}, & \text{if} \quad k \leq -m-1, \\ (\rho_j^{k+m}, \ldots, \rho_j, 1, 0, \ldots, 0), & \text{if} \quad -m \leq k \leq h, \\ \rho_j^{k-h} \boldsymbol{d}_{j,h}, & \text{if} \quad k \geq h. \end{cases}$$

Therefore,

$$\Gamma^{\|\cdot\|} = \sum_{j=1}^{J} \sum_{\vartheta \in S_1} w_{j,\vartheta} \sigma^{\alpha} \pi_j^{\alpha} \left[\sum_{k=-m}^{h-1} \|\boldsymbol{d}_{j,k}\|^{\alpha} \delta_{\left\{\frac{\vartheta \boldsymbol{d}_{j,k}}{\|\boldsymbol{d}_{j,k}\|}\right\}} + \sum_{k=h}^{+\infty} |\rho_j|^{\alpha(k-h)} \|\boldsymbol{d}_{j,h}\|^{\alpha} \delta_{\left\{\frac{\vartheta \rho_j^{k-h} \boldsymbol{d}_{j,h}}{|\rho_j|^{k-h} \|\boldsymbol{d}_{j,h}\|}\right\}} \right].$$

Moreover,

$$\begin{aligned} &\sum_{j=1}^{J} \sum_{\vartheta \in S_1} w_{j,\vartheta} \sigma^{\alpha} \pi_j^{\alpha} \sum_{k=h}^{+\infty} |\rho_j|^{\alpha(k-h)} \|\boldsymbol{d}_{j,h}\|^{\alpha} \delta_{\left\{\mathrm{sign}(\rho_j)^{k-h} \frac{\vartheta \boldsymbol{d}_{j,h}}{\|\boldsymbol{d}_{j,h}\|}\right\}} \\ &\qquad = \sum_{j=1}^{J} \sum_{\vartheta \in S_1} \sigma^{\alpha} \pi_j^{\alpha} \|\boldsymbol{d}_{j,h}\|^{\alpha} \frac{1}{2} \left[\sum_{k=h}^{+\infty} |\rho_j|^{\alpha(k-h)} + \vartheta \beta_j \sum_{k=h}^{+\infty} (\rho_j^{<\alpha>})^{k-h} \right] \delta_{\left\{\frac{\vartheta \boldsymbol{d}_{j,h}}{\|\boldsymbol{d}_{j,h}\|}\right\}} \\ &\qquad = \sum_{j=1}^{J} \sum_{\vartheta \in S_1} \sigma^{\alpha} \pi_j^{\alpha} \frac{1}{1 - |\rho_j|^{\alpha}} \|\boldsymbol{d}_{j,h}\|^{\alpha} \bar{w}_{j,\vartheta} \delta_{\left\{\frac{\vartheta \boldsymbol{d}_{j,h}}{\|\boldsymbol{d}_{j,h}\|}\right\}}. \end{aligned}$$

Finally, noticing that for $k = -m$ and any $j \in \{1, \ldots, J\}$, $\boldsymbol{d}_{j,k} = (1, 0, \ldots, 0)$,

$$\begin{aligned} \Gamma^{\|\cdot\|} &= \sum_{j=1}^{J} \sum_{\vartheta \in S_1} \sigma^{\alpha} \pi_j^{\alpha} \left[w_{j,\vartheta} \sum_{k=-m}^{h-1} \|\boldsymbol{d}_{j,k}\|^{\alpha} \delta_{\left\{\frac{\vartheta \boldsymbol{d}_{j,k}}{\|\boldsymbol{d}_{j,k}\|}\right\}} + \frac{\bar{w}_{j,\vartheta}}{1 - |\rho_j|^{\alpha}} \|\boldsymbol{d}_{j,h}\|^{\alpha} \delta_{\left\{\frac{\vartheta \boldsymbol{d}_{j,h}}{\|\boldsymbol{d}_{j,h}\|}\right\}} \right] \\ &= \sum_{j=1}^{J} \sum_{\vartheta \in S_1} \sigma^{\alpha} \pi_j^{\alpha} \left[w_{j,\vartheta} \left(\delta_{\{(\vartheta,0,\ldots,0)\}} + \sum_{k=-m+1}^{h-1} \|\boldsymbol{d}_{j,k}\|^{\alpha} \delta_{\left\{\frac{\vartheta \boldsymbol{d}_{j,k}}{\|\boldsymbol{d}_{j,k}\|}\right\}} \right) + \frac{\bar{w}_{j,\vartheta}}{1 - |\rho_j|^{\alpha}} \|\boldsymbol{d}_{j,h}\|^{\alpha} \delta_{\left\{\frac{\vartheta \boldsymbol{d}_{j,h}}{\|\boldsymbol{d}_{j,h}\|}\right\}} \right] \\ &= \sum_{\vartheta \in S_1} \left[w_{\vartheta} \delta_{\{(\vartheta,0,\ldots,0)\}} + \sum_{j=1}^{J} \sigma^{\alpha} \pi_j^{\alpha} \left(w_{j,\vartheta} \sum_{k=-m+1}^{h-1} \|\boldsymbol{d}_{j,k}\|^{\alpha} \delta_{\left\{\frac{\vartheta \boldsymbol{d}_{j,k}}{\|\boldsymbol{d}_{j,k}\|}\right\}} + \frac{\bar{w}_{j,\vartheta}}{1 - |\rho_j|^{\alpha}} \|\boldsymbol{d}_{j,h}\|^{\alpha} \delta_{\left\{\frac{\vartheta \boldsymbol{d}_{j,h}}{\|\boldsymbol{d}_{j,h}\|}\right\}} \right) \right], \end{aligned}$$

where we have used the definition $w_{\vartheta} = \sum_{j=1}^{J} \sigma^{\alpha} \pi_j^{\alpha} w_{j,\vartheta}$.

7.8. Proof of Proposition 3.3

Lemma 7.2. *Let $\Gamma^{\|\cdot\|}$ be the spectral measure given in Lemma 3.3 with $\sigma > 0$ and assume that the ρ_j's are all positive. Letting $(\vartheta_0, j_0, k_0) \in \mathcal{I}$, consider*

$$I_0 := \left\{ \frac{\vartheta' \boldsymbol{d}_{j',k'}}{\|\boldsymbol{d}_{j',k'}\|} : \quad \frac{\vartheta' f(\boldsymbol{d}_{j',k'})}{\|\boldsymbol{d}_{j',k'}\|} = \frac{\vartheta_0 f(\boldsymbol{d}_{j_0,k_0})}{\|\boldsymbol{d}_{j_0,k_0}\|} \ \text{ for } \ (\vartheta', j', k') \in \mathcal{I} \right\}.$$

For $m \geq 1$, and $0 \leq k_0 \leq h$, then

$$I_0 = \left\{ \frac{\vartheta_0 \boldsymbol{d}_{j_0,k'}}{\|\boldsymbol{d}_{j_0,k'}\|} : \quad 0 \leq k' \leq h \right\}.$$

For $m \geq 1$, and $-m \leq k_0 \leq -1$, then

$$I_0 = \begin{cases} \left\{ \dfrac{\vartheta_0 \boldsymbol{d}_{j_0,k_0}}{\|\boldsymbol{d}_{j_0,k_0}\|} \right\}, & \text{if} \quad -m+1 \leq k_0 \leq -1 \\ \\ \left\{ \dfrac{\vartheta_0 \boldsymbol{d}_{0,k_0}}{\|\boldsymbol{d}_{0,k_0}\|} \right\} = \{(\vartheta_0, 0, \ldots, 0)\}, & \text{if} \quad k_0 = -m. \end{cases}$$

For $m = 0$, then

$$I_0 = \left\{ \frac{\vartheta_0 \boldsymbol{d}_{j',k'}}{\|\boldsymbol{d}_{j',k'}\|} : \quad (j',k') \in \{1,\ldots,J\} \times \{1,\ldots,h\} \cup \{(0,0)\} \right\}.$$

Proof. The key observation is that the parameter $\sigma > 0$ appears as a multiplicative factor in the spectral measure $\Gamma^{\|\cdot\|}$ but does **not** affect the normalized directions $\vartheta' \boldsymbol{d}_{j',k'}/\|\boldsymbol{d}_{j',k'}\|$ or their projections $\vartheta' f(\boldsymbol{d}_{j',k'})/\|\boldsymbol{d}_{j',k'}\|$. This is because σ only scales the overall magnitude of the spectral measure but does not change the geometric structure of the charged points on the unit cylinder. More precisely, from Lemma 3.3, the spectral measure takes the form:

$$\Gamma^{\|\cdot\|} = \sigma^\alpha \sum_{\vartheta \in S_1} \left[w_\vartheta \delta_{\{(\vartheta,0,\ldots,0)\}} + \sum_{j=1}^{J} \pi_j^\alpha \left(w_{j,\vartheta} \sum_{k=-m+1}^{h-1} \|\boldsymbol{d}_{j,k}\|^\alpha \delta_{\left\{ \frac{\vartheta \boldsymbol{d}_{j,k}}{\|\boldsymbol{d}_{j,k}\|} \right\}} + \frac{\bar{w}_{j,\vartheta}}{1-|\rho_j|^\alpha} \|\boldsymbol{d}_{j,h}\|^\alpha \delta_{\left\{ \frac{\vartheta \boldsymbol{d}_{j,h}}{\|\boldsymbol{d}_{j,h}\|} \right\}} \right) \right],$$

The factor σ^α multiplies the entire spectral measure uniformly, but the support of $\Gamma^{\|\cdot\|}$ (i.e., the set of points where $\Gamma^{\|\cdot\|}$ assigns positive mass) consists exactly of the normalized directions:

$$\operatorname{supp}(\Gamma^{\|\cdot\|}) = \left\{ (\vartheta, 0, \ldots, 0), \frac{\vartheta \boldsymbol{d}_{j,k}}{\|\boldsymbol{d}_{j,k}\|} : \vartheta \in S_1, j \in \{1,\ldots,J\}, k \in \{-m+1,\ldots,h\} \right\}$$

Since the condition defining I_0 involves only the equality of normalized projections:

$$\frac{\vartheta' f(\boldsymbol{d}_{j',k'})}{\|\boldsymbol{d}_{j',k'}\|} = \frac{\vartheta_0 f(\boldsymbol{d}_{j_0,k_0})}{\|\boldsymbol{d}_{j_0,k_0}\|}$$

and since these normalized directions are independent of σ, the analysis proceeds exactly as in the case $\sigma = 1$.

Case $m \geq 1$ and $k_0 \in \{0,\ldots,h\}$

If $k' \in \{-m,\ldots,-1\}$, the $(m+1)$-th component of $f(\boldsymbol{d}_{j',k'})$ is zero, whereas the $(m+1)$-th component of $f(\boldsymbol{d}_{j_0,k_0})$ is $\rho_{j_0}^{k_0} \neq 0$. This geometric relationship is unaffected by σ.

Necessarily, $\vartheta' f(\boldsymbol{d}_{j',k'})/\|\boldsymbol{d}_{j',k'}\| \neq \vartheta_0 f(\boldsymbol{d}_{j_0,k_0})/\|\boldsymbol{d}_{j_0,k_0}\|$ and

$$I_0 = \left\{ \frac{\vartheta' \boldsymbol{d}_{j',k'}}{\|\boldsymbol{d}_{j',k'}\|} : \quad \frac{\vartheta' f(\boldsymbol{d}_{j',k'})}{\|\boldsymbol{d}_{j',k'}\|} = \frac{\vartheta_0 f(\boldsymbol{d}_{j_0,k_0})}{\|\boldsymbol{d}_{j_0,k_0}\|} \text{ for } (\vartheta',j',k') \in \{-1,+1\} \times \{1,\ldots,J\} \times \{0,\ldots,h\} \right\}.$$

Now, with $k' \in \{0, \dots, h\}$, we have that

$$f(\boldsymbol{d}_{j',k'}) = (\rho_{j'}^{k'+m}, \dots, \rho_{j'}^{k'+1}, \rho_{j'}^{k'}),$$
$$f(\boldsymbol{d}_{j_0,k_0}) = (\rho_{j_0}^{k_0+m}, \dots, \rho_{j_0}^{k_0+1}, \rho_{j_0}^{k_0}),$$

and by (3.3) we also have that

$$\|\boldsymbol{d}_{j',k'}\| = \|(\rho_{j'}^{k'+m}, \dots, \rho_{j'}^{k'+1}, \rho_{j'}^{k'}, \overbrace{0, \dots, 0}^{h})\|,$$
$$\|\boldsymbol{d}_{j_0,k_0}\| = \|(\rho_{j_0}^{k_0+m}, \dots, \rho_{j_0}^{k_0+1}, \rho_{j_0}^{k_0}, \underbrace{0, \dots, 0}_{h})\|.$$

The key observation is that these norms and the resulting normalized directions are independent of σ. Thus,

$$\begin{aligned}
\frac{\vartheta' f(\boldsymbol{d}_{j',k'})}{\|\boldsymbol{d}_{j',k'}\|} = \frac{\vartheta_0 f(\boldsymbol{d}_{j_0,k_0})}{\|\boldsymbol{d}_{j_0,k_0}\|} & \\
\iff \frac{\vartheta' \rho_{j'}^{k'} f\left(\boldsymbol{d}_{j',0}\right)}{|\rho_{j'}|^{k'}\|\boldsymbol{d}_{j',0}\|} &= \frac{\vartheta_0 \rho_{j_0}^{k_0} f\left(\boldsymbol{d}_{j_0,0}\right)}{|\rho_{j_0}|^{k_0}\|\boldsymbol{d}_{j_0,0}\|} \\
\iff \frac{\vartheta' \rho_{j'}^{\ell}}{\|\boldsymbol{d}_{j',0}\|} &= \frac{\vartheta_0 \rho_{j_0}^{\ell}}{\|\boldsymbol{d}_{j_0,0}\|}, \qquad \ell = 0, \dots, m \\
\iff \vartheta'\vartheta_0 \frac{\|\boldsymbol{d}_{j_0,0}\|}{\|\boldsymbol{d}_{j',0}\|} &= \left(\frac{\rho_{j_0}}{\rho_{j'}}\right)^{\ell}, \quad \ell = 0, \dots, m \\
\iff \rho_{j'} = \rho_{j_0} \quad &\text{and} \quad \vartheta'\vartheta_0 = 1 \\
\iff j' = j_0 \quad &\text{and} \quad \vartheta' = \vartheta_0,
\end{aligned}$$

because the ρ_j's are assumed to be non-zero and distinct.

Case $m \geq 1$ and $k_0 \in \{-m, \dots, -1\}$

By comparing the place of the first zero component, it is easy to see that

$$\frac{\vartheta' f(\boldsymbol{d}_{j',k'})}{\|\boldsymbol{d}_{j',k'}\|} = \frac{\vartheta_0 f(\boldsymbol{d}_{j_0,k_0})}{\|\boldsymbol{d}_{j_0,k_0}\|} \implies k' = k_0.$$

$$f(\boldsymbol{d}_{j',k'}) = (\overbrace{\rho_{j'}^{k'+m}, \dots, \rho_{j'}, 1, 0, \dots, 0}^{m+1}),$$
$$f(\boldsymbol{d}_{j_0,k_0}) = (\underbrace{\rho_{j_0}^{k_0+m}, \dots, \rho_{j_0}, 1, 0, \dots, 0}_{m+1}),$$

and we also have that

$$\|\boldsymbol{d}_{j',k'}\| = \|(\overbrace{\rho_{j'}^{k'+m}, \dots, \rho_{j'}, 1, 0, \dots, 0}^{m+1}, \overbrace{0, \dots, 0}^{h})\|,$$
$$\|\boldsymbol{d}_{j_0,k_0}\| = \|(\underbrace{\rho_{j_0}^{k_0+m}, \dots, \rho_{j_0}, 1, 0, \dots, 0}_{m+1}, \underbrace{0, \dots, 0}_{h})\|.$$

As $k' = k_0 \leq -1$, the condition becomes:

$$\begin{aligned}\frac{\vartheta' f(\boldsymbol{d}_{j',k'})}{\|\boldsymbol{d}_{j',k'}\|} = \frac{\vartheta_0 f(\boldsymbol{d}_{j_0,k_0})}{\|\boldsymbol{d}_{j_0,k_0}\|} \\ \iff \frac{\vartheta' \rho_{j'}^{\ell}}{\|\boldsymbol{d}_{j',k_0}\|} = \frac{\vartheta_0 \rho_{j_0}^{\ell}}{\|\boldsymbol{d}_{j_0,k_0}\|}, \quad \ell = 0, \dots, m + k_0, \text{ and } k' = k_0 \\ \iff \vartheta'\vartheta_0 \frac{\|\boldsymbol{d}_{j_0,k_0}\|}{\|\boldsymbol{d}_{j',k_0}\|} = \left(\frac{\rho_{j_0}}{\rho_{j'}}\right)^{\ell}, \quad \ell = 0, \dots, m + k_0, \text{ and } k' = k_0.\end{aligned}$$

Now if $-m + 1 \leq k_0 \leq -1$,

$$\begin{aligned}\vartheta'\vartheta_0 \frac{\|\boldsymbol{d}_{j_0,k_0}\|}{\|\boldsymbol{d}_{j',k_0}\|} = \left(\frac{\rho_{j_0}}{\rho_{j'}}\right)^{\ell}, \quad \ell = 0, 1, \dots, m + k_0, \text{ and } k' = k_0 \\ \iff \vartheta' = \vartheta_0 \quad \text{and} \quad j' = j_0 \quad \text{and} \quad k' = k_0.\end{aligned}$$

If $k_0 = -m$, given that $(\vartheta_0, j_0, k_0) \in \mathcal{I} = S_1 \times \Big(\{1, \dots, J\} \times \{-m, \dots, -1, 0, 1, \dots, h\} \cup \{(0, -m)\}\Big)$, then necessarily $j_0 = 0$. Furthermore, as $k' = k_0 = -m$, we similarly have that $j' = j_0 = 0$ and thus $\boldsymbol{d}_{j',k_0} = \boldsymbol{d}_{j_0,k_0} = \boldsymbol{d}_{0,-m} = (1, 0, \dots, 0)$.

Hence

$$\begin{aligned}\vartheta'\vartheta_0 \frac{\|\boldsymbol{d}_{j_0,k_0}\|}{\|\boldsymbol{d}_{j',k_0}\|} = \left(\frac{\rho_{j_0}}{\rho_{j'}}\right)^{\ell}, \quad \ell = 0, \text{ and } k' = k_0 = -m \text{ and } j' = j_0 = 0, \\ \iff \vartheta' = \vartheta_0 \text{ and } k' = k_0 = -m \text{ and } j' = j_0 = 0\end{aligned}$$

Case $m = 0$

If $k_0 \in \{1, \dots, h\}$ then $f(\boldsymbol{d}_{j_0,k_0}) = \rho_{j_0}^{k_0}$ and by (3.3), $\|\boldsymbol{d}_{j_0,k_0}\| = |\rho_{j_0}|^{k_0}$. Thus, $\vartheta_0 f(\boldsymbol{d}_{j_0,k_0})/\|\boldsymbol{d}_{j_0,k_0}\| = \vartheta_0$.

If $k_0 = -m = 0$, then $j_0 = 0$ and $f(\boldsymbol{d}_{j_0,k_0}) = 1$ and $\vartheta_0 f(\boldsymbol{d}_{j_0,k_0})/\|\boldsymbol{d}_{j_0,k_0}\| = \vartheta_0$.

The same holds for $(\vartheta', j', k') \in \mathcal{I}$ and we obtain that

$$\frac{\vartheta' f(\boldsymbol{d}_{j',k'})}{\|\boldsymbol{d}_{j',k'}\|} = \frac{\vartheta_0 f(\boldsymbol{d}_{j_0,k_0})}{\|\boldsymbol{d}_{j_0,k_0}\|} \iff \vartheta' = \vartheta_0.$$

Proof. By Proposition 3.2,

$$\mathbb{P}_x^{\|\cdot\|}\Big(\boldsymbol{X}_{\boldsymbol{t}}, A_{\vartheta,j,k} \Big| B(V_0)\Big) \underset{x\to\infty}{\longrightarrow} \frac{\Gamma^{\|\cdot\|}\left(\left\{\frac{\vartheta' \boldsymbol{d}_{j',k'}}{\|\boldsymbol{d}_{j',k'}\|} \in A_{\vartheta,j,k} : \frac{\vartheta' f(\boldsymbol{d}_{j',k'})}{\|\boldsymbol{d}_{j',k'}\|} \in V_0\right\}\right)}{\Gamma^{\|\cdot\|}\left(\left\{\frac{\vartheta' \boldsymbol{d}_{j',k'}}{\|\boldsymbol{d}_{j',k'}\|} \in C_{m+h+1}^{\|\cdot\|} : \frac{\vartheta' f(\boldsymbol{d}_{j',k'})}{\|\boldsymbol{d}_{j',k'}\|} \in V_0\right\}\right)}. \tag{7.51}$$

Focusing on the denominator, we have by (3.16)

$$\Gamma^{\|\cdot\|}\left(\left\{\frac{\vartheta' \boldsymbol{d}_{j',k'}}{\|\boldsymbol{d}_{j',k'}\|} \in C_{m+h+1}^{\|\cdot\|} : \frac{\vartheta' f(\boldsymbol{d}_{j',k'})}{\|\boldsymbol{d}_{j',k'}\|} \in V_0\right\}\right) = \Gamma^{\|\cdot\|}\left(\left\{\frac{\vartheta' \boldsymbol{d}_{j',k'}}{\|\boldsymbol{d}_{j',k'}\|} \in C_{m+h+1}^{\|\cdot\|} : \frac{\vartheta' f(\boldsymbol{d}_{j',k'})}{\|\boldsymbol{d}_{j',k'}\|} = \frac{\vartheta_0 f(\boldsymbol{d}_{j_0,k_0})}{\|\boldsymbol{d}_{j_0,k_0}\|}\right\}\right)$$

We will now distinguish the cases arising from the application of Lemma 7.2. Recall that we assume for this proposition that the ρ_j's are positive. Thus, $\text{sign}(\rho_j) = 1$ and $\bar{\beta}_j = \beta_j \frac{1 - |\rho_j|^{\alpha}}{1 - \rho_j^{<\alpha>}} = \beta_j$ and $\bar{w}_{j,\vartheta} = w_{j,\vartheta}$ in (3.15) for all j's and $\vartheta \in \{-1, +1\}$.

Case $m \geq 1$ and $0 \leq k_0 \leq h$

By Lemma 7.2,

$$\Gamma^{\|\cdot\|}\left(\left\{\frac{\vartheta' \boldsymbol{d}_{j',k'}}{\|\boldsymbol{d}_{j',k'}\|} \in C^{\|\cdot\|}_{m+h+1} : \quad \frac{\vartheta' f(\boldsymbol{d}_{j',k'})}{\|\boldsymbol{d}_{j',k'}\|} = \frac{\vartheta_0 f(\boldsymbol{d}_{j_0,k_0})}{\|\boldsymbol{d}_{j_0,k_0}\|}\right\}\right)$$
$$= \Gamma^{\|\cdot\|}\left(\left\{\frac{\vartheta_0 \boldsymbol{d}_{j_0,k'}}{\|\boldsymbol{d}_{j_0,k'}\|} : \quad 0 \leq k' \leq h\right\}\right)$$
$$= \sigma^\alpha \pi^\alpha_{j_0}\left[w_{j_0,\vartheta_0}\sum_{k'=0}^{h-1}\|\boldsymbol{d}_{j_0,k'}\|^\alpha + \frac{\bar{w}_{j_0,\vartheta_0}}{1-|\rho_{j_0}|^\alpha}\|\boldsymbol{d}_{j_0,h}\|^\alpha\right]$$

By (3.3), for $k' \in \{0,1,\ldots,h\}$

$$\|\boldsymbol{d}_{j_0,k'}\| = \|(\rho_{j_0}^{k'+m},\ldots,\rho_{j_0}^{k'+1},\rho_{j_0}^{k'},\underbrace{0,\ldots,0}_{h})\|$$
$$= |\rho_{j_0}|^{k'-h}\|(\rho_{j_0}^{m+h},\ldots,\rho_{j_0}^{h+1},\rho_{j_0}^{h},\underbrace{0,\ldots,0}_{h})\|$$
$$= |\rho_{j_0}|^{k'-h}\|\boldsymbol{d}_{j_0,h}\|.$$

Thus,

$$\Gamma^{\|\cdot\|}\left(\left\{\frac{\vartheta' \boldsymbol{d}_{j',k'}}{\|\boldsymbol{d}_{j',k'}\|} \in C^{\|\cdot\|}_{m+h+1} : \quad \frac{\vartheta' f(\boldsymbol{d}_{j',k'})}{\|\boldsymbol{d}_{j',k'}\|} = \frac{\vartheta_0 f(\boldsymbol{d}_{j_0,k_0})}{\|\boldsymbol{d}_{j_0,k_0}\|}\right\}\right)$$
$$= \sigma^\alpha \pi^\alpha_{j_0} w_{j_0,\vartheta_0}\|\boldsymbol{d}_{j_0,h}\|^\alpha\left[\sum_{k'=0}^{h-1}|\rho_{j_0}|^{\alpha(k'-h)} + \frac{1}{1-|\rho_{j_0}|^\alpha}\right]$$
$$= \sigma^\alpha \pi^\alpha_{j_0} w_{j_0,\vartheta_0}\|\boldsymbol{d}_{j_0,h}\|^\alpha \frac{|\rho_{j_0}|^{-\alpha h}}{1-|\rho_{j_0}|^\alpha}.$$

Similarly for the numerator in (7.51), by (3.17),

$$\Gamma^{\|\cdot\|}\left(\left\{\frac{\vartheta' \boldsymbol{d}_{j',k'}}{\|\boldsymbol{d}_{j',k'}\|} \in A_{\vartheta,j,k} : \quad \frac{\vartheta' f(\boldsymbol{d}_{j',k'})}{\|\boldsymbol{d}_{j',k'}\|} \in V_0\right\}\right)$$
$$= \Gamma^{\|\cdot\|}\left(\left\{\frac{\vartheta_0 \boldsymbol{d}_{j_0,k'}}{\|\boldsymbol{d}_{j_0,k'}\|} \in A_{\vartheta,j,k} : \quad 0 \leq k' \leq h\right\}\right)$$

$$= \begin{cases} \Gamma^{\|\cdot\|}\left(\left\{\dfrac{\vartheta_0 \boldsymbol{d}_{j_0,k}}{\|\boldsymbol{d}_{j_0,k}\|}\right\}\right), & \text{if} \quad j = j_0 \quad \text{and} \quad \vartheta = \vartheta_0, \\ \Gamma^{\|\cdot\|}(\emptyset), & \text{if} \quad j \neq j_0 \quad \text{or} \quad \vartheta \neq \vartheta_0, \end{cases}$$

$$= \begin{cases} \sigma^\alpha \pi^\alpha_{j_0} w_{j_0,\vartheta_0}\|\boldsymbol{d}_{j_0,h}\|^\alpha |\rho_{j_0}|^{\alpha(k-h)}\delta_{\{\vartheta_0\}}(\vartheta)\delta_{\{j_0\}}(j), & \text{if} \quad 0 \leq k \leq h-1, \\ \sigma^\alpha \pi^\alpha_{j_0} w_{j_0,\vartheta_0}\|\boldsymbol{d}_{j_0,h}\|^\alpha \dfrac{1}{1-|\rho_{j_0}|^\alpha}\delta_{\{\vartheta_0\}}(\vartheta)\delta_{\{j_0\}}(j), & \text{if} \quad k = h. \end{cases}$$

The σ^α terms cancel out in the ratio.

Case $m \geq 1$ and $-m \leq k_0 \leq -1$

We have by Lemma 7.2

$$\Gamma^{\|\cdot\|}\left(\left\{\frac{\vartheta' \boldsymbol{d}_{j',k'}}{\|\boldsymbol{d}_{j',k'}\|} \in C^{\|\cdot\|}_{m+h+1} : \quad \frac{\vartheta' f(\boldsymbol{d}_{j',k'})}{\|\boldsymbol{d}_{j',k'}\|} = \frac{\vartheta_0 f(\boldsymbol{d}_{j_0,k_0})}{\|\boldsymbol{d}_{j_0,k_0}\|}\right\}\right) = \Gamma^{\|\cdot\|}\left(\left\{\frac{\vartheta_0 \boldsymbol{d}_{j_0,k_0}}{\|\boldsymbol{d}_{j_0,k_0}\|}\right\}\right).$$

If $-m+1 \leq k_0 \leq -1$,

$$\Gamma^{\|\cdot\|}\left(\left\{\frac{\vartheta_0 \boldsymbol{d}_{j_0,k_0}}{\|\boldsymbol{d}_{j_0,k_0}\|}\right\}\right) = \sigma^\alpha \pi^\alpha_{j_0} w_{j_0,\vartheta_0} \|\boldsymbol{d}_{j_0,k_0}\|^\alpha,$$

and

$$\begin{aligned}
&\Gamma^{\|\cdot\|}\left(\left\{\frac{\vartheta' \boldsymbol{d}_{j',k'}}{\|\boldsymbol{d}_{j',k'}\|} \in A_{\vartheta,j,k} : \quad \frac{\vartheta' f(\boldsymbol{d}_{j',k'})}{\|\boldsymbol{d}_{j',k'}\|} \in V_0\right\}\right) \\
&\qquad = \Gamma^{\|\cdot\|}\left(A_{\vartheta,j,k} \cap \left\{\frac{\vartheta_0 \boldsymbol{d}_{j_0,k_0}}{\|\boldsymbol{d}_{j_0,k_0}\|}\right\}\right) \\
&\qquad = \begin{cases} \Gamma^{\|\cdot\|}\left(\left\{\dfrac{\vartheta_0 \boldsymbol{d}_{j_0,k_0}}{\|\boldsymbol{d}_{j_0,k_0}\|}\right\}\right), & \text{if } j = j_0 \text{ and } \vartheta = \vartheta_0, \text{ and } k = k_0, \\ \Gamma^{\|\cdot\|}(\emptyset), & \text{if } j \neq j_0 \text{ or } \vartheta \neq \vartheta_0 \text{ or } k \neq k_0, \end{cases} \\
&\qquad = \sigma^\alpha \pi^\alpha_{j_0} w_{j_0,\vartheta_0} \|\boldsymbol{d}_{j_0,k_0}\|^\alpha \delta_{\{\vartheta_0\}}(\vartheta)\delta_{\{j_0\}}(j)\delta_{\{k_0\}}(k).
\end{aligned}$$

If $k_0 = -m$, then $\boldsymbol{d}_{j_0,k_0} = \boldsymbol{d}_{0,-m} = (1,0,\ldots,0)$, and

$$\Gamma^{\|\cdot\|}\left(\left\{\frac{\vartheta_0 \boldsymbol{d}_{j_0,k_0}}{\|\boldsymbol{d}_{j_0,k_0}\|}\right\}\right) = \Gamma^{\|\cdot\|}\Big(\{\vartheta_0(1,0,\ldots,0)\}\Big) = \sigma^\alpha w_{\vartheta_0},$$

and

$$\begin{aligned}
&\Gamma^{\|\cdot\|}\left(\left\{\frac{\vartheta' \boldsymbol{d}_{j',k'}}{\|\boldsymbol{d}_{j',k'}\|} \in A_{\vartheta,j,k} : \quad \frac{\vartheta' f(\boldsymbol{d}_{j',k'})}{\|\boldsymbol{d}_{j',k'}\|} \in V_0\right\}\right) \\
&\qquad = \Gamma^{\|\cdot\|}\left(A_{\vartheta,j,k} \cap \left\{\frac{\vartheta_0 \boldsymbol{d}_{j_0,k_0}}{\|\boldsymbol{d}_{j_0,k_0}\|}\right\}\right) \\
&\qquad = \begin{cases} \Gamma^{\|\cdot\|}\Big(A_{\vartheta,j,k} \cap \{\vartheta_0(1,0,\ldots,0)\}\Big), & \text{if } \vartheta = \vartheta_0, \text{ and } k = k_0 = -m, \text{ and } j = j_0 = 0 \\ \Gamma^{\|\cdot\|}(\emptyset), & \text{if } \vartheta \neq \vartheta_0 \text{ or } k \neq k_0, \text{ or } j \neq j_0 \end{cases} \\
&\qquad = \sigma^\alpha w_{\vartheta_0} \delta_{\{\vartheta_0\}}(\vartheta)\delta_{\{j_0\}}(j)\delta_{\{k_0\}}(k).
\end{aligned}$$

Again, the σ^α terms cancel out in the ratio.

Case $m = 0$

By Lemma 7.2, as the ρ_j's are positive

$$\Gamma^{\|\cdot\|}\left(\left\{\frac{\vartheta' \boldsymbol{d}_{j',k'}}{\|\boldsymbol{d}_{j',k'}\|} \in C^{\|\cdot\|}_{m+h+1} : \quad \frac{\vartheta' f(\boldsymbol{d}_{j',k'})}{\|\boldsymbol{d}_{j',k'}\|} = \frac{\vartheta_0 f(\boldsymbol{d}_{j_0,k_0})}{\|\boldsymbol{d}_{j_0,k_0}\|}\right\}\right)$$
$$= \Gamma^{\|\cdot\|}\left(\left\{\frac{\vartheta_0 \boldsymbol{d}_{j',k'}}{\|\boldsymbol{d}_{j',k'}\|} \in C^{\|\cdot\|}_{m+h+1} : \quad (j',k') \in \{1,\dots,J\} \times \{0,\dots,h\} \cup \{(0,0)\}\right\}\right)$$

Given that $w_{\vartheta_0} = \sum_{j'=1}^J \pi_{j'}^\alpha w_{j',\vartheta_0}$ and $\|\boldsymbol{d}_{j',k'}\| = |\rho_{j'}|^{k'}$, for any $1 \le j' \le J$, $1 \le k' \le h$,

$$\Gamma^{\|\cdot\|}\left(\left\{\frac{\vartheta' \boldsymbol{d}_{j',k'}}{\|\boldsymbol{d}_{j',k'}\|} \in C^{\|\cdot\|}_{m+h+1} : \quad \frac{\vartheta' f(\boldsymbol{d}_{j',k'})}{\|\boldsymbol{d}_{j',k'}\|} = \frac{\vartheta_0 f(\boldsymbol{d}_{j_0,k_0})}{\|\boldsymbol{d}_{j_0,k_0}\|}\right\}\right)$$
$$= \sigma^\alpha w_{\vartheta_0} + \sigma^\alpha \sum_{j'=1}^J \pi_{j'}^\alpha w_{j',\vartheta_0}\left[\sum_{k'=1}^{h-1} \|\boldsymbol{d}_{j',k'}\|^\alpha + \frac{\|\boldsymbol{d}_{j',h}\|^\alpha}{1-|\rho_{j'}|^\alpha}\right]$$
$$= \sigma^\alpha \sum_{j'=1}^J \pi_{j'}^\alpha w_{j',\vartheta_0}\left[1 + \sum_{k'=1}^{h-1} |\rho_{j'}|^{\alpha k'} + \frac{|\rho_{j'}|^{\alpha h}}{1-|\rho_{j'}|^\alpha}\right]$$
$$= \sigma^\alpha \sum_{j'=1}^J \pi_{j'}^\alpha w_{j',\vartheta_0}\left[\frac{1-|\rho_{j'}|^{\alpha h}}{1-|\rho_{j'}|^\alpha} + \frac{|\rho_{j'}|^{\alpha h}}{1-|\rho_{j'}|^\alpha}\right]$$
$$= \sigma^\alpha \sum_{j'=1}^J \pi_{j'}^\alpha w_{j',\vartheta_0} \frac{1}{1-|\rho_{j'}|^\alpha}.$$

Similarly, by (3.17),

$$\Gamma^{\|\cdot\|}\left(\left\{\frac{\vartheta' \boldsymbol{d}_{j',k'}}{\|\boldsymbol{d}_{j',k'}\|} \in A_{\vartheta,j,k} : \quad \frac{\vartheta' f(\boldsymbol{d}_{j',k'})}{\|\boldsymbol{d}_{j',k'}\|} \in V_0\right\}\right)$$
$$= \Gamma^{\|\cdot\|}\left(A_{\vartheta,j,k} \cap \left\{\frac{\vartheta_0 \boldsymbol{d}_{j',k'}}{\|\boldsymbol{d}_{j',k'}\|} \in C^{\|\cdot\|}_{m+h+1} : \quad (j',k') \in \{1,\dots,J\} \times \{0,\dots,h\} \cup \{(0,0)\}\right\}\right)$$

$$= \begin{cases} \Gamma^{\|\cdot\|}\left(\left\{\dfrac{\vartheta_0 \boldsymbol{d}_{j,k}}{\|\boldsymbol{d}_{j,k}\|}\right\}\right), & \text{if } \vartheta = \vartheta_0, \\ \Gamma^{\|\cdot\|}(\emptyset), & \text{if } \vartheta \ne \vartheta_0, \end{cases}$$

$$= \begin{cases} \sigma^\alpha \sum_{j'=1}^J \pi_{j'}^\alpha w_{j',\vartheta_0} \delta_{\{\vartheta_0\}}(\vartheta), & \text{if } \quad k = 0, \\ \sigma^\alpha \pi_j^\alpha w_{j,\vartheta_0} |\rho_j|^{\alpha k} \delta_{\{\vartheta_0\}}(\vartheta), & \text{if } \quad 1 \le k \le h-1, \\ \sigma^\alpha \pi_j^\alpha w_{j,\vartheta_0} \dfrac{|\rho_j|^{\alpha h}}{1-|\rho_j|^\alpha} \delta_{\{\vartheta_0\}}(\vartheta), & \text{if } \quad k = h. \end{cases}$$

The conclusion follows.

References

Acharya, V., and Rajan, R. 2024. Liquidity, Liquidity Everywhere, Not A Drop To Use - Why Flooding Banks With Central Bank Reserves May Not Expand Liquidity. *Journal of Finance*, 79(5), 2943-2991.

Acharya, V., Crosignani, M., Eisert, T., and Eufinger, C. 2024. Zombie Credit and (Dis-)Inflation: Evidence from Europe. *Journal of Finance*, 79(3), 1883-1929.

Agliari, A., Naimzada, A., Pecora, N. (2018). Boom-bust dynamics in a stock market participation model with heterogeneous traders. *Journal of Economic Dynamics and Control*, 91, 458-468.

Allen, F., Barlevy, G., and Gale, D. 2023. Risk premia, asset price bubbles, and monetary policy. *Journal of Behavioral and Experimental Finance*.

Andrews, B., Calder, M., and R., Davis. 2009. Maximum likelihood estimation for α-stable autoregressive process. *Annals of Statistics*, 37, 1946-1982.

Basrak, B., Planinić, H., and P., Soulier. 2016. An invariance principle for sums and record times of regularly varying stationary sequences. *Probability Theory and Related Fields*, 1-46.

Basrak, B., and J., Segers. 2009. Regularly varying multivariate time series. *Stochastic processes and their applications*, 119, 1055-1080.

Behme, A. D. 2011. Distributional properties of solutions of $dV_t = V_t - dU_t + dL_t$ with Lévy noise. *Advances in Applied Probability*, 43(3), 688-711.

Behme, A., Lindner, A., and R., Maller. 2011. Stationary solutions of the stochastic differential equation with Lévy noise. *Stochastic Processes and their Applications*, 121, 91-108.

Blanchard, O.J., and Watson, M.W. 1982. Bubbles, Rational Expectations and Financial Markets. *NBER Working Papers*, 0945.

Biagini, F., and Mancin, J. 2017. Financial asset price bubbles under model uncertainty. *Probability, Uncertainty and Quantitative Risk*, 2(1), 1-29.

Biagini, F., and Nedelcu, S. 2015. The Formation of Financial Bubbles in Defaultable Markets. *SIAM J. Fin. Math.*, 6(1), 530-558.

Biagini, F., Föllmer, H., and Nedelcu, S. 2014. Shifting martingale measures and the birth of a bubble as a submartingale. *Finance and Stochastics*, 18(2), 297-326.

Brockwell, P.J., and Davis, R.A. 1991. *Time series: theory and methods*. Springer science & business media.

Carvalho, V.M., Martin, A., and Ventura, J. 2012. Understanding bubbly episodes. *American Economic Review*, 102(3), 95-100.

Cavaliere, G., Nielsen, H.B., and Rahbek, A. 2020. Bootstrapping noncausal autoregressions: with applications to explosive bubble modeling. *Journal of Business & Economic Statistics*, 38(1), 55-67.

Chen, B., Choi, J., and J. C., Escanciano. 2017. Testing for fundamental vector moving average representations. *Quantitative Economics*, 8, 149-180.

Cioczek-Georges, R., and M. S., Taqqu. 1994. How do conditional moments of stable vectors depend on the spectral measure? *Stochastic processes and their applications*, 54, 95-111.

Cioczek-Georges, R., and M. S., Taqqu. 1998. Sufficient conditions for the existence of conditional moments of stable

random variables. *Stochastic Processes and Related Topics*, Birkhäuser Boston, 35-67.

Cubadda, G., Hecq, A., Telg, S. (2019). Detecting Co-Movements in Non-Causal Time Series. *Oxford Bulletin of Economics and Statistics*, 81(3), 697-715.

Erdős, P. and A. H., Stone. 1970. On the sum of two Borel sets. *Proceedings of the American Mathematical Society*, 25, 304-306.

de Truchis, G., Fries, S., Thomas, A. (2025). Forecasting Extreme Trajectories Using Seminorm Representations *Working Paper 2025-06*, Chaire Économie du Climat, Paris.

de Truchis, G., Thomas, A., L. Vaudrée (2025). Deconvolution and Filtering of Non-Causal Alpha-Stable Processes *On going paper.*

de Truchis, G., Dumitrescu, E.I., Fries, S., and Thomas, A. 2024. Bet on a bubble asset? An optimal portfolio allocation strategy. *Mimeo*

Dumitrescu, E.I., and Thomas, A. 2024. Learning the predictive density of mixed-causal ARMA processes. *Mimeo*

Doukhan, P. 1994. Mixing: Properties and Examples. *Lecture Notes in Statistics, Vol. 85. New York: Springer-Verlag.*

Fries, S., Zakoian, J. M. (2019). Mixed causal-noncausal ar processes and the modelling of explosive bubbles. *Econometric Theory*, 35(6), 1234-1270.

Fries, S. (2022) Conditional Moments of Noncausal Alpha-Stable Processes and the Prediction of Bubble Crash Odds. *Journal of Business & Economic Statistics*, 40:4, 1596-1616

Gouriéroux, C., and J., Jasiak (2016). Filtering, prediction and simulation methods for noncausal processes. *Journal of Time Series Analysis*, 37, 405-430.

Gouriéroux, C., and J., Jasiak (2017). Noncausal vector autoregressive process: Representation, identification and semi-parametric estimation. *Journal of Econometrics*, 200, 118-134.

Gourieroux, C., Jasiak, J. (2018). Misspecification of noncausal order in autoregressive processes. *Journal of Econometrics*, 205(1), 226-248.

Gourieroux, C., Jasiak, J., Monfort, A. (2020). Stationary bubble equilibria in rational expectation models. *Journal of Econometrics*, 218(2), 714-735.

Gouriéroux, C., and J.-M., Zakoian. 2015. On uniqueness of moving average representations of heavy-tailed stationary processes. *Journal of Time Series Analysis*, 36, 876-887.

Gouriéroux, C. and J.-M., Zakoian. 2017. Local explosion modelling by non-causal process. *Journal of the Royal Statistical Society: Series B (Statistical Methodology)*. 79, 737-756.

Gourieroux, C., Jasiak, J., and Monfort, A. 2020. Stationary bubble equilibria in rational expectation models. *Journal of Econometrics*, 218(2), 714-735.

Gourieroux, C., Jasiak, J., & Tong, M. (2021). Convolution-based filtering and forecasting: An application to WTI crude oil prices. *Journal of Forecasting, 40(7), 1230-1244.*

Hashimoto, K., and Im, R. 2016. Bubbles and unemployment in an endogenous growth model. *Oxford Economic Papers*, 68(4), 1084-1106.

Hashimoto, K., and Im, R. 2019. Asset bubbles, labour market frictions and R&D-based growth. *Canadian Journal of Economics*, 52(2), 822-846.

Hecq, A., Lieb, L., and S. M., Telg. 2016. Identification of mixed causal-noncausal models in finite samples. *Annals*

of Economics and Statistics, 123/124, 307-331.

Hecq, A., Telg, S., and L., Lieb. 2017. Do seasonal adjustments induce noncausal dynamics in inflation rates? *Econometrics*, 5, 48.

Hecq, A., Voisin, E. (2021). Forecasting bubbles with mixed causal-noncausal autoregressive models. *Econometrics and Statistics*, 20, 29-45.

Hencic, A., and C., Gouriéroux. 2015. Noncausal autoregressive model in application to bitcoin/usd exchange rates. *Econometrics of Risk*, Springer International Publishing, 17-40.

Hirano, T., and Toda, A. A. 2024. Bubble economics. *Journal of Mathematical Economics*, 111(C).

Hirano, T., Kishi, K., and Toda, A. A. 2025. Bursting Bubbles in a Macroeconomic Model. *CIGS Working Paper Series No. 25-001E*, Canon Institute for Global Studies.

Hirano, T., and Toda, A. A. 2025. Housing Bubbles with Phase Transitions. *Working Paper*, arXiv:2303.11365 [econ.TH].

Hugonnier, J. 2012. Rational asset pricing bubbles and portfolio constraints. *Journal of Economic Theory*, 147(6), 2260-2302.

Janßen, A. (2019). Spectral tail processes and max-stable approximations of multivariate regularly varying time series. *Stochastic Processes and their Applications*, 129(6), 1993-2009.

Janßen, A., and J., Segers. 2014. Markov tail chains. *Journal of Applied Probability*, 51, 1133-1153.

Jarrow, R., Protter, P., and Shimbo, K. 2010. Asset Price Bubbles in Incomplete Markets. *Mathematical Finance*, 20, 145-185.

Jarrow, R.A., Protter, P., and Roch, A.F. 2012. A liquidity-based model for asset price bubbles. *Quantitative Finance*, 12(9), 1339-1349.

Knight, J. L., Yu, J. (2002). Empirical characteristic function in time series estimation. *Econometric Theory*, 18(3), 691-721.

Lanne, M., and P., Saikkonen. 2011. Noncausal autogressions for economic time series. *Journal of Time Series Econometrics*, 3.

Lanne, M., and P., Saikkonen. 2013. Noncausal vector autoregression. *Econometric Theory*, 29, 447-481.

Lux, T., and Sornette, D. (2002). On rational bubbles and fat tails. *Journal of Money, Credit, and Banking*, 34(3), 589-610.

Martin, A., and Ventura, J. 2012. Economic Growth with Bubbles. *American Economic Review*, 102(6), 3033-58.

Meinguet, T., and J., Segers. 2010. Regularly varying time series in Banach spaces. arXiv preprint arXiv:1001.3262.

Miao, J. 2014. *Economic Dynamics in Discrete Time*. MIT Press, Cambridge, MA.

Miao, J., Wang, P., and Xu, L. 2016. Stock market bubbles and unemployment. *Economic Theory*, 61(2), 273-307.

Michau, J.-B., Ono, Y., and Schlegl, M. 2024. Optimal monetary policy and rational asset bubbles. *European Economic Review*, 170, Article 104884.

Planinić, H., and P., Soulier. 2017. The tail process revisited. *Extremes*, 1-29.

Protter, P. 2012. A Mathematical Theory of Financial Bubbles. *SSRN Electronic Journal*, 2081.

Rootzén, H. (1978): Extremes of moving averages of stable processes. *The Annals of Probability*, 847-869.

Saikkonen, P., and R., Sandberg. 2016. Testing for a unit root in noncausal autoregressive models. *Journal of Time*

Series Analysis, 37, 99-125.

Samorodnitsky, G., and M. S., Taqqu. 1994. *Stable non-Gaussian random processes*, Chapman & Hall, London, 516-536

Soulier, P., Dombry, C., Hashorva, E. (2018). The tail measure and tail spectral process of regularly varying time series. *The Annals of Applied Probability*, 6(28), 3884-3921.

Tirole, J. 1985. Asset bubbles and overlapping generations. *Econometrica*, 1499-1528.

Xu, D. and Knight, J. (2010). Continuous empirical characteristic function estimation of mixtures of normal parameters. *Econometric Reviews*, 30(1) 25–50.